4-1992

Computational Simulation of Flow through Elbows in the Approach Piping Systems to a Headbox

Kasinathan Ramanathan
Western Michigan University

COMPUTATIONAL SIMULATION OF FLOW THROUGH ELBOWS IN THE APPROACH PIPING SYSTEMS TO A HEADBOX

by

K. Ramanathan

A Thesis
Submitted to the
Faculty of The Graduate College
in partial fulfillment of the
requirements for the
Degree of Master of Science
Department of Paper and Printing
Science and Engineering

Western Michigan University
Kalamazoo, Michigan
April 1992

COMPUTATIONAL SIMULATION OF FLOW THROUGH ELBOWS IN THE APPROACH PIPING SYSTEMS TO A HEADBOX

K. Ramanathan, M.S.

Western Michigan University, 1992

The successful operation of the wet end in a paper machine is highly dependent on the approach piping system. Sheet basis weight stability and ease of making wet end adjustments are greatly impaired by improperly designed approach piping systems. Most problems in headbox approach piping occur when the flow splits, combines, and passes through elbows.

Elbows create cross flows, flow separation, and eddies, and play an important role in the uniform and stable delivery of the pulp into the headbox. The effect due to an elbow lasts for a considerable distance downstream of the elbow and is severe when two elbows are in the system. Although elbows are commonly used in practice, many questions regarding their optimum arrangement still remain unanswered. The present study gave answers for the optimum arrangement of elbows and provides a convenient and effective guide to improve the design of the approach piping system.

ACKNOWLEDGEMENTS

I would like to thank Dr. Nick Triantafillopoulos, advisor and thesis committee chairperson, for his valuable suggestions, support, and time for this study; Dr. David K. Peterson, advisor, for his valuable suggestions, time, and help; Dr. Raja Aravamuthan, advisor, for his valuable suggestions and time; Mr. Richard Reames for permitting me to use his computer to carry out this research and for his encouragement and support; Dr. Pradeep Sagdeo for his help in solving problems; Dr. Jimmy Li, Creare.X, Inc., Hanover, NH. for his enormous help in getting the new FLUENT/BFC code and for designing the strategies to solve the problem; Creare.X, Inc. for donating the FLUENT/BFC code to Western Michigan University, Kalamazoo; Dr. Harley Behm, Mr. George Kohrman and Dr. Dennis Pence, University Computing Services, for their help in obtaining the new code; and Ms. Elaine, University Computing Services, for providing research account and required diskquota and CPU time in VAX/VMS computer.

K. Ramanathan

Order Number 1348309

Computational simulation of flow through elbows in the approach piping systems to a headbox

Ramanathan, Kasinathan, M.S.

Western Michigan University, 1992

U·M·I
300 N. Zeeb Rd.
Ann Arbor, MI 48106

TABLE OF CONTENTS

Table of Contents--Continued

CHAPTER

Table of Contents--Continued

CHAPTER

LIST OF TABLES

LIST OF FIGURES

List of Figures--Continued

List of Figures--Continued

List of Figures--Continued

CHAPTER I

INTRODUCTION

The piping arrangement before a headbox is part of the system in a papermachine design. The function of the approach piping system is to deliver the stock into headbox from the fan pump. The successful operation of the wet end in a paper machine is strongly dependent on this system. Sheet basis weight uniformity and ease of making wet end adjustments are greatly impaired by an improperly designed approach piping system (1).

In order to have consistently uniform flow to the headbox inlet, the following requirements need to be satisfied:

1. Correct pipe diameter to attain proper stock velocities in order to maintain dispersion of fibers and also promote clean pipe lines.

2. Flanges with gaskets should be concentric with the pipe inside diameter to avoid stock buildup.

3. All interior pipe surfaces must be polished to the extent that the surface will not "pick" the fibers of a cotton ball.

4. Long radius elbows with adequate distance between/after elbows to decouple the elbow effect (2).

The above requirements illustrate that the approach piping system needs special attention in design, unlike other pipe line design in the mill. Any deviations from the above requirements will affect the papermachine performance. It is therefore important to design and install an optimum and efficient approach piping system.

CHAPTER II

LITERATURE REVIEW

Overview

In the design of an approach piping system, little attention has been paid to flow velocities around bends or elbows. In early times, when piping was made out of brass rather than stainless steel, mills made pipe lines four times larger than necessary by modern standards. When it came time for a rebuild, they sold the piping for scrap to pay for new stainless steel piping (3). Now, of course, piping design is a more exact science.

The modern design of approach piping system takes into consideration the following factors:

1. Stock piping should be sized to deliver dilute stock at velocities of approximately 3 m/sec (4).

2. At higher stock velocities, for example 4.5 m/sec, the chances for flow separation in fittings and cross sectional area changes of the pipe increase. At stock velocities below 3 m/sec, particularly around 1.5 m/sec, there is the possibility for heavy filler dropout and air entrapment at the top of pipelines, especially on those machines operating without a deaeration system (4).

3. Flow complications should be kept to an absolute minimum. In practice, long-radius elbow (i.e., the radius of curvature of elbow is equal to one-and-one half times the diameter of the pipe) is used in approach piping systems (4).

4. The usual specification of a ten pipe diameter spacing between the last elbow and the headbox manifold will eliminate only the grossest of flow anomalies, such as flow separation and recirculation coming from the elbow.

The fluid flow in an approach flow system is defined as "pipe flow" (5). In order to optimize the design of the approach piping design, there is a need to study the fluid dynamics of pipe flow. Therefore, it is pertinent to review the literature of pipe flow, including bends and elbows.

Background

In the papermaking process, water is used not only to transport fibers but also to achieve good mixing of fibers and fillers for good sheet formation. The pipe flows may be either laminar or turbulent, depending on the characteristic Reynolds number (Re). Laminar flow is the one in which the fluid flows in laminae or layers; there is no macroscopic mixing of adjacent fluid layers. In contrast, turbulent flow involves eddies, whirls and vortices due to small velocity fluctuations superimposed on the mean motion

of flow. Whether a flow is laminar or turbulent depends on certain parameters of pipe flows. The nature of the flow is determined by the value of the dimensionless Reynolds number, Re, defined as:

$$Re = \rho DV/\mu \qquad (1)$$

where ρ = density of the fluid; D = pipe diameter; V = average flow velocity; μ = viscosity of the liquid.

Laminar flow ends at approximately Re = 2400. Under ordinary condition of flow, the flow is turbulent at Reynolds number above 4000. Between 2100 and 4000, a transition region is found where the type of flow may be either laminar or turbulent, depending upon conditions at the entrance of the tube and on the distance from the entrance. For a papermachine with a capacity of 350 t/day, the diameter of the approach pipe need to be 0.6 m for the velocity of the pulp suspension to be 3 m/sec (5). In this case the Re is about 3 million, which indicates that the flow in the approach piping system to a headbox is turbulent.

Turbulent Flow in a Pipe

Turbulent flow is a very complex process. Although a considerable amount of knowledge has been developed, the field of turbulent flow remains among the least understood areas of fluid mechanics. A distinguishing feature of

turbulent flow is that it is irregular and random. Many important turbulent flow properties (e.g., pressure drop, heat transfer) depend strongly on the existence and nature of the turbulent fluctuations. The main characteristic of this flow is that, in addition to the time-averaged flow velocity, a fluctuating velocity component also exists. A typical velocity trace measured at a given location in the flow field is shown in Figure 1.

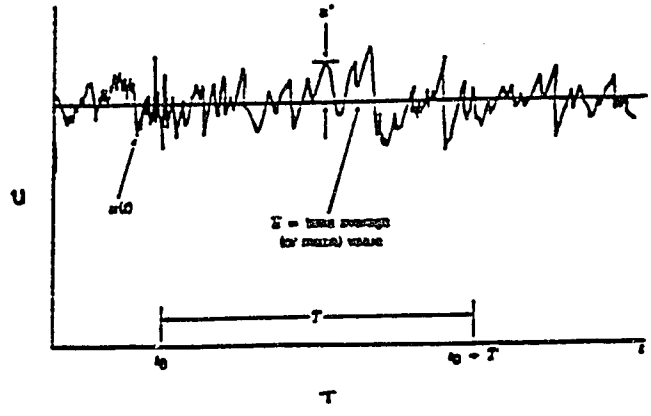

Figure 1. The Nature of Velocity in Turbulent Flow (7).

Thus, turbulent flows can be described in terms of their mean velocity values (denoted with an overbar) on which the fluctuations (denoted with a prime) are superimposed. If $u = u(x,y,z,t)$ is the velocity component, then its mean (or time averaged) value, $\bar{u}$ is equal to

$$\bar{u} = 1/T \int u(x,y,z,t)\, dt \qquad (2)$$

where T is the time interval. The fluctuating part of the velocity, u', is the time varying portion that deviates from the average value:

$$u = \bar{u} + u' \text{ or } u' = u - \bar{u} \qquad (3)$$

Turbulent flow comprises many eddies of various sizes coexisting in the flowing stream. Large eddies are continually formed and break down into smaller eddies, which finally disappear.

Turbulent flow fields are characterized by two average parameters: intensity and scale. The first measures the intensity of the field and refers to the speed of rotation of the eddies as well as the energy contained in an eddy of a specific size. The second measures the size of the eddies. The turbulent intensity, I, is defined as the square root of the mean square of the fluctuating velocity divided by the average velocity.

$$I = \sqrt{(\bar{u}')^2} / \bar{u} = [(1/T)\int (u')^2 \, dt]^{1/2} / \bar{u} \qquad (4)$$

The larger the turbulence intensity, the larger the fluctuations of the velocity. In highly turbulent fields, such as those immediately downstream of turbulence-producing grids, intensity may reach values of 5 to 10%. In unobstructed flows, intensities are less and of the order of 0.5 to 2.0% (7).

When the fluid passes through a pipe, the velocity is

not uniform across the pipe because of the formation of the boundary layer. The formation and behavior of boundary layers are important for a fluid flow in a pipe.

Flow in Boundary Layers

A boundary layer is defined as that part of a moving fluid in which the fluid motion is influenced by the presence of a solid boundary (8). For example, referring to Figure 2, the velocity of the fluid upstream from the leading edge of the plate is uniform across the entire

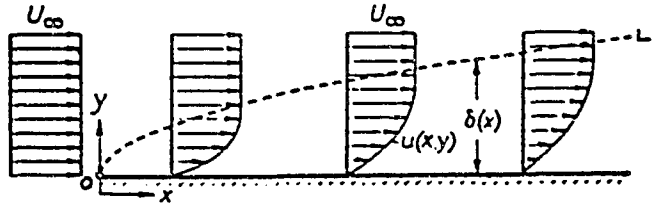

Figure 2. Boundary Layer on a Flat Plate in Parallel Flow (8).

fluid stream. However, while the velocity of the fluid at the interface between the solid and fluid is zero, the velocity increases with the distance from the plate. The dotted line OL is so drawn that the velocity changes are confined between this line and the trace of the wall. This imaginary line separates the fluid stream into two parts; one in which the fluid velocity is constant and the other

in which the velocity varies from zero at the wall to a velocity substantially equal to that of the undisturbed fluid far away from the wall. For fully-developed laminar and turbulent flows (Re, 10^4), the profiles are depicted in Figure 3. For laminar flow the average velocity over the whole cross section of the pipe is precisely 0.5 times the maximum velocity at the center. For turbulent flow with the curve is somewhat flattened in the center and the

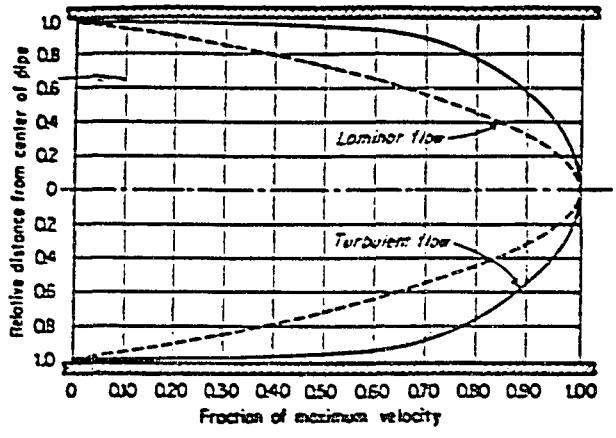

Figure 3. Velocity Distribution of a Fluid Across a Pipe (9).

average velocity is about 0.8 times that of the maximum. This value of 0.8 varies with the Reynolds number.

Turbulent Velocity Profiles

The fully-developed turbulent flow in a pipe can be broken into three regions which are characterized by their

distances from the wall. These are (a) the viscous sublayer very near the pipe wall, (b) the overlap region or buffer layer, and (c) the outer turbulent layer. Within the viscous sublayer, the viscous shear stress is dominant compared with the turbulent stress and the random nature of the flow is essentially absent. In the outer turbulent layer the Reynolds stress is dominant, and there is considerable mixing and randomness to the flow. The character of the flow within these two regions is entirely different. For example, within the viscous sublayer the fluid viscosity is an important parameter while the density is unimportant. In the outer layer the opposite is true.

In the viscous sublayer the velocity profile can be written in dimensionless form as:

$$\bar{u}/u^* = yu^*/v \qquad (5)$$

where y = R-r is the distance measured from the wall, u is the time average x component of velocity, and $u^* = (\tau_w/\rho)^{1/2}$ is termed the friction velocity. Dimensional analysis arguments can show that, in the overlap region, the velocity should vary as the logarithm of y (7). The following expression has been proposed:

$$\bar{u}/u^* = 2.5 \ln (yu^*/v) + 5.0 \qquad (6)$$

where the coefficients 2.5 and 5.0 have been determined experimentally.

In the central region (i.e., the outer turbulent layer) the expression

$$(V_c - \bar{u})/u^* = 2.5 \ln(R/y) \qquad (7)$$

where V_c is the centerline velocity. This relationship is in agreement with experimental data (7). Another form of this relationship often used is the empirical power-law velocity profile

$$\bar{u}/V_c = (1 - r/R)^{1/n} \qquad (8)$$

Hence, the value of n is a function of the Reynolds number Re. The one-seventh power law velocity profile (n = 7) is usually used as a reasonable approximation for many practical flows (7).

Flow Over Curved Sections

Bending of the flow in curved pipes generates centrifugal forces directed from the center of curvature to the outer wall of the pipe (10). The appearance of centrifugal forces and the development of boundary layers at the walls explain the occurrence of secondary flows in curved tubes. These centrifugal forces induce an increase of the pressure at the outer wall and a decrease at the inner wall as the flow passes from the straight to the curved section of the pipe. Consequently, the flow velocity will correspondingly

be lower at the outer wall and larger at the inner wall as shown in Figure 4.

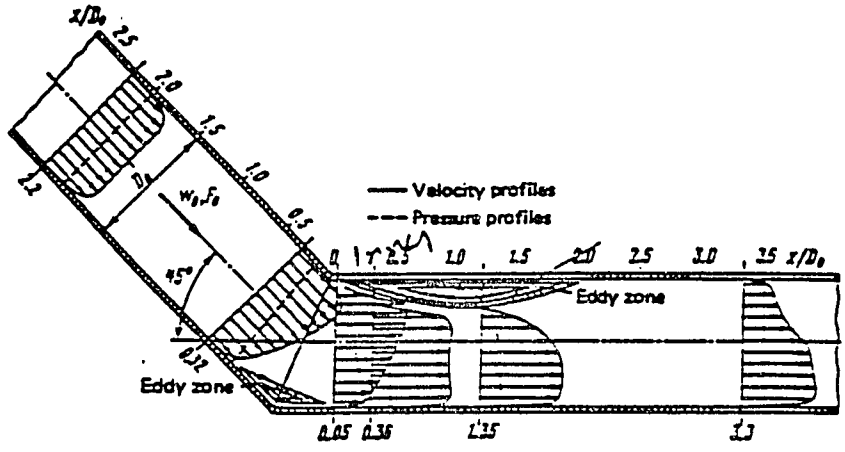

Figure 4. Variation of Velocity and Pressure Profiles in an Elbow and a Straight Section Downstream (10).

In this bend, a "diffuser effect" occurs near the outer wall, and a "bellmouth effect" appears near the inner wall. Similar phenomena appear after turning the passage of flow from the curved into the straight section, but in the reverse order. The diffuser-type phenomena lead to flow separation from both walls. An eddy zone, formed as a result of flow separation from the inner wall, propagates far ahead and across greatly reducing the cross-section of the main stream. Separation of the laminar layer at the point closest to the beginning of the curvature of the bend

naturally produces an extensive eddy zone at the inner wall.

Flow separates along the inner wall and remains so for a considerable distance downstream of the elbow as shown in Figure 5.

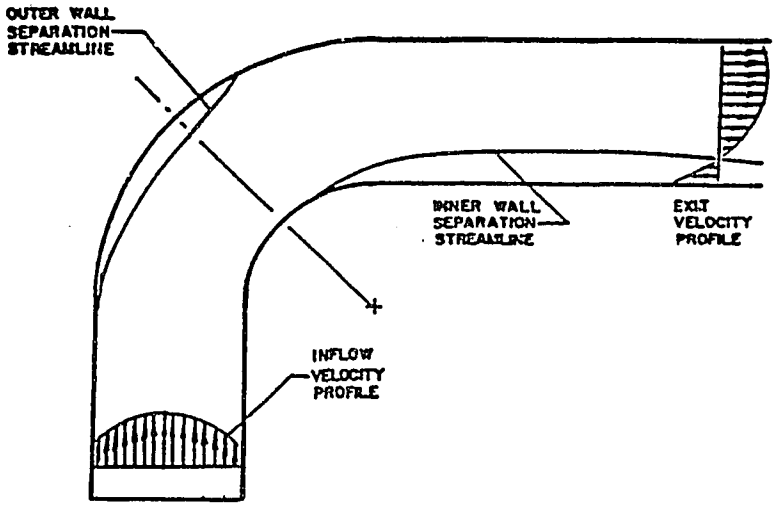

Figure 5. Flow Separation in a 90° Elbow (4).

If the flow velocities are high enough, there is also the potential for separation along the outer wall. However, because of the favorable pressure gradient in the existing quadrant, the flow will reattach itself. The picture depicted here is for relatively uniform inflow velocity profiles, which implies a considerable length of straight pipe upstream of the bend. This situation is more complicated if there are two elbows in series, separated

only by short distances of straight pipe. In that case the velocity profile at the exit of the elbow is extremely difficult, if not impossible to predict (4).

Flow in Bends With Sharp Corners

Other conditions being equal, the curved tube offers the largest resistance to flow in the case when the inner wall is a sharp corner (10), i.e., the flow separates from this wall more vigorously. Both the intensity of vortex formation and the resistance on the wall increase proportionally with the bend angle. Rounding of the elbow corners makes flow separation much smoother and, consequently, reduces resistance. In contrast, if the outer corner of the elbow is left sharp and only the inner corner is rounded, the minimal resistance of 90° elbow will be attained at r_o/b_o = 1.2-1.5 (r_o is the radius of curvature; b_o is the diameter of the pipe). With the further increase in r_o/b_o, the resistance will grow noticeably (10). This is due to the fact that, if the inner corner is rounded, the cross-sectional area at the place of bending increases, and, hence, the average velocity decreases. As a result the diffuser-separation of flow increases.

Rounding-off of the outer corner and keeping the inner corner sharp does not lead to a noticeable decrease in elbow resistance. On the other hand, an increase in the

radius of curvature of the outer wall causes an increase in elbow resistance. This indicates that it is not sufficient to round off the outer wall alone (with the inner corner kept sharp), because the cross-sectional area of flow decreases and the diffuser losses increase. Additionally, variations of the surface ratio at the entrance and exit from an elbow alter the flow resistance (10). The diffuser effects become larger with an increase in the cross sectional area downstream of the bend. This intensifies flow separation and formation of vortices.

Effect of Two Elbows

The flow resistance of combined bends or elbows depends on the relative distance between the two units. In sharply bent channels, the interaction between paired elbows is mainly determined by the position and the magnitude of the separation zones downstream of the first bend. In the case of smooth elbows the combined effect depends on the distance between the two elbows and the orientation of the second elbow; whether the second elbow is in the same plane or out-of-plane. Double elbow combination where minimal pipelengths separate the elbows can produce very energetic, long-lasting, swirling flows (11).

Elbows as Mixture Devices

Yeh and Mattingly (12) studied the effects of elbows

using laser Doppler velocimetry and concluded that two elbows in series can act as excellent systems for fluid mixing. They found that closely coupled double elbow with out-of-plane piping produced very energetic, long lasting mixing flows. In contrast, the spaced double elbow out-of-plane configuration produces less effective mixing. In contrast, a single elbow produces energetic mixing which is not as long-lasting in the downstream pipeflow as in the closely coupled double elbow. For the double elbow out-of-plane configuration, the local swirl intensity is intense and the swirl angle approximates 20 degrees near the pipe wall, at the upstream location. For the double elbow piping, the most active mixing region is near the wall, while there is little mixing activity at the pipe center-line. As for the single elbow case, mixing at the center-line of the pipe is important. This is because there is only one large swirling eddy produced in the double elbow case, but two counter-rotating swirling eddies produced in the single elbow piping.

The major conclusions from the above literature review are:

1. Elbows result in flow separation and formation of eddies. These secondary fluid motions cause restriction of the flow not only within the curved section itself but also in downstream straight-pipe sections.

2. Elbows with sharp corners are not desirable since they offer large resistance and vigorous flow separations.

3. The elbow effect is worse if two elbows are in series since the combined elbow effects last for a long distance, compared to a singe elbow configuration.

There are many unanswered questions regarding the proper approach to piping design, particularly in situation involving elbows or bends. The solutions to this problem are (a) use of venturi elbow, (b) use of bends with turning vanes, or (c) having sufficient pipe length downstream of an elbow to eliminate the elbow effects. A venturi elbow offers less resistance than the standard elbow by about 30-40%, but venturi elbows complicate piping design where the designer is trying to keep stock velocities within fairly narrow limits (4). In case of bends with turning vanes, the flow is straightened within three diameters from the exit, but there are problems of fiber stabling and stringing (4). None of these solutions is considered the ultimate as far as papermachine approach flow component systems are concerned (4). The literature does not give the exact length of pipe required to completely eliminate the effect of the elbow. Hence, it is obvious that additional work needs to be carried out in this field.

CHAPTER III

PROBLEM STATEMENT

The performance of the papermachine headbox is influenced by the presence of elbows in the approach piping systems. Elbows create eddies and flow separations, but these effects need to be eliminated before the stock enters the headbox in order to facilitate a uniform paper with good formation. The transition from circular pipes to the rectangular flow domains of the headboxes must be done without flow separation.

Considering these issues, there are still many unanswered questions regarding the optimum arrangement of elbows. In particular, consider the two elbows in series configured in Figure 6.

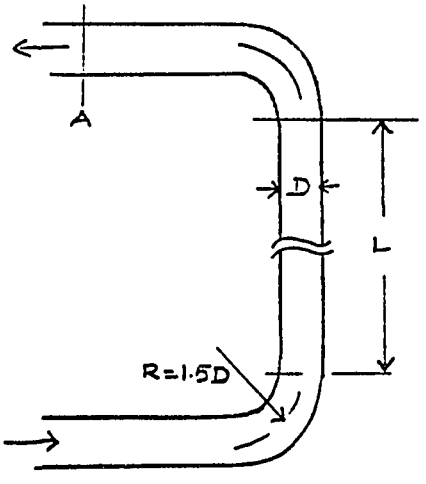

Figure 6. Two Elbows in Series.

If length L is short, flow profiles at location 'A' would be different than if L is very long. These questions need to be considered.

1. What length of pipe, L, is required so that further increases in length will not significantly affect the profiles at section A?

2. How far downstream of the second elbow does the flow attain uniform profiles?

3. What should be the length of pipeline after the second elbow if the two elbows are close?

4. What is the length of the pipeline required after an elbow to completely eliminate its effect?

5. Are there any differences in the effect of elbows if they are 90^0 out-of-plane?

CHAPTER IV

SIGNIFICANCE OF THE PROBLEM AND RATIONALE

Approach piping needs to be properly designed for optimum headbox performance. Pipes longer than the optimum would result in higher construction costs and frictional losses which would require higher pumping energy. In contrast, insufficient pipe length after an elbow would result in basis weight variations in the cross direction of the machine, nonuniform filler distribution in the sheet, and less retention (13). In particular, a problem with a short pipeline between the last elbow and the headbox manifold transition piece is higher ash content in the sheet at the back side than at the front. Because of the flow separation and acceleration of flow at the outer wall due to the elbow, a larger amount of fillers enters the backside of the headbox than at the front side. This causes nonuniformity of the ash profile in the sheet.

To solve the above problems, experimental methods are not very suitable, since the fluid flowing through the approach system contains pulp even though it is dilute. Available experimental facilities like LDV (Laser Doppler Velocimetry) measurements cannot be used to determine the velocity profile in suspensions with fiber concentrations

above 0.2%. There are many flow variables like velocity, pressure, temperature, and consistency in the approach flow system which vary for different papermachines. Hence, the experiments have to be repeated with all the possible combinations of variables which is a tedious and complex task.

Numerical simulation using computational fluid dynamics can eliminate the problems associated with experiments. In particular, no experimental probe that can disturb the flow is needed. Once the model is verified, different initial conditions can be implemented and results can be obtained for different cases.

The present study would contribute to identifying the optimum pipe length between or after elbows. This could save costs while improving paper quality. Accurate numerical prediction of the approach piping flow would provide a convenient and effective guide to improve the design of approach piping system. Such a system would deliver a uniform, steady, and stable flow to the headbox.

CHAPTER V

OBJECTIVES

The main objective of this study is to model flows and computationally simulate the approach piping system to headboxes containing elbows. The specific objectives are:

1. To develop a model and verify its results with the available experimental results in the literature.

2. To find the optimum length of pipe required downstream of an elbow to completely eliminate elbow effects.

3. To find the optimum distance required downstream of a second elbow if two elbows are present in a system.

4. To find the minimum distance required between two elbows.

5. To find the effects of elbows, when they are located 90° out-of-plane.

CHAPTER VI

EXPERIMENTAL DESIGN

The methodology is comprised of modeling the flow and computationally simulating these flow variables such as velocity (streamwise, vertical), pressure, kinetic energy of turbulence and eddy dissipation rate in the flow field. Computational modeling will be done using the fluid dynamics code FLUENT/BFC (Version 3.02, Trademark of Creare Inc., Hannover, NH) (14). Hence, it is necessary to review the general scope of the computational fluid dynamics and the characteristics of FLUENT/BFC before discussing the methodology implemented in this project.

Scope of Computational Fluid Dynamics

Computational fluid dynamics is certainly not pure theoretical analysis. If anything, it is closer to the experimental branch. The performance of each particular calculation on a computer closely resembles the performance of a physical experiment, in that the analyst "turns on" the equations and waits to see what happens, just as in physical experiments. Though numerical simulation cannot replace experiments they have some exclusive advantages over physical experiments (15):

1. No experimental probe that can disturb the flow is needed.

2. Flow parameters such as initial and boundary conditions can be chosen with flexibility.

3. The adequacy of basic constitutive fluid equations can be tested.

4. The numerics can do what is difficult to do with experiments--they can test the sensitivity of flow phenomena to theoretical assumptions and observe the response of the simulated system to new and unusual conditions.

Implementing an accurate modeling and simulation of a physical system involves four basic steps (15): (1) the development of a model based on current understanding of theory and on experimental data (2) discretization of the geometrical domain of interest (3) application of a computational (numerical) method to solve the system of governing equations and (4) analysis of the numerical solution. Once the model is conceptualized, the spatial region (geometric domain) of the fluid-flow field is divided into a large number of small subregions by superimposing a grid pattern over the domain. A higher concentration of grid points should be designed in regions with increasing flow activity or complexity to provide sufficient resolution that accurately represents the flow.

Computational Fluid Dynamics (CFD) provide approximate solutions of the governing conservation equations for fluid

flow by utilizing one of several numerical techniques to solve a set of discretized algebraic equations (15). The integral or partial-differential forms of these equations are solved on digital computers and the results may be displayed in a manner similar to experimentally visualizing the flow and analyzing laboratory data.

Because the accuracy of a numerical solution depends on the approximations originally made, it must be verified by comparing model predictions to both analytical and experimental data. When inconsistencies occur, complicating effects not previously considered should be accounted for in the model. Numerical results are also strongly affected by grid design, convergence and stability of the solution scheme, and the specified initial and boundary conditions. Thus, simulation and experiment are complementary in the sense that simulations should be calibrated by experiments, and then experiments can be interpreted based on simulations.

Once the model is verified, the simulation can be used to interpret measurements and observations, evaluate new ideas, extend theoretical models into new parameter regimes, help in engineering design processes, and quantitatively test existing theories (15). Consequently, CFD can provide useful information on fluid flow aspects of design and on the effect of process and fluid variables on the characteristics of the flow. The CFD code used for

this research work is FLUENT/BFC and it would be appropriate to review its main features.

Characteristics of FLUENT/BFC (14)

FLUENT/BFC is a general-purpose computer program for modeling transport processes involving fluid flow and heat transfer in arbitrary geometries. Current capabilities of the program include simulation of laminar and turbulent flows, subsonic and supersonic viscous flows, incompressible flows, time-dependent and stationary flows, isothermal flows and flows with heat transfer involving Newtonian and power law non-Newtonian fluids.

The FLUENT/BFC solves the transient or steady two-dimensional (planar as well as axi-symmetric) or the three dimensional Navier-Stokes and energy equations for laminar or turbulent, incompressible or compressible flows in general curvilinear geometries. Curvilinear flow geometries, which simple coordinate systems such as the Cartesian or cylindrical-polar coordinates cannot accurately represent, are modeled without compromise. An interactive computer aided design (CAD) interface helps analyst construct the geometry to be modeled.

FLUENT/BFC consists of three modules: PreBFC, SolvBFC and PostBFC. Their description and functions are as follows:

1. PreBFC is the preprocessor module which is an

interactive menu-driven program with the following functions:

1. Geometry modeling: CAD tools are available for constructing geometries using points, curves, surfaces and other entities with integrated display capabilities.

2. Grid generation: FLUENT/BFC has a built-in option with flexible grid generation capability for creating in single or multiple connected domains.

3. Physical property input and equation solution control.

4. Boundary condition specification.

2. SolvBFC: SolvBFC is the module which solves the governing equations of flow in generalized curvilinear coordinates using iteration method.

3. PostBFC: PostBFC is a post-processor module used to manipulate and display the data generated by SolvBFC. The problem geometry and the grid can be displayed, along with the flow field plotted in the form of vectors and profiles. Distribution of scalar quantities such as velocity magnitude, stream function, temperature, etc., can be plotted as color filled contours.

Appendix A depicts the theory utilized by the FLUENT/BFC computational code (15).

Methodology

Overview

The experimental design involved two parts: (1) Developing a model and verifying it with the available experimental data, and (2) Determining the optimum distance required downstream of an elbow or between elbows, using the verified model.

In approach piping system, long radius elbows are used. Hence it is necessary to develop a model containing a long radius elbow. In order to rely on the result of the model developed, verification of the experiments is needed. Model development and simulation involved implementing the exact geometry and boundary conditions of the experiments. Experimental results such as streamwise and vertical velocity are available at different distances downstream of the elbow from National Institute of Standards and Technology, Gaithersburg, MD (10). The simulated velocity profiles were compared with experimental profiles to verify the model. All initial and boundary conditions were simulated exactly the same way as they appeared in these experiments. However, some assumptions were made because the exact values of some of the variables (such as pressure and turbulent intensity) were not monitored during the experiments. The inlet velocity of the fluid was fully-developed. This condition was implemented by modeling

adequate length (about 25 diameters distance) of pipe before the elbow that would develop the flow. Downstream of the elbow is a long pipe (about 90 diameters length) sufficient enough to study the elbow effects.

Once the model was verified, the next step was to perform numerical experiments to investigate the effect of elbows using the verified model. These numerical experiments involved single and double elbow cases. Single elbow cases were run for three different Reynolds numbers to see if there was any difference in the effect of elbows when the Reynolds number is changed. One of the single elbow cases had a Reynolds number similar to the conditions of practical interest. The double elbow cases were of out-of-plane type. The second elbow was placed at different distances from the first elbow and in each case the distance required downstream of second elbow to get fully developed flow was studied. This give an answer for the optimum distance between two elbows. Another set of models were in-plane type. These were modeled like out-of-plane cases at different distances between the two elbows. This to find out if there were any differences in the effect of elbows if they were 90° off the plane.

In real mill situations, dilute pulp slurry flows through the approach systems with a consistency of about 0.4% to 1.0%. While simulating mill conditions, the fluid was assumed to be water. There have been many studies on

pulp flow in a circular pipe. Dilute pulp slurry at consistency below 0.5% behaves like a Newtonian fluid and above this consistency it is a pseudoplastic fluid (18). In a study conducted at the Tokyo Institute of Technology, Japan with fiber suspensions of consistencies between 0.15% to 0.62%, it was found that the velocity profile of dilute pulp suspension in the above consistency range was almost the same as water in the turbulent region of flow (19). The critical Reynolds number for transition from laminar to turbulent was almost the same as water. Friction played a minimal role at high Reynolds numbers (in mill situations the Re is very high), because the inertial force is superior to viscous forces and the velocity profile is flat at the center (19).

Before introducing model verification and numerical experiments, it is appropriate to explain how the experiments were conducted and the procedure used to develop the model.

LDV Measurements of Pipe Flow

Numerical results were compared with the experimental results conducted by Yeh and Mattingly (10) at the NIST (National Institute of Standards and Technology, National Engineering Laboratory, Gaithersburg, Maryland). They used Laser Doppler Velocimetry (LDV). The pipeflows were produced in smooth, stainless steel piping. The joints

were arranged through weld-neck type flanges where special attention had been paid to smooth, concentric alignments for all welded joints. All flange joints were concentrically aligned with pins. Where steel pipe joined the glass tube test section, extreme care was taken to produce a concentric joint with no steps in the inner diameter. The facility had a 5 cm diameter stainless steel piping with a long radius elbow of radius of curvature 7.5 cm. The source of flow was a centrifugal pump and a heat exchanger provided constant temperature flow up to Reynolds number, W_bD/v exceeding 10^5 (where W_b is the bulk flow velocity and v is the fluid kinematic viscosity). The thin-walled, round-glass pipe that represented the test section was contained in a water filled enclosure having flat, thick optical glass sides so that the laser beams were minimally deflected by the curvature of the round glass pipe.

The piping elbow configurations selected were the single, standard, long-radius elbow and double elbow arrangements. The double elbow configurations were of the "out-of-plane" type. The experiments were conducted at a Reynolds number of 10^5 with water as the fluid. Measurements like streamwise and vertical velocities were collected at different distances from the elbow outlet. These were collected along both vertical and horizontal direction. These data were compared with the results obtained by simulation.

Model Development

Overview

The numerical work involves (a) development of a model for verification and (b) conducting numerical experiments to determine the optimum distance required after an elbow or between elbows. Initially, it was decided to attempt to simulate the flow characteristics by developing a two-dimensional model using FLUENT. The result from the two dimensional model did not compare well with the experimental results of Yeh and Mattingly (11). Figure 7 compares the simulated result from the two-dimensional model and the experimental results at 1.5 diameter distance from the elbow.

To increase the accuracy of the two-dimensional model, more nodes were added in the flow domain and more iterations were tried. Numerical results did not compare well with the experimental results. The flow velocity is supposed to be high near the inner wall and low at the outer wall at the elbow. At the exit of the elbow the reverse should happen (9). Figure 8, which depicts the streamwise velocity, does not show above phenomenon at the elbows.

This may be due to the fact that the two-dimensional model did not represent the pipe flow and was closer to the open channel flow. Another reason might be that smooth

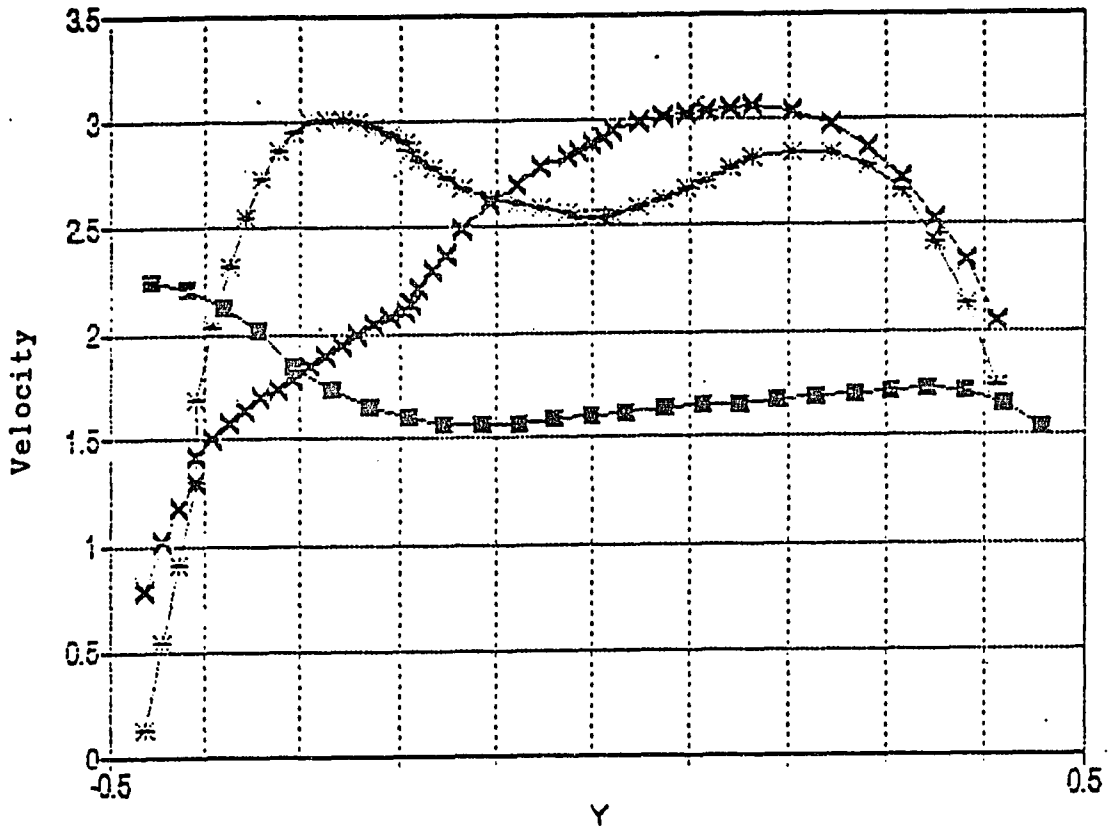

Legand. Experimental profile
Simulated profile after 150 iterations
Simulated profile after 1080 iterations

Figure 7. Comparison of Streamwise Velocity Along Vertical Direction From Two-Dimensional Model With Experimental Results (11).

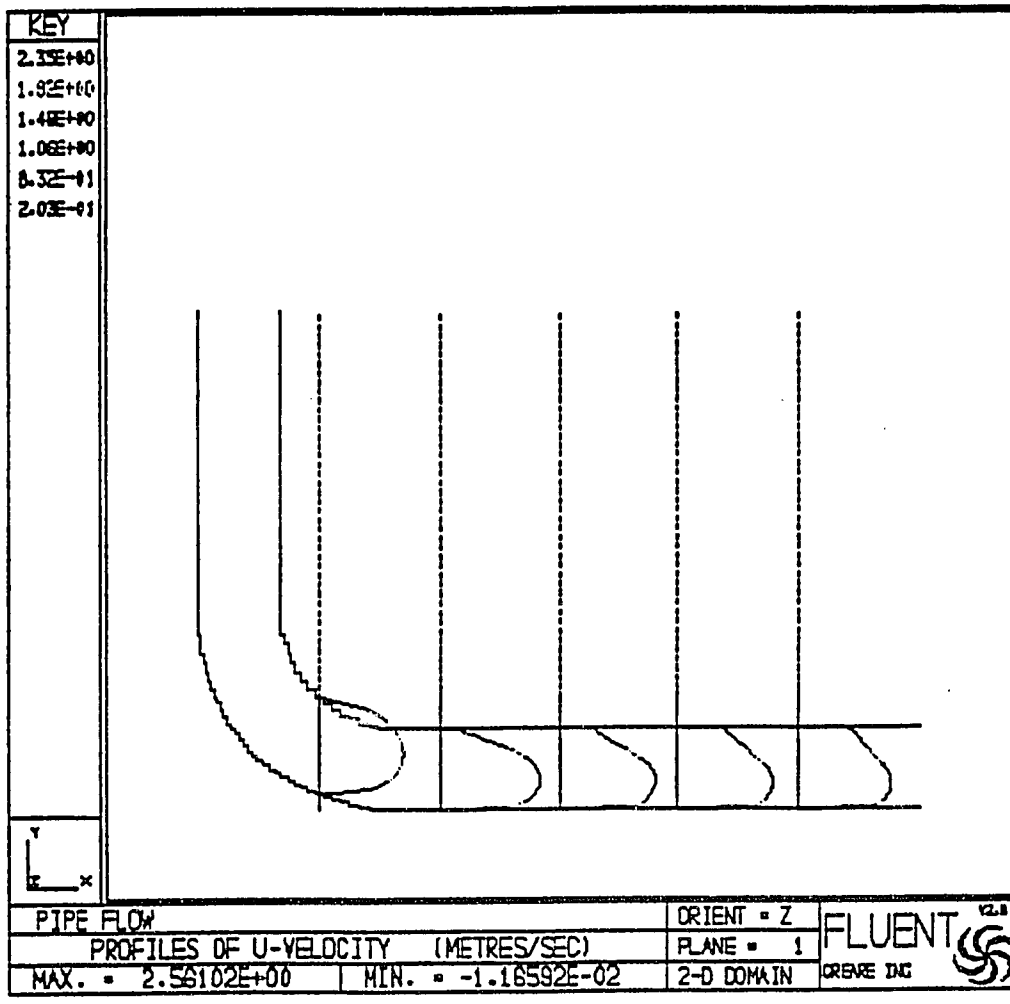

Figure 8. Streamwise Velocity Profiles From Two-Dimensional Model.

elbow could not be implemented because the conventional FLUENT was based on the Cartesian Coordinate (rectangular coordinate system) System. Hence the elbow was created with lot of stair steps at the boundaries, something which had an influence on the global picture of the flow. Addition of more and more nodes at the elbow resulted in the small step sizes, but steps could never be eliminated.

With the use of FLUENT/BFC, the above difficulty was eliminated. With the built in computer aided design (CAD), smooth curving was possible and the elbow could be implemented exactly. The model was developed using the preBFC module from FLUENT/BFC.

Geometry Definition

The BFC has menus in a treelike structure. Under the geometry setup menu in the preBFC module, geometry parameter like points, arcs, curves or surfaces can be created. Figures 9-11 illustrate the geometry description such as important points, curve and surface. In the development of geometry, the first point defined was the origin labelled 00 at coordinate (0,0,0). The first surface created was the inlet. A circular region in physical space was mapped to a rectangular in the computational space. Hence a circle had to be created with four curves which required four points in its circumference. The inlet of the pipe was depicted as circle which had a center point and four

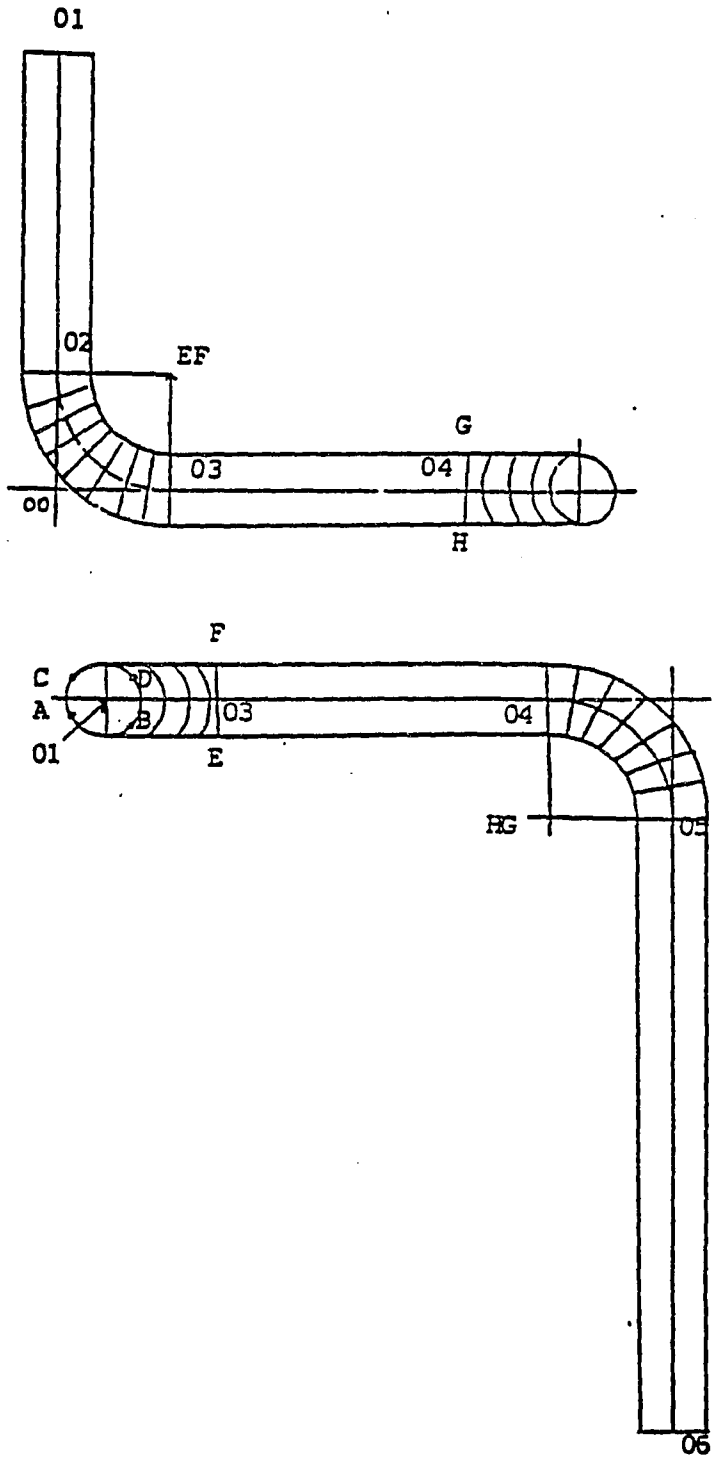

Figure 9. Important Points in the Geometry.

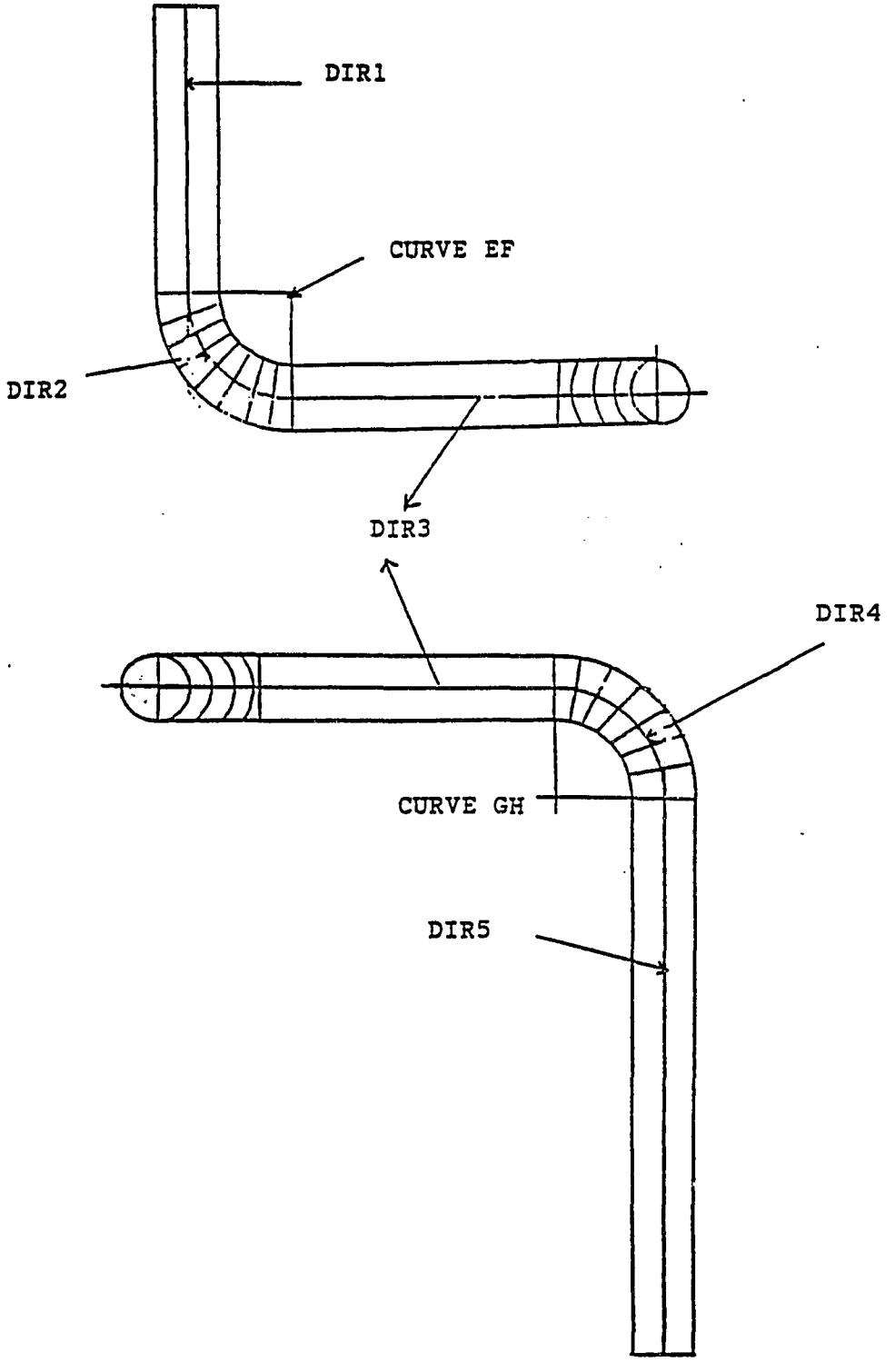

Figure 10. Important Curves in the Geometry.

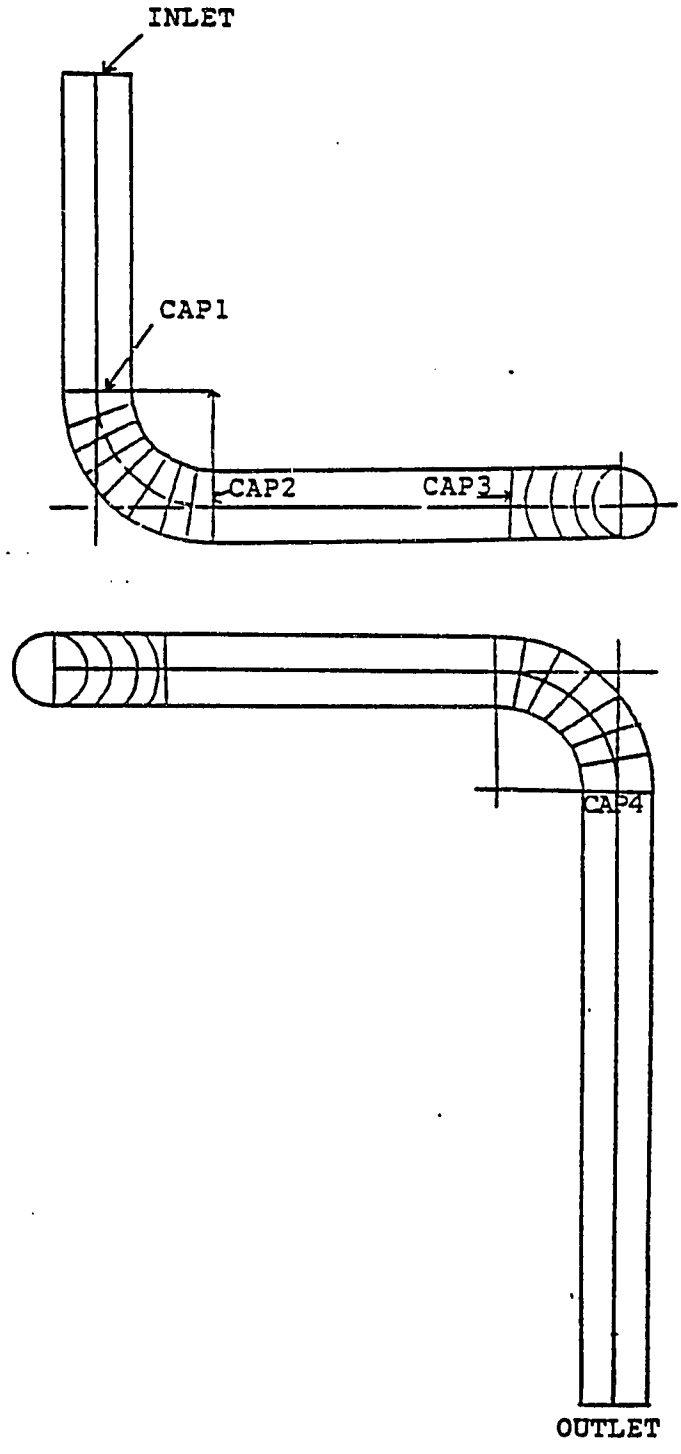

Figure 11. Important Surfaces in the Geometry.

more points in its circumference. The center point of the inlet 01 was created 25 diameters from the origin such that the fluid passing this long pipe would become fully developed when it reaches the elbow. Another point, such as A, was defined in the Z-direction at a distance equivalent to the radius of the pipe with the same X and Y coordinates as the origin. An arc of 90° was drawn using the center point and A. The arc ended in another point B located at the circumference of the pipe inlet. The same procedure was followed to make three more arcs each of 90°, thus creating points C, D, and E. Finally the points E and A were merged. All of the four arcs jointly made the inlet surface of the pipe.

The next step was to generate an inlet pipe section before the elbow. This was done by defining a point 02 at a distance of 25 diameters from point 01 in the Y direction. Both the points 01 and 02 were joined together with a curve named DIR1. This represented the center axis of the inlet pipe. Then the entire inlet section of the pipe was generated by sweeping the inlet surface along the directrix DIR1. Because the cylindrical body had to be mapped as a rectangular body in computational space, it was necessary to supply five labels for the additional surfaces that are created by the sweep operation. These surfaces were labelled as FRONT1, REAR1, LEFT1, RIGHT1 and CAP1. In addition, the orientation of the swept surfaces to the

directrix had to be specified whether FIXED or NORMAL. In this case, since DIR1 is a straight line, the orientation of the surface to the directrix had no effect.

The next step was to create the first 90° elbow section. This was generated by sweeping CAP1 through a 90° circular arc. To create a circular arc, a pivot axis had to be created. A pivot point E was created at 1.5 diameters distance in X and Y coordinates. Another pivot point F was created at the same distance as E in X and Y direction and with the distance equal to the radius of the pipe in Z direction. The points E and F were joined together to form the pivot curve EF. With the pivot curve defined, CREATE-ARC option was used to generate a 90° degree curve to be used as the directrix curve. The right hand rule convention was used for the sign of the angle; the angle specified here was -90°. The arc named as DIR2 created an end point called 03. Then, the 90° elbow section was generated by sweeping CAP1 in the direction of the directrix curve DIR2. Here the orientation was set to NORMAL so that the sweep surface CAP1 always remained perpendicular to the directrix DIR2. The five sides of the elbow created during the sweeping process were named FRONT2, REAR2, LEFT2, RIGHT2 and CAP2.

The third section of the pipeline, which was a straight section like the entrance section, was generated

by sweeping surface CAP2 along a straight line directrix DIR3. For the single elbow case, the pipe length after the elbow was 93 diameters. In double elbow cases, the distance between the elbow was varied between 5 and 15 diameter distances. The point 04 was defined at 93 diameters distance form the exit of the elbow. The points 03 and 04 were connected yielding the directrix curve DIR3. The straight section of the pipe was created by sweeping the surface CAP2 along the directrix curve DIR3. The surfaces created by this sweeping action were named as FRONT3, REAR3, BOTTOM3, TOP3 and OUTLET. For the double elbow case another elbow and a straight section were defined in the same way as above by taking into account of orientation of the curve. After these procedures, the geometry file were appropriately named and saved. Appendix B shows the log file (code) to develop the above geometry for a two elbow case with fifteen diameter spacing.

Grid Generation and Mapping

After the generation of the geometrical flow domain of the flow, a three-dimensional grid was generated within the domain. This process involves transformation of the physical domain (the real domain) to a computational domain (the transformed domain) since FLUENT/BFC solves the transport equations in curvilinear coordinates system. Establishing the correspondence between the physical domain

and the computational domain is the task of the mapping process. Figure 12 shows a geometry of a two elbow model in physical and computational space.

The first step in grid generation was to set the grid size and then map the boundaries of the geometry. In two elbow cases with 15 diameters spacing, the grid size was 157 X 11 X 11 in the X, Y and Z directions respectively. Thus the domain was made up of 18,997 computational cells. There were 21 surfaces to be mapped. When mapping a surface it is necessary to specify the i,j, and k indices of the three corner points of the surface. Upon mapping, the grid can be interpolated throughout the entire region. Table 1 shows the number of nodes assigned to each surface in each direction. Under this mapping process, the physical geometry and the physical grid were transformed into a corresponding computational grid for a rectangular region with uniform grid spacing. Figure 13 shows the finite difference grid at various cross-sections of the geometry. Figures in Appendix C present the cell types generated while developing the model and mapping. The cells at the outer boundary W_1 are of WALL type with zone number. Figure 44(p.141) is the first plane of the geometry in computational space which is inlet to the model. The cells in the interior are denoted by I_1 and represents cells with an inlet. Figure 45(p.142) depicts the a plane in the flow domain of the computational space. The cells

Table 1

Mapping of Nodes in 15 Diameters Spaced Double Elbow Model

SURFACE	I1	J1	K1	I2	J2	K2	I3	J3	K3
INLET	1	1	11	1	1	1	1	11	1
FRONT1	1	1	11	22	1	11	22	11	11
LEFT1	1	1	11	22	1	11	22	1	1
REAR1	1	1	1	22	1	1	22	11	1
RIGHT1	1	11	11	22	11	11	22	11	1
FRONT2	22	1	11	37	1	11	37	11	11
LEFT2	22	1	11	37	1	11	37	1	1
REAR2	22	1	1	37	1	1	37	11	1
RIGHT2	22	11	11	37	11	11	37	11	1
FRONT3	37	1	11	47	1	11	47	11	11
BOTTOM3	37	1	11	47	1	11	47	1	1
REAR3	37	1	1	47	1	1	47	11	1
TOP3	37	11	11	47	11	11	47	11	1
FRONT4	47	1	11	62	1	11	62	11	11
BOTTOM4	47	1	11	62	1	11	62	1	1
REAR4	47	1	1	62	1	1	62	11	1
TOP4	47	11	11	62	11	11	62	11	1
LEFT5	62	1	11	152	1	11	152	11	11
BOTTOM5	62	1	11	152	1	11	152	1	1
RIGHT5	62	1	1	152	1	1	152	11	1
TOP5	62	11	11	152	11	11	152	11	1

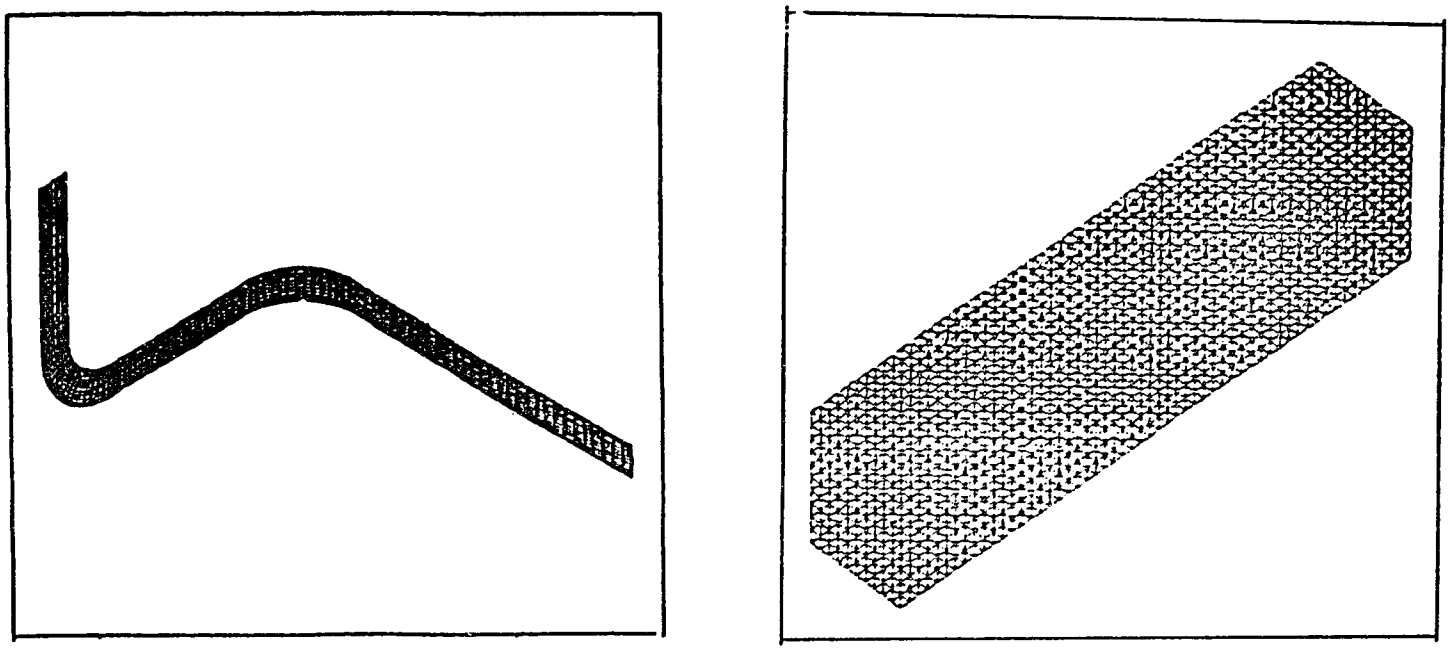

Figure 12. Fifteen Diameters Spaced Double Elbow Model at Different Domain: (a) Physical Domain; (b) Computational Domain.

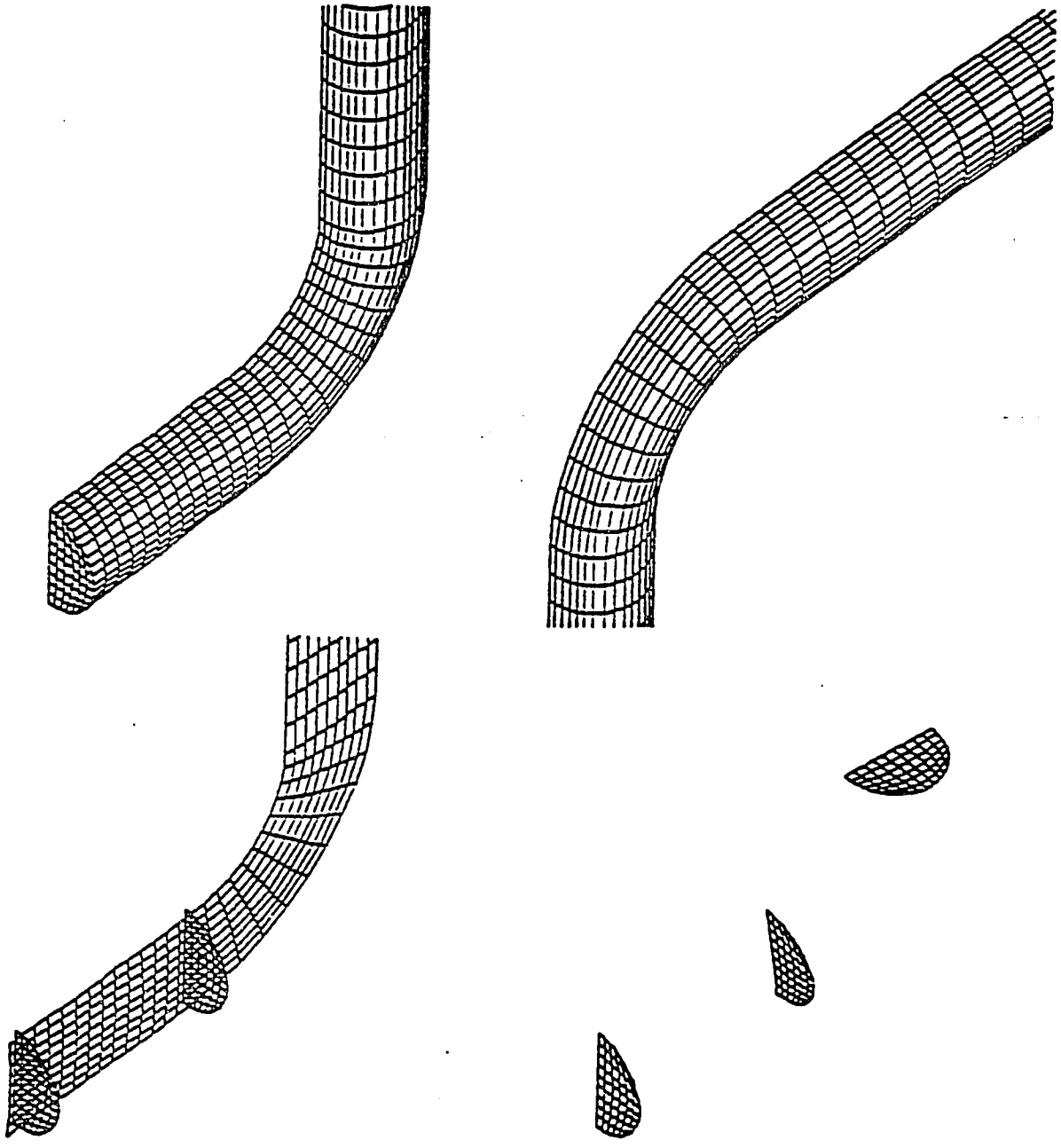

Figure 13. Finite Difference Grid at Various Cross Sections of the Geometry.

in the interior of the domain are all "live" cells denoted by ".". Figure 46(p.143) is the last plane of the geometry in the computational space and denotes an outlet. The cells in the interior of the domain are denoted by "o" which represents the outlet.

Defining Physical Properties and Boundary Conditions

Defining physical properties should precede setting the boundary conditions so that the correct equations are solved by the program. Fluid parameters like density and viscosity were specified here. In the "VISCOSITY" Table, the turbulent flow modeling option was switched on and then the inlet conditions were defined. Following are the some of the flow variables defined.

Density = 1000 kg/m^3

Viscosity = $9*10^{-4}$ kg/m.s

Velocity = 1.85 m/sec

Turbulent intensity = 5%

The computational solutions are based on the following assumptions:

1. The fluid is incompressible and Newtonian.
2. Walls are perfect and rigid.
3. No-slip conditions exist at the flow walls.
4. A fully developed turbulent profile is at the inlet of elbow.
5. No acceleration is present due to gravity.

The last step before quitting the preBFC program was to save the grid, physical properties, and boundary conditions in a case file.

Calculation of Flow Variables

For calculation, "solvBFC" module was used. Because the governing equations were highly non-linear, an iterative process was adopted. The number of iterations required to obtain a solution depended on the nature and the complexity of the flow field, the initial conditions, and the number of grid points used. For each variable such as velocity (U, V and W components) and pressure, the FLUENT gave a measure of the total error (residuals) in the mass continuity equation, summed for all computational cells of the domain. Residuals for each flow variable, which gave a measure of the magnitude of the correction made at each iteration, were normalized by dividing the residual from the second iteration. Normalized residuals of the order of 10^{-3} were considered adequate for representing a converged solution. The variables were checked after a few additional iterations to ensure that they did not change significantly.

After the calculations were completed and the convergence criteria satisfied, the results were saved in a data file. The data were examined by using postBFC module.

CHAPTER VII

RESULTS AND DISCUSSION

The aim of this investigation was to numerically investigate the turbulent pipe flow in single and double elbows as it relates to piping arrangements in the approach systems to papermachine headboxes. Although there have been guidelines established to allow selection of piping, knowledge of the effects of elbows is lacking. In particular, it is not known how far ahead of the tapered section of a headbox an elbow must be placed to avoid disturbing the uniformity of the flow delivered to the papermachine. Experiments to investigate these effects are tedious and time consuming. However, availability of CFD codes allows the performance of these experiments in a computer. This study utilizes the FLUENT/BFC code to set up models for studying elbow effects and for performing numerical experiments. In these experiments it is easy to change initial and/or boundary conditions to observe the effects on flow with the computer.

The present investigation studied the effects of single and double elbows in turbulent pipe flow fields. In the case of a single elbow, the fluid passes from vertical (positive Y-direction upward) to horizontal pipe (positive

X-direction is downstream). In double elbows the fluid turns around after the second elbow along the Z-direction if it is out-of-plane or flows upward in Y-direction if it is in-plane. The mean velocities in the X-, Y- and Z directions were denoted as U, V and W respectively. Figure 14 depicts the above coordinate system of the physical system.

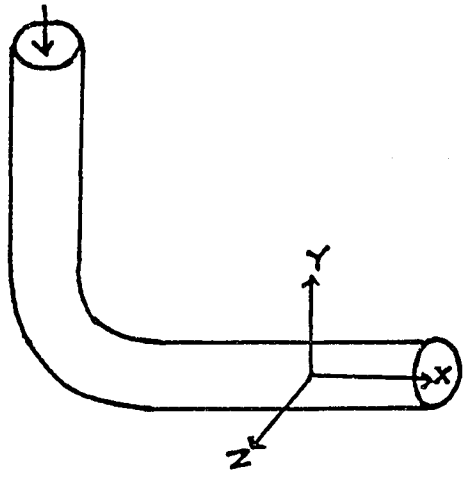

Figure 14. Elbow Orientation and Coordinate System.

Numerical results were taken after the solution was converged to a residual of 10^{-3} for velocity and pressure. A sensitivity analysis for the convergence of solution was made to determine the variation of the solution with the number of iterations. Table 2 shows the velocity profile at different iterations. There were 12 nodes placed across the cross section of the pipe from bottom to top which means that the pipe was divided into 12 parts.

Table 2

Sensitivity Analysis of Solution Convergence

Nodal Points	Number of Iterations 40	90	150	225	300	425
1	0.00	0.00	0.00	0.00	0.00	0.00
2	1.47	1.39	1.39	1.40	1.40	1.40
3	1.87	1.81	1.81	1.82	1.82	1.82
4	2.06	2.09	2.10	2.10	2.10	2.10
5	2.12	2.28	2.25	2.25	2.25	2.25
6	2.14	2.30	2.32	2.32	2.32	2.32
7	2.14	2.30	2.32	2.32	2.32	2.32
8	2.12	2.28	2.25	2.25	2.25	2.25
9	2.06	2.09	2.25	2.10	2.10	2.10
10	1.87	1.81	2.10	1.82	1.82	1.82
11	1.47	1.39	1.82	1.40	1.40	1.40
12	0.00	0.00	0.00	0.00	0.00	0.00
Length of Pipe Required to Get Fully Developed Flow in Diameters	28	49	65	66	67	67

Velocity values are given for each node in m/sec. With the increase in the number of iterations from 40 to 225, the length of pipe required to get fully developed flow also increases. Similarly, the numerical values of the velocity also changes up to 225 iterations. All of the

cases were run for 425 iterations to get stable results and the residuals were of the order of 10^{-03} for both the velocity and pressure. The required CPU time for 425 iterations was about 39 hours on a VAX/VMS-6520 computer. Results were compared to three significant digits. All the quantities were non-dimensionalized using the bulk average velocity to normalize velocities and the inner pipe diameter to normalize length.

The different computational models that were simulated are as follows.

(a) Single elbow:

  (i) Reynolds number 10^4

  (ii) Reynolds number 10^5

  (iii) Reynolds number 10^6

(b) Double elbows:

  (i) Out-of-plane

    (1) Five diameters spacing, Re 10^5

    (2) Ten diameters spacing, Re 10^5

    (3) Fifteen diameters spacing, Re 10^5

  (ii) In-plane

    (1) Five diameters spacing, Re 10^5

    (2) Fifteen diameters spacing, Re 10^5

Figure 15 presents different models with single and double elbows. All the above cases were run for long radius elbow (R = 1.5D) with water as fluid. Fluid with

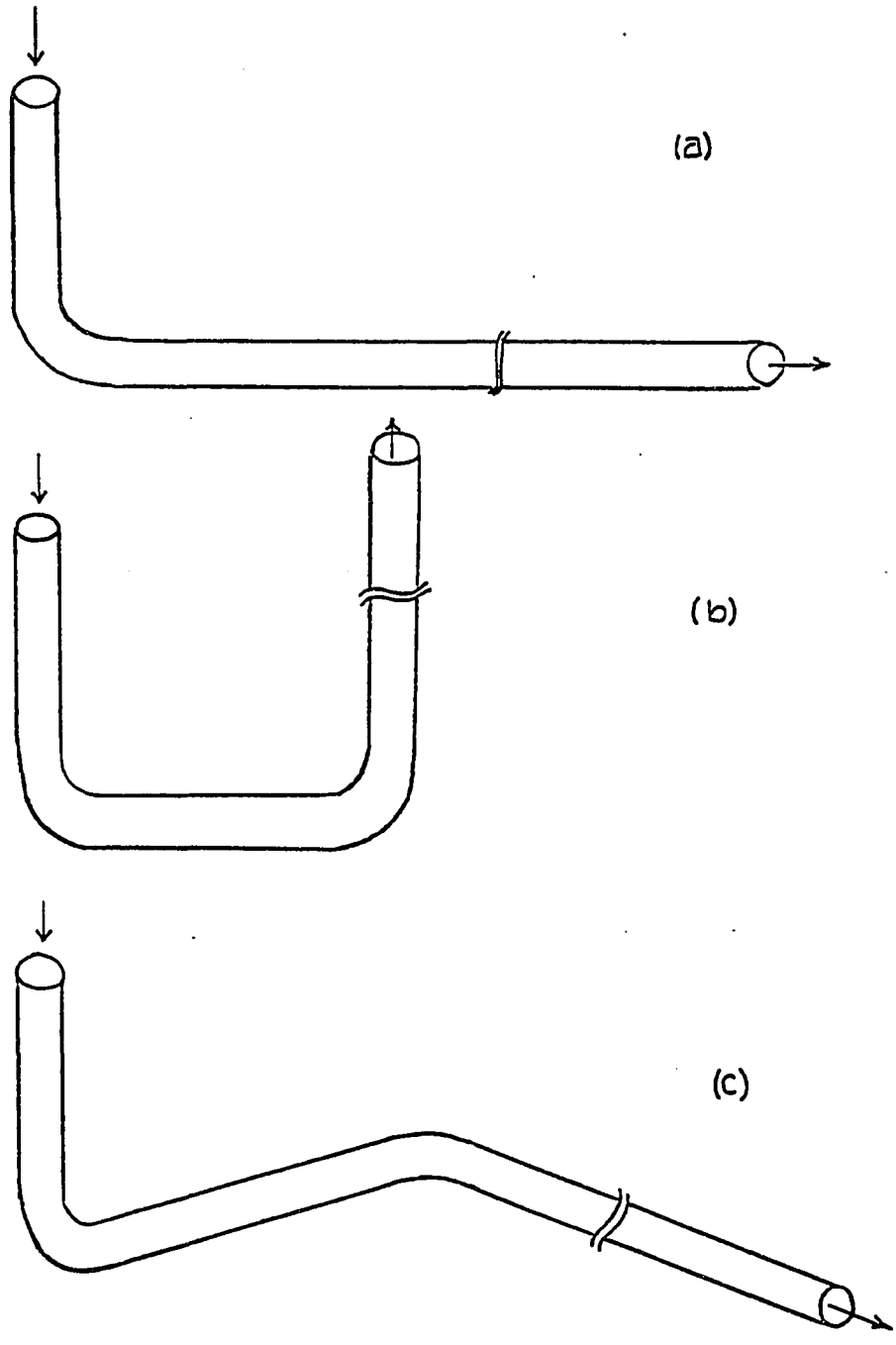

Figure 15. Geometry of Different Models: (a) Single Elbow (Front View); (b) Double Elbows, In-Plane (Front View); (c) Double Elbows, Out-of-Plane (Isometric).

uniform velocity enters the inlet of the pipe, which then flows through the 25 diameters long pipe and becomes fully developed when it reaches the elbow. All the double elbow cases (both out-of-plane and in-plane) and single elbow case with Reynolds number 10^5 were simulated with same initial conditions (like velocity, pressure, turbulence intensity, viscosity, and density) for the purpose of comparison. The single elbow case with $Re=10^6$ was simulated for mill conditions such as velocity and diameter of pipe. In all the cases, acceleration due to gravity was absent. Table 3 depicts the different physical parameters defined in the above models.

Table 3

Physical Parameters of Different Computational Models

Type	Re	Velocity m/sec
Single elbow	10^4	0.20
Single elbow	10^5	1.85
Single elbow (Pipe dia .6 m)	$2*10^6$	3.65
Double elbows 5 Diameters spacing out-of-plane	10^5	1.85
Double elbows 10 Diameters spacing out-of-plane	10^5	1.85

Table 3--Continued

Type	Re	Velocity m/sec
Double elbows 15 Diameters spacing out-of-plane	10^5	1.85
Double elbows 5 Diameters spacing in-plane	10^5	1.85
Double elbows 15 Diameters spacing in-plane	10^5	1.85

Results were analyzed for two purposes: (1) Model verification, and (2) Numerical experimentation with single and double elbows to determine the length of pipe required after single and double elbows to completely eliminate the elbow effects.

Model Verification

Verification of the numerical model was based on the comparison with experimental time-averaged velocity of streamwise and vertical components. Swirl angles were also calculated from the computational velocity components and were compared with experimental results. In addition, the numerical velocity profiles were compared with analytical solutions.

Comparison of Velocity Profiles With Experimental Results

Simulated results of both vertical and horizontal velocity components were compared with experimental results at different axial locations downstream of the elbow. These results are presented and compared with experimental profiles in Figures 16-19 at 1.5, 5.0 and 22 diameters distance from elbow. All lengths were normalized with respect to half pipe diameters and the results are presented in non-dimensionalized form. In the legends of these Figures, "L" is used to indicate long radius elbow. When this "L" is followed by a letter designation such as "-Y", it indicates a negative spatial displacement with respect to the origin of the computational coordinate system. In the experimental results, the dashed line is the corresponding power law profile for a smooth pipe. Overall, numerical results compared well with experimental measurements of velocity with the LDA. Both numerical and simulated results had the same trend.

To find the variation of the simulated results from the experimental results, both were drawn together on one graph. Figure 20 has both experimental and simulated results of streamwise velocity along horizontal axis. Figure 21 has both experimental and simulated results of streamwise velocity along vertical axis. At 1.5 and 5 diameters distance both experimental and simulated results

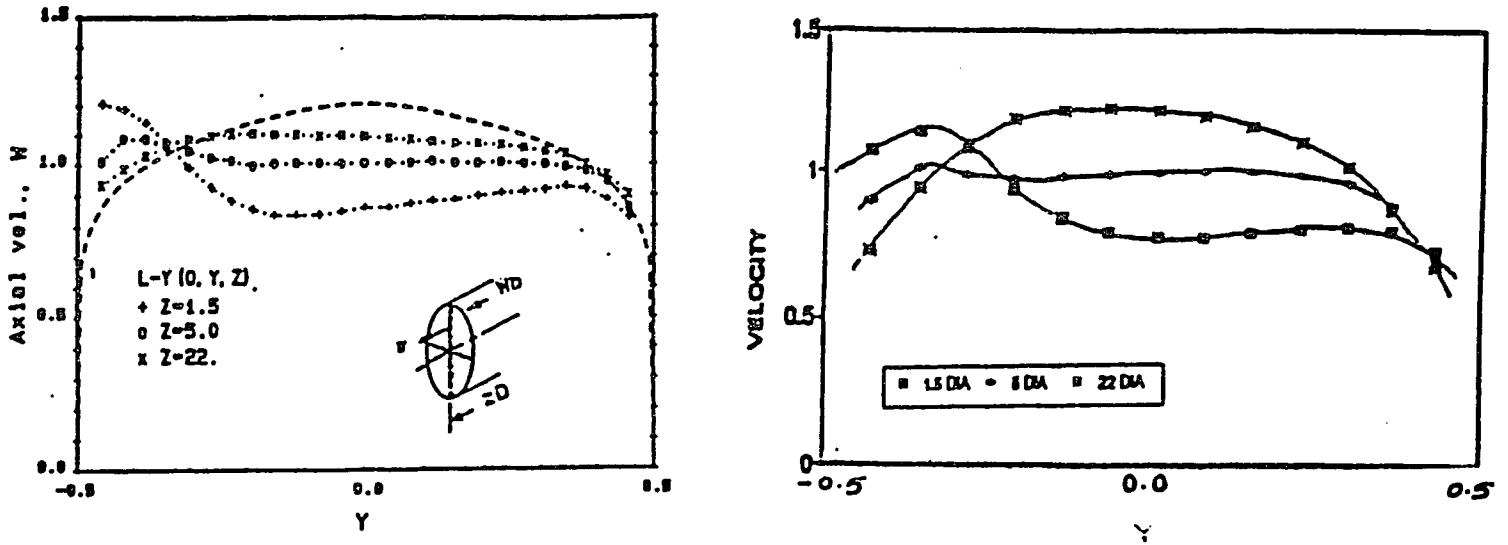

(a) (b)

Figure 16. Comparison of Streamwise Velocity Along Vertical Axis: (a) Experimental Results; (b) Simulated Results.

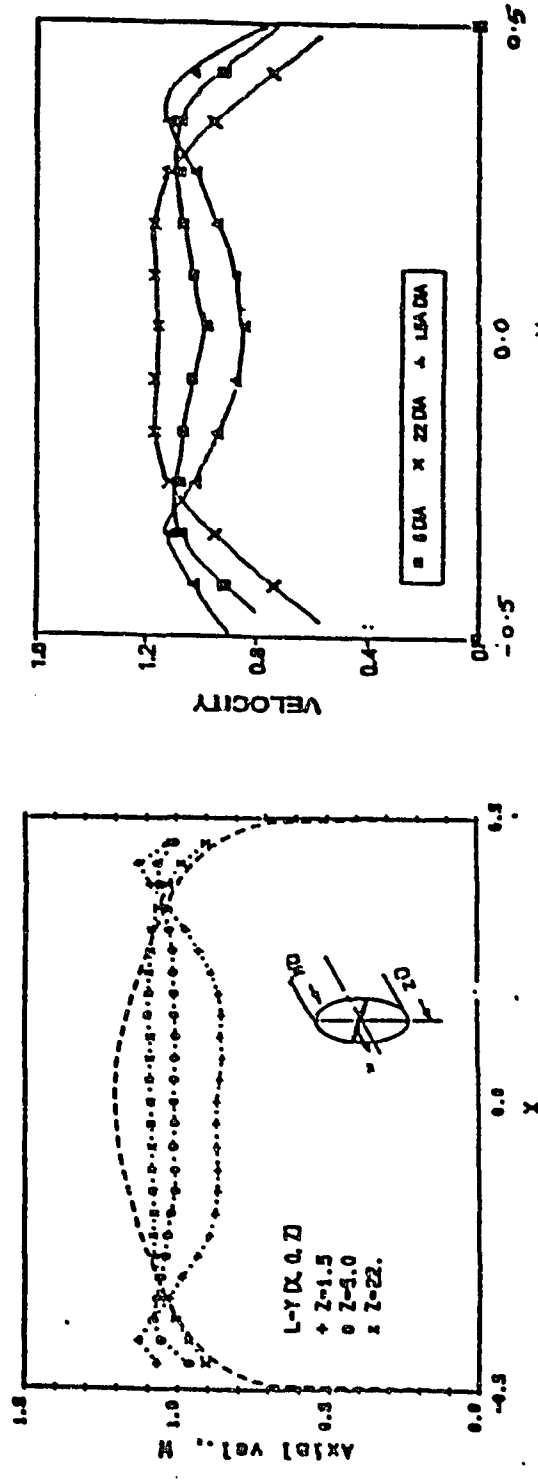

Figure 17. Comparison of Streamwise Velocity Along Horizontal Axis (a) Experimental Results; (b) Simulated Results.

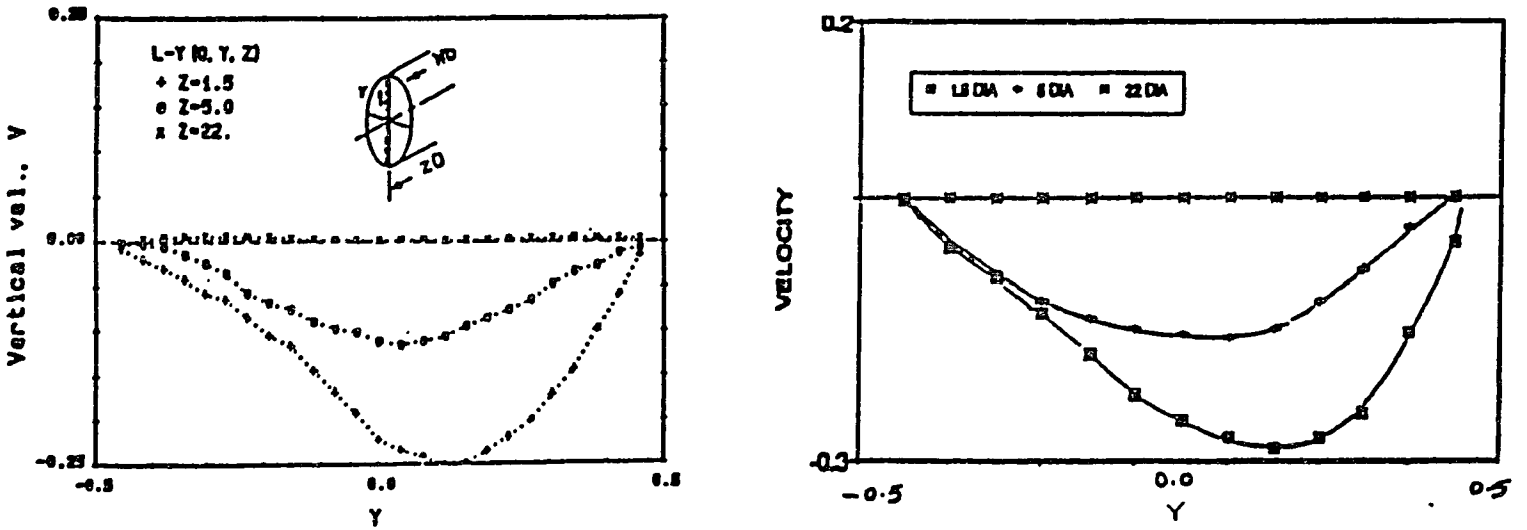

(a) (b)

Figure 18. Comparison of Vertical Velocity Along Vertical Axis: (a) Experimental Results; (b) Simulated Results.

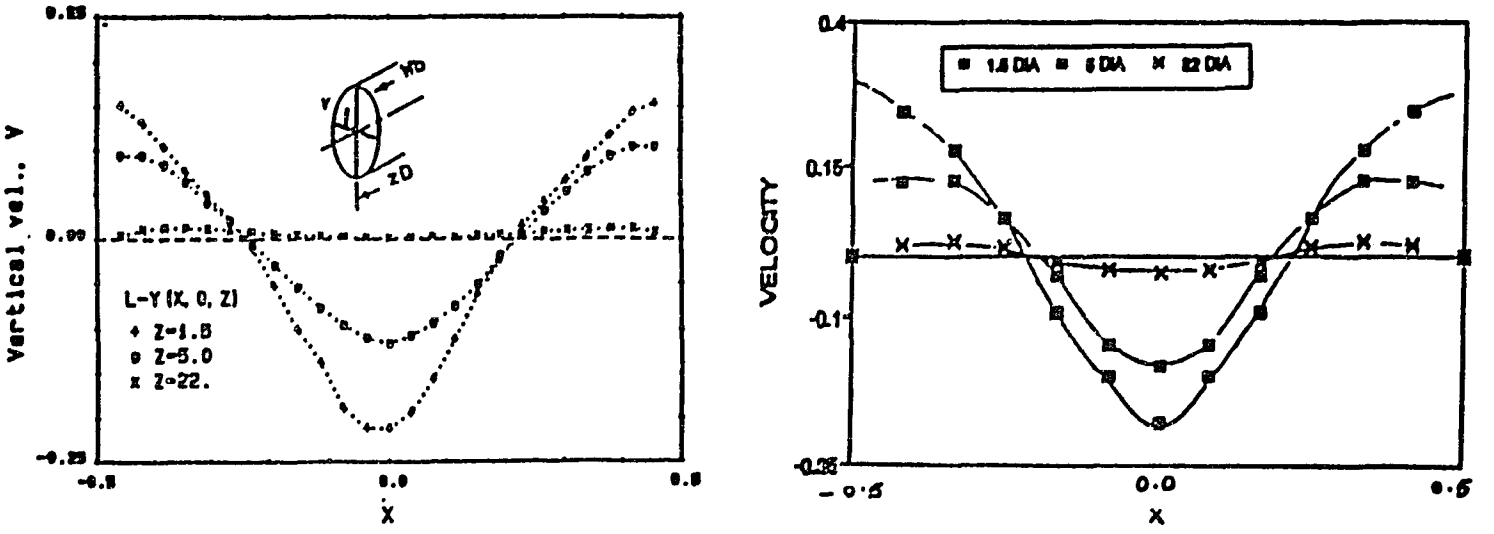

Figure 19. Comparison of Vertical Velocity Along Horizontal Axis: (a) Experimental Results; (b) Simulated Results.

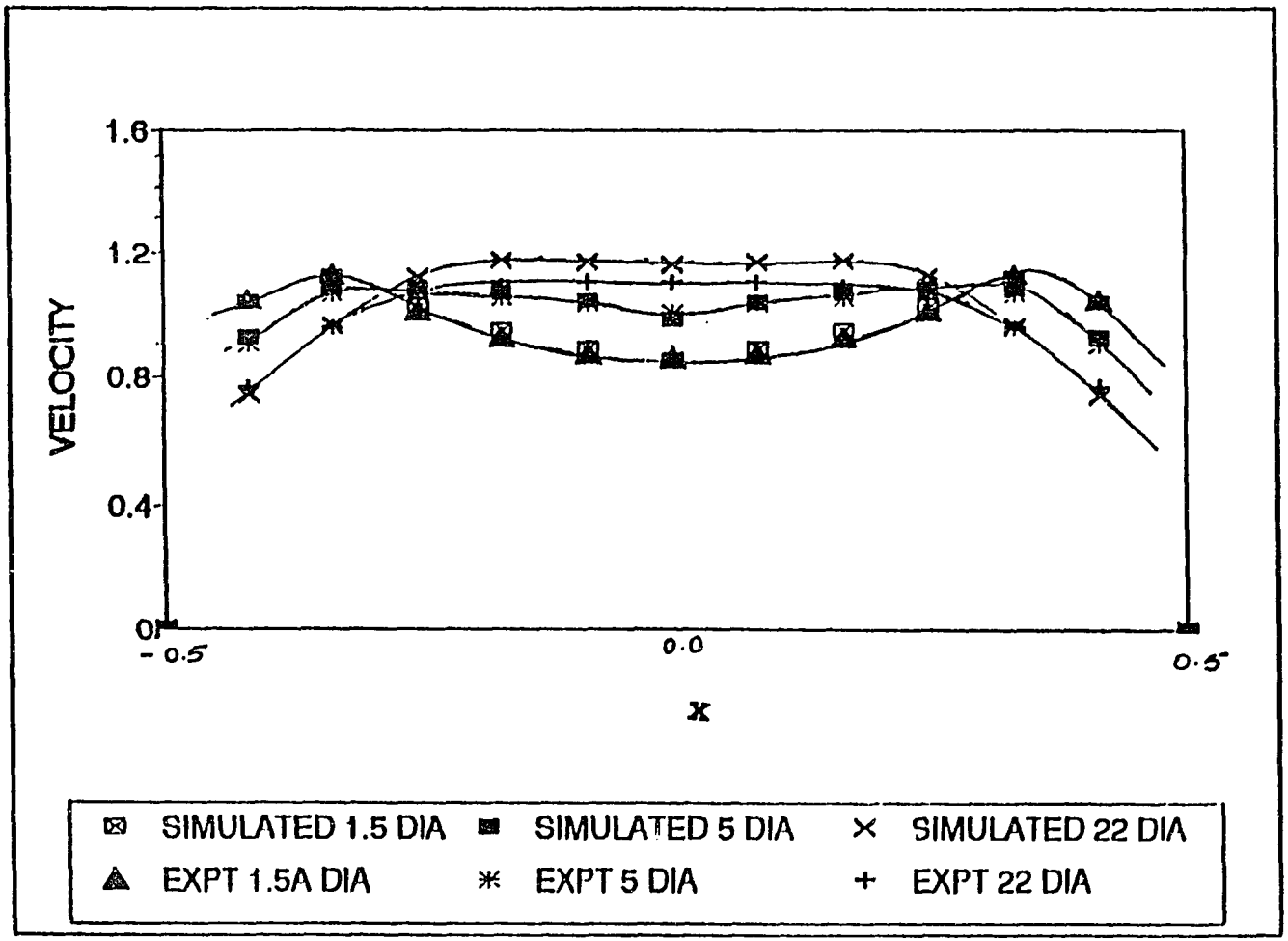

Figure 20. Comparison of Experimental and Simulated Velocity Profiles Along Horizontal Axis.

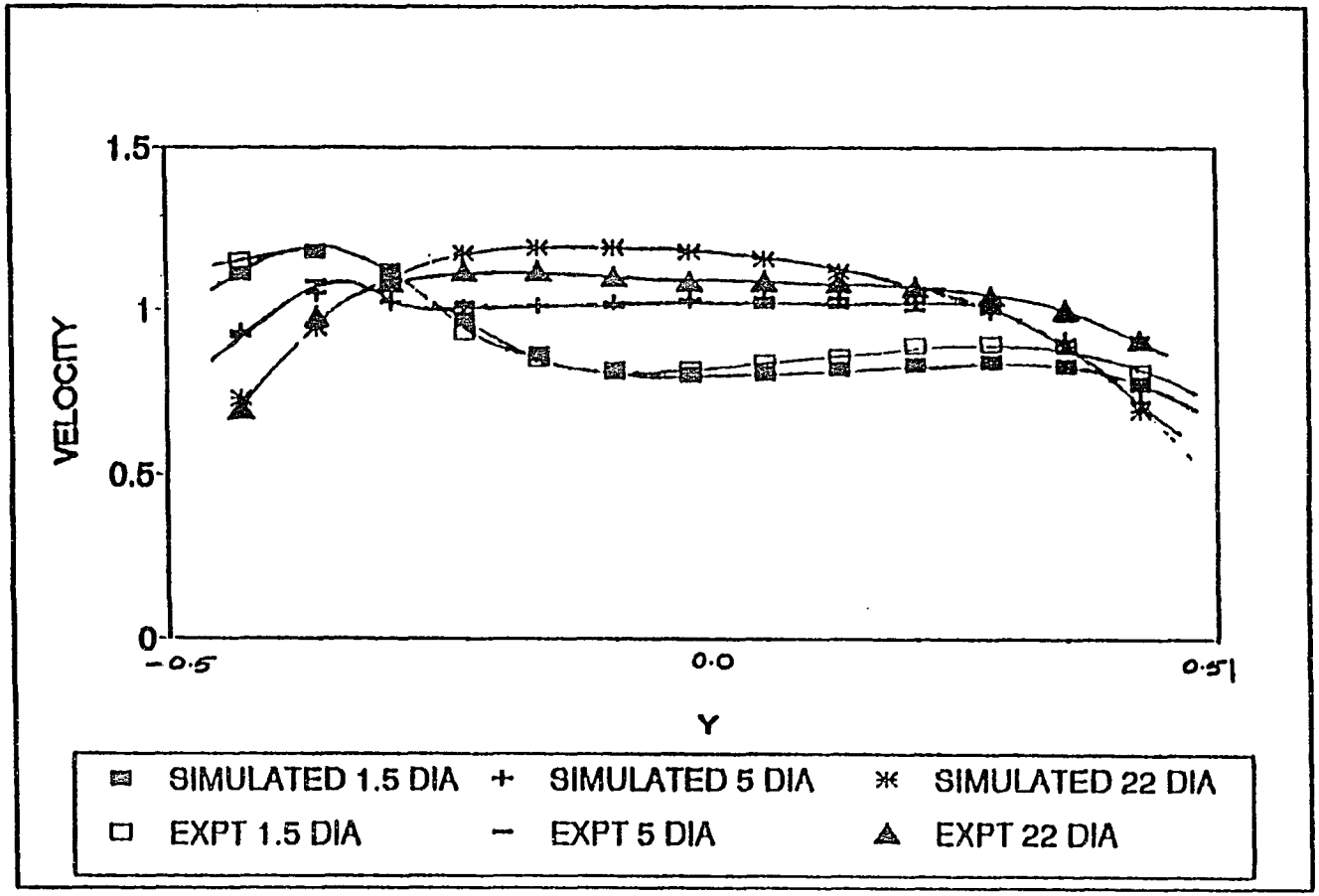

Figure 21. Comparison of Experimental and Simulated Velocity Profiles Along Vertical Axis.

were almost identical in both the cases. At 22 diameters distance, the magnitudes of the simulated results were higher than the experimental results. Along the horizontal axis, the deviation was about 6.14% more than experimental curve. Along the vertical axis, it varied by 5.98% more than the experimental curve at the middle. In Figure 21, the simulated results have lower values by about 4% than the experimental curve at the outer wall of the pipe at 1.5 diameters distance. However, the simulated curves in both the vertical and horizontal directions had almost the same trend as the experimental curve except that the value was high.

The following discussions compare the simulated profiles with the power law profiles which are fully developed theoretical turbulent profiles. This shows how the velocity distribution would be affected after the fluid passes through the elbow.

Figures 16 and 17 present profiles of the streamwise velocity along vertical and horizontal axis, respectively. The profile at the exit of the elbow, i.e., at 1.5 diameters distance downstream, was much affected and deviated from the power law profile by about 25-30%. Near the pipe wall there are layers of fluid which move faster than the power law values by about 5-18%. As the flow develops downstream these deviations diminish.

Figures 18 and 19 present the profiles of vertical

velocity along horizontal and vertical diameters, respectively. The experimental profiles for the fully developed flows are shown by the dashed line which is everywhere zero. Figure 18 indicates that at 1.5 diameters distance, the vertical velocities were 28% more near the wall and 26% lower at the center of the pipe than for the fully developed profile. At 5 diameters distance it was about 12% more near the wall and about 12% less at the middle of the pipe than the fully developed profile. At 22 diameters the profile was close to the fully developed profile which still varies by 1.5% more at the pipe and lower at the middle.

Figure 19 shows that the vertical velocity along the vertical diameters was negative everywhere. At 1.5 diameters distance the magnitude of the negative velocity is 27% less than the fully developed velocity. At 5 diameters distance it was lower by 14% at the middle than the fully developed velocity. At 22 diameters distance the velocity values almost matched with the fully developed profile. The vertical velocity components created by the elbow persisted for at least 22 diameters distance.

The elbow effect was quantified by the onset of secondary recirculations in the vicinity of the curved pipe section. The developed secondary flow across the cross-section of the pipe combined with the main flow and gave rise to a spiral flow.

The qualitative behavior of the secondary flow can be explained with the help of centrifugal force and the boundary layer theory. Figure 22 shows two counter rotating

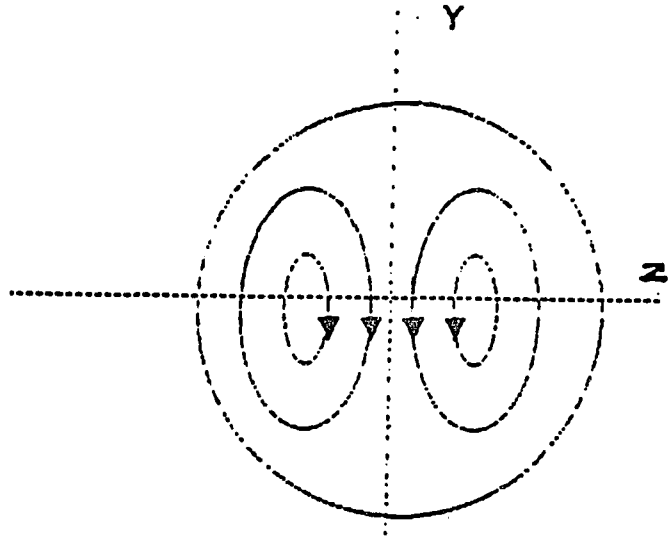

Figure 22. Counter Rotating Eddies at the Exit of an Elbow

flows at the exit of the elbow. Velocity at the centerline of the pipe is maximum and the velocity near the wall is retarded owing to the formation of a boundary layer. When the fluid turns at the elbow due to the centrifugal force, the pressure is high at the outer wall and low near the inner wall. Thus a circulating current is set up by these pressure differences and results in the formation of two eddies in opposite direction which when combined with the main flow gives rise to spiral motion. As the distance increases the intensity of the secondary flows decreases

and after 32 diameters the secondary flow completely disappears.

Table 4 and Figure 23 present the streamwise velocity profiles at different distances downstream of a single elbow along the vertical axis for the Reynolds number of 10^5. Fully developed flow is identified by its axi symmetric nature (velocity is same at all points at the circumference for any radius from the center within the pipe). In this case, it required about 67 diameters distance to completely eliminate the elbow effects. However, there was very little difference after 45 diameters distance.

Table 5 and Figure 24 show the velocity profile along the horizontal direction. The profiles along the horizontal direction were axisymmetric at all the distances from the elbow and they became fully developed before the profiles along the vertical axis. The profile along the horizontal direction had peak values at both the edge and lower value at the middle. As the distance increases, the velocity increased at the middle and decreased at the edges. This trend continues until the flow was fully developed. Along the horizontal axis, 60 diameters distance were needed whereas along the vertical axis 67 diameters distance were needed to get fully developed flow.

It is noteworthy that development of secondary flows near the exit from the elbow arises from three-dimensional effects. Thus, their existence cannot be predicted by a

Table 4

Numerical Values of Streamwise Velocity Along Vertical Axis After the Elbow, Single Elbow, Re 10^5

Node Points	Distance from Elbow in Diameters															
	0	1	2	3	4	5	6	7	8	9	10	11	13	15	17	19
1	0.00	0.00	0.00	0.00	0.00	0.00	0.00	0.00	0.00	0.00	0.00	0.00	0.00	0.00	0.00	0.00
2	1.96	2.07	1.99	1.87	1.80	1.78	1.79	1.80	1.82	1.83	1.83	1.83	1.82	1.80	1.77	1.75
3	2.06	2.10	1.99	1.90	1.88	1.91	1.96	2.01	2.06	2.10	2.14	2.17	2.22	2.26	2.28	2.29
4	2.00	1.93	1.82	1.79	1.83	1.90	1.96	2.02	2.07	2.11	2.15	2.18	2.24	2.29	2.33	2.36
5	1.88	1.76	1.69	1.73	1.82	1.90	1.97	2.03	2.07	2.11	2.15	2.17	2.22	2.26	2.30	2.33
6	1.73	1.62	1.63	1.72	1.82	1.91	1.98	2.03	2.07	2.11	2.14	2.16	2.20	2.24	2.27	2.30
7	1.58	1.52	1.60	1.73	1.84	1.92	1.98	2.03	2.07	2.10	2.12	2.14	2.18	2.20	2.23	2.25
8	1.46	1.47	1.60	1.75	1.85	1.93	1.98	2.02	2.05	2.08	2.10	2.11	2.14	2.15	2.17	2.18
9	1.39	1.46	1.62	1.76	1.86	1.92	1.96	1.99	2.02	2.03	2.05	2.06	2.07	2.07	2.07	2.07
10	1.38	1.48	1.63	1.76	1.83	1.88	1.91	1.93	1.94	1.95	1.95	1.95	1.94	1.93	1.92	1.91
11	1.42	1.49	1.61	1.70	1.74	1.76	1.77	1.76	1.74	1.73	1.71	1.70	1.67	1.66	1.64	1.64
12	1.44	1.42	1.46	1.47	1.45	1.43	1.41	1.39	1.37	1.36	1.34	1.33	1.31	1.29	1.28	1.27
13	0.00	0.00	0.00	0.00	0.00	0.00	0.00	0.00	0.00	0.00	0.00	0.00	0.00	0.00	0.00	0.00

Table 4--Continued

Node Points	Distance from Elbow in Diameters															
	21	24	27	30	33	36	39	42	45	48	51	54	57	61	67	75
1	0.00	0.00	0.00	0.00	0.00	0.00	0.00	0.00	0.00	0.00	0.00	0.00	0.00	0.00	0.00	0.00
2	1.73	1.69	1.66	1.63	1.59	1.56	1.53	1.50	1.48	1.46	1.45	1.45	1.44	1.44	1.44	1.44
3	2.29	2.26	2.20	2.13	2.07	2.02	1.98	1.94	1.91	1.89	1.88	1.87	1.87	1.86	1.86	1.86
4	2.40	2.45	2.48	2.47	2.43	2.37	2.31	2.26	2.22	2.19	2.17	2.16	2.16	2.16	2.16	2.16
5	2.37	2.41	2.46	2.50	2.52	2.50	2.47	2.42	2.39	2.36	2.34	2.33	2.33	2.32	2.32	2.32
6	2.32	2.36	2.40	2.43	2.46	2.48	2.48	2.47	2.45	2.43	2.42	2.42	2.41	2.41	2.41	2.41
7	2.26	2.29	2.31	2.34	2.37	2.40	2.42	2.43	2.44	2.44	2.44	2.44	2.44	2.44	2.44	2.44
8	2.18	2.19	2.21	2.23	2.26	2.29	2.32	2.35	2.37	2.39	2.40	2.40	2.41	2.41	2.41	2.41
9	2.07	2.07	2.08	2.10	2.12	2.16	2.20	2.23	2.26	2.29	2.30	2.31	2.32	2.32	2.32	2.32
10	1.90	1.90	1.91	1.92	1.95	1.98	2.02	2.06	2.09	2.12	2.13	2.14	2.15	2.15	2.16	2.16
11	1.63	1.63	1.64	1.66	1.68	1.71	1.75	1.78	1.81	1.83	1.85	1.85	1.86	1.86	1.86	1.86
12	1.27	1.27	1.27	1.28	1.30	1.33	1.35	1.38	1.40	1.42	1.43	1.44	1.44	1.44	1.44	1.44
13	0.00	0.00	0.00	0.00	0.00	0.00	0.00	0.00	0.00	0.00	0.00	0.00	0.00	0.00	0.00	0.00

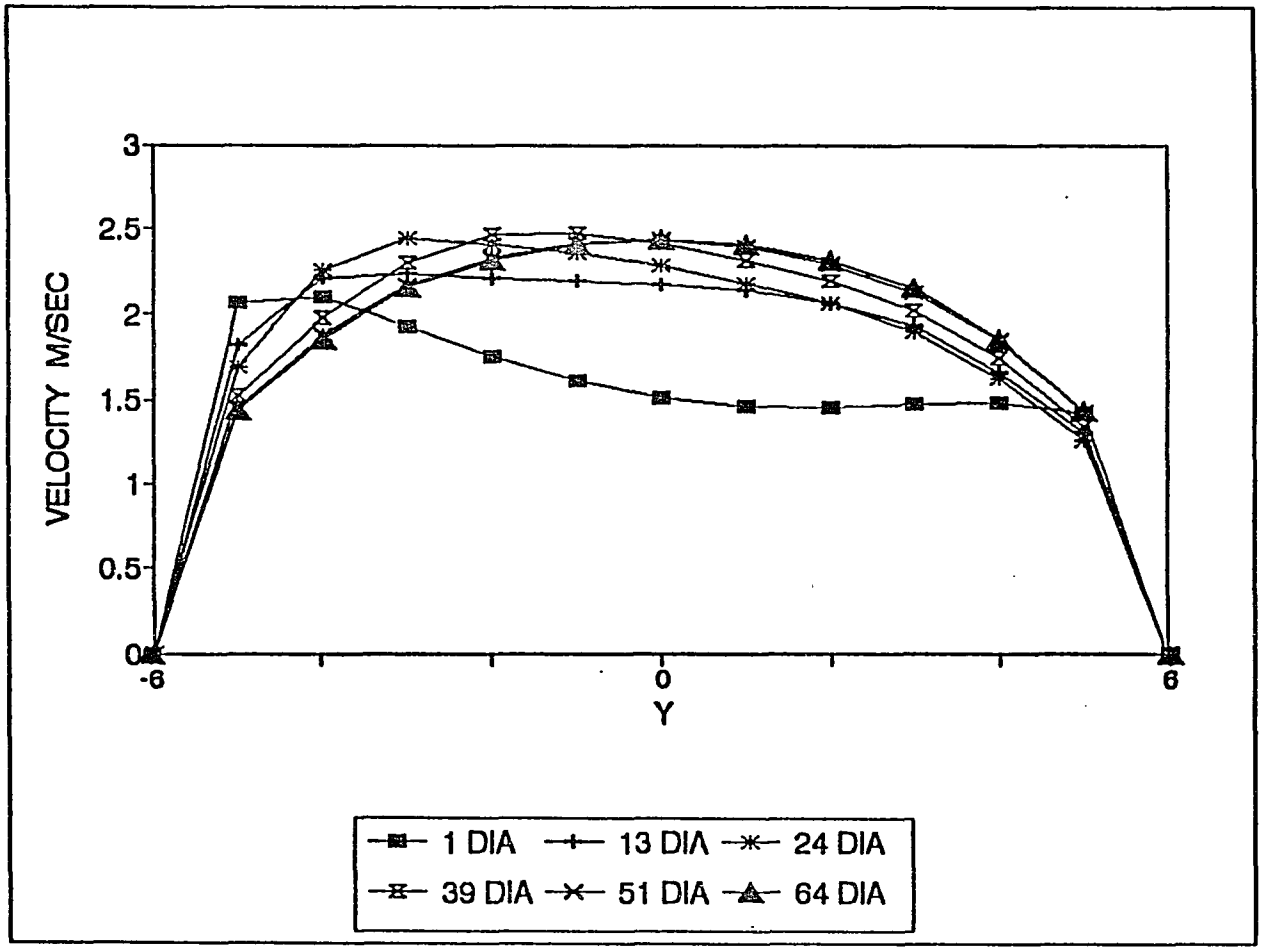

Figure 23. Streamwise Velocity Profiles Along Vertical Axis, Single Elbow, Re 10^5.

Table 5

Numerical Values of Velocity for Single Elbow Case Along Horizontal Axis, Re 10^5

Nodes	1	10	25	40	60
1	0.00	0.00	0.00	0.00	0.00
2	1.97	1.54	1.42	1.41	1.40
3	2.09	1.95	1.86	1.83	1.82
4	2.00	2.12	2.19	2.12	2.10
5	1.81	2.13	2.27	2.28	2.25
6	1.59	2.05	2.25	2.34	2.32
7	1.59	2.05	2.25	2.34	2.32
8	1.81	2.13	2.27	2.28	2.25
9	2.00	2.12	2.19	2.12	2.10
10	2.09	1.95	1.86	1.83	1.82
11	1.97	1.54	1.42	1.41	1.40
12	0.00	0.00	0.00	0.00	0.00

two-dimensional model such as the one developed with the original FLUENT code. Three dimensionality, however, can be more clearly demonstrated by considering the swirl angle of flow.

Comparison of Swirl Angle With Experimental Results

Swirl angle is a measure of the degree of flow relative to the stream direction which was calculated from

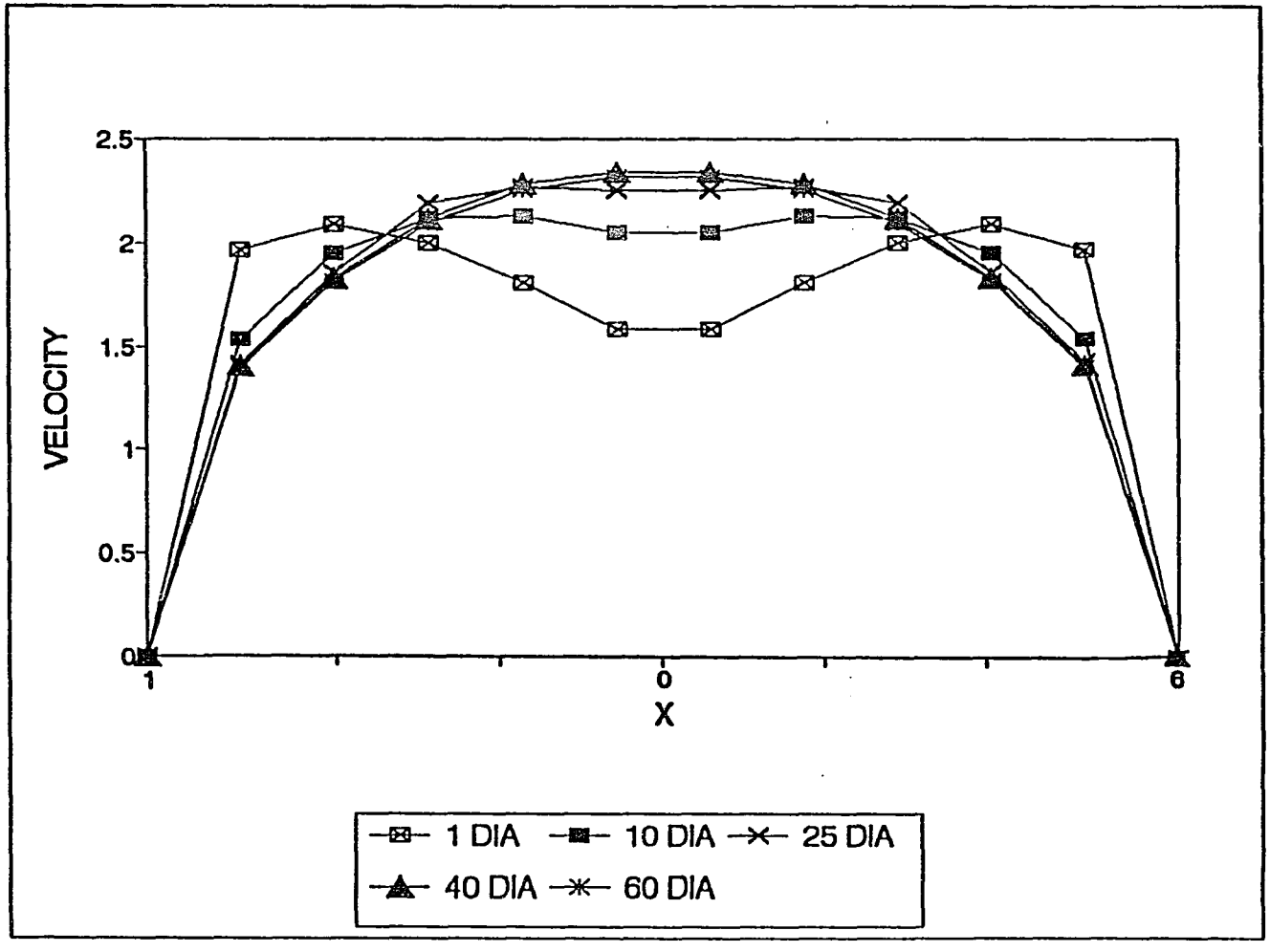

Figure 24. Streamwise Velocity Profiles Along Horizontal Axis, Single Elbow, Re 10^5.

numerical results using the relation O = arctan(V/U), where V is the vertical and U is the streamwise velocity components, respectively.

Figures 25 and 26 compare the numerical and experimental results of swirl angle at three different axial locations. The simulated results agree qualitatively with experimental results and both sets of data have the same trend. As in the case of the velocity profiles, numerical experiments (Figures 25 and 26) overestimate the swirl angles measured in physical experiments. At 1.5 diameters distance, the simulated angles were higher than the experimental results by 6 to 7% both along vertical and horizontal axes. These differences increase to 11 to 12% at five-diameters distance and dropped again to 7 to 8% at 22 diameters distance.

At the most downstream location, the swirl angle profiles from both numerical and experimental results were qualitatively closer to each other. At that point, the values of the swirl angle were almost zero. It can be noted that the swirl angle distribution more closely approximated the mean vertical velocity distribution. The profile along the horizontal axis was symmetrical about the center of the pipe which did not happen along the vertical axis. The results indicated that skew angle levels for Re 10^5 reached -14° along the pipe centerline. Subsequent profiles showed that these extreme levels of swirl angle at

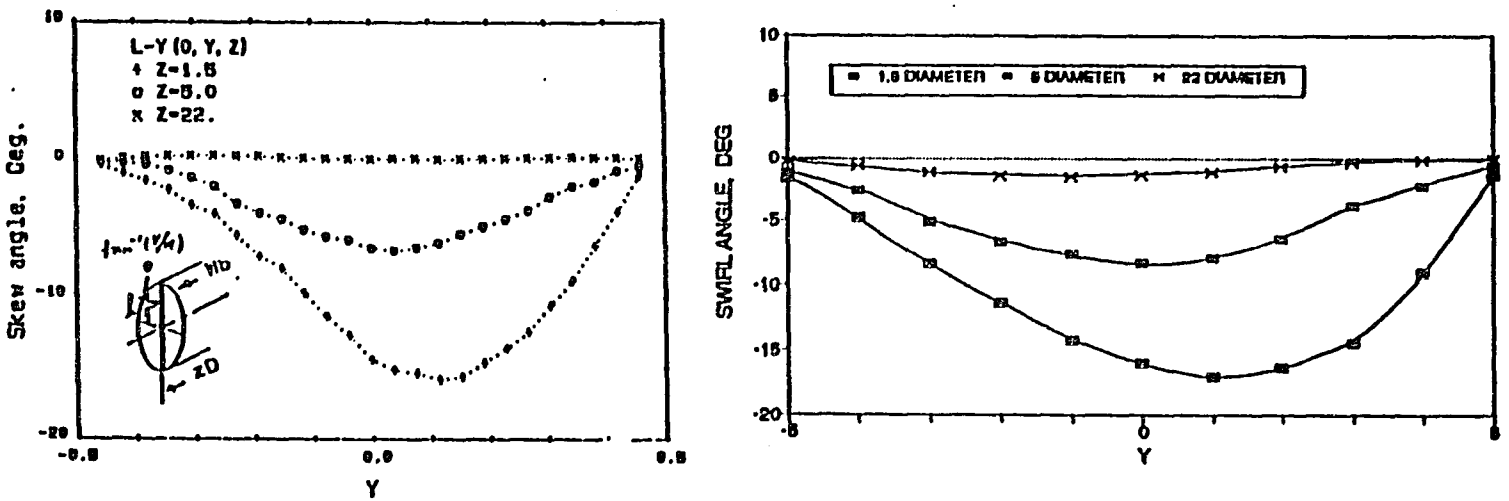

Figure 25. Comparison of Experimental and Simulated Swirl Angle Along Vertical Axis: (a) Experimental Swirl Angle; (b) Simulated Swirl Angle.

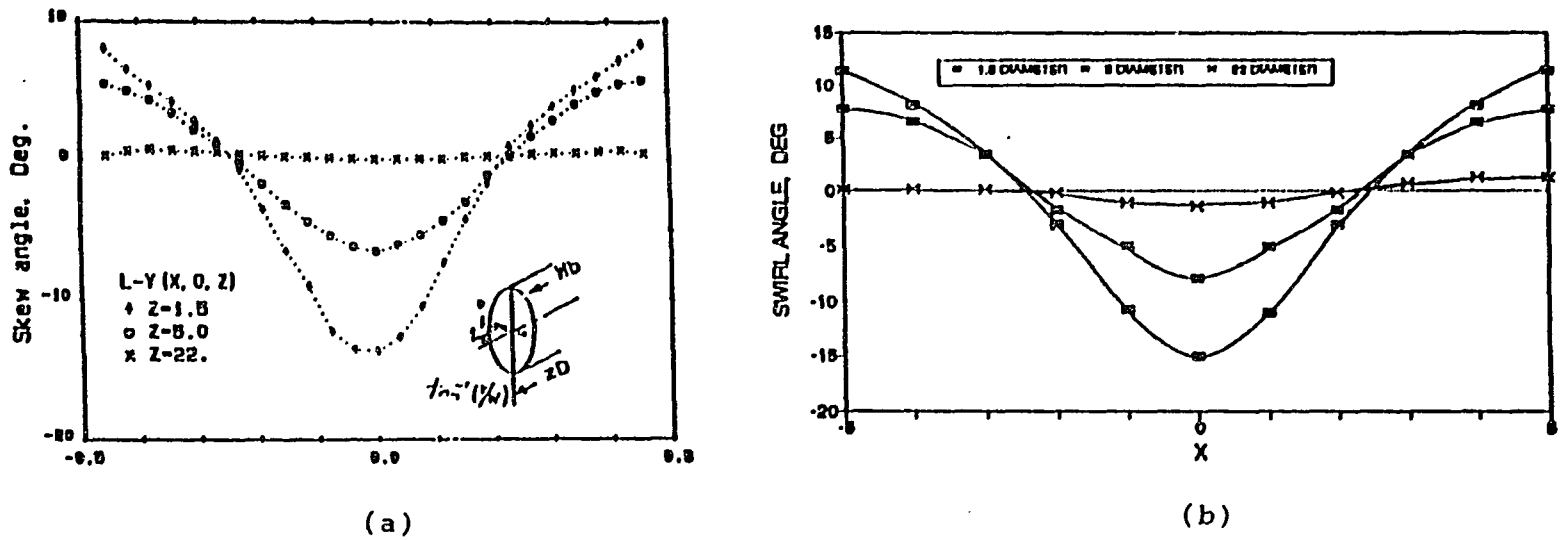

(a) (b)

Figure 26. Comparison of Experimental and Simulated Swirl Angle Along Horizontal Axis: (a) Experimental Swirl Angle; (b) Simulated Swirl Angle.

the pipe centerline rapidly diminished to about 0° after 22 diameters distance.

Comparison with Analytical Solutions

The simulated results were qualitatively in good agreement with the analytical solutions. The analytical solutions indicated that, at close proximity to the elbow downstream, there was a pressure gradient across the cross section of the pipe. This originated from the differential centrifugal forces acting upon the fluid element in the curved streamlines of the flow inside the elbow. In the elbow the pressure was low at the inner wall and hence the velocity was high. At the exit of the elbow the situation was reverse, i.e., the velocity was high at the outer wall and low at the inner wall (10). This can be illustrated in the numerical profiles appearing on Figure 27. Quantitatively, however, the numerical results overestimated the strength of the flow downstream of the elbow.

The reasons for the deviation of the simulated results are unclear. Possible causes may be the following: The numerical solution was solved based on a perfectly smooth pipe walls while the physical walls had some roughness. With increasing roughness, the velocity profile will be flater. Since in experimental pipe had roughness, the experimental profile are flater than the simulated profile. Another reason could be due to the turbulent intensity

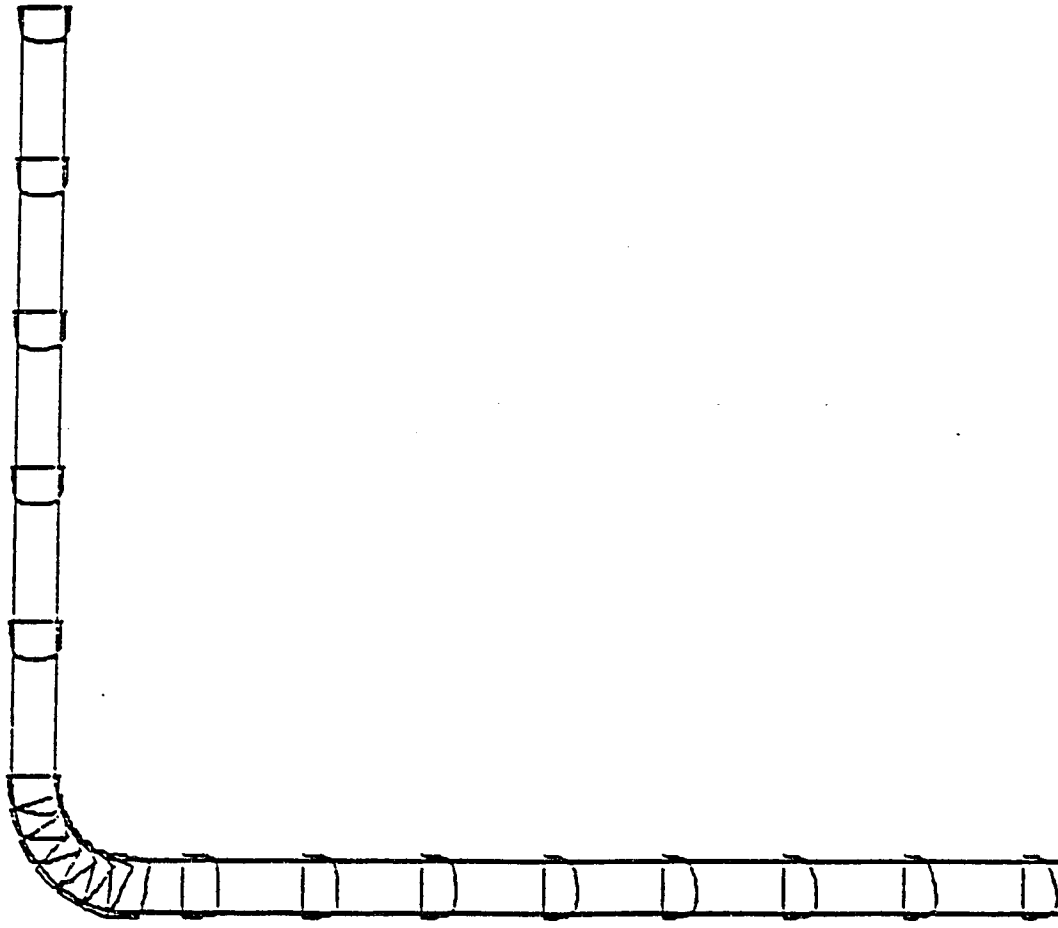

Figure 27. Profiles of Velocity Magnitude Before and After an Elbow.

which was not monitored during experiments by Yeh and Mattingly (11). For numerical simulation turbulent intensity was assumed to be 5% (22). The turbulent intensity, which is the square root of the mean square of the fluctuating velocity, is an important variable in predicting the flow field in the geometry domain of interest. Since FLUENT/BFC is overestimating the flow field, the assumed turbulent intensity may be higher than that of the experiment. Other reasons could be due to the large number of computational cells in the flow field and more iterations which would result in round-off error.

Flow separation at the inner wall could not be seen both in experiments and in simulation. This might be due to the fact that at this high Reynolds number the boundary layer was thin. Also the velocity in the viscous sublayer was high enough to be turblent. From Figure 23, it can be seen that the velocity near the inner wall is about 1.2 m/sec which shows that the flow is turbulent near the inner wall. However, the fluid velocity at the inner wall is less by about 41% than the at the outer wall.

Effect of Elbows on Pressure Profiles

Table 6 and Figure 28 present the pressure profiles across an elbow. The pressure was high at the outerwall and low at the inner wall, because of the centrifugal force. This variation across the cross direction is not

Table 6

Pressure Values at the Elbow, Re 10^5

	ELBOW ENTRANCE	NODE 1	NODE 2	NODE 3	NODE 4	NODE 5
13	-4.38E+02	-1.35E+03	-1.55E+03	-1.64E+03	-1.67E+03	-1.64E+03
12	-4.38E+02	-1.35E+03	-1.55E+03	-1.64E+03	-1.67E+03	-1.64E+03
11	-4.35E+02	-1.18E+03	-1.32E+03	-1.39E+03	-1.42E+03	-1.42E+03
10	-4.30E+02	-9.81E+02	-1.07E+03	-1.12E+03	-1.15E+03	-1.15E+03
9	-4.20E+02	-7.65E+02	-8.21E+02	-8.41E+02	-8.55E+02	-8.55E+02
8	-4.08E+02	-5.57E+02	-5.80E+02	-5.75E+02	-5.72E+02	-5.72E+02
7	-3.95E+02	-3.68E+02	-3.60E+02	-3.31E+02	-3.09E+02	-3.09E+02
6	-3.82E+00	-2.08E+02	-1.70E+02	-1.19E+02	-7.76E+01	-7.76E+01
5	-3.70E+00	-8.07E+01	-1.38E+01	5.57E+01	1.14E+02	1.14E+02
4	-3.62E+00	1.29E+01	1.05E+02	1.89E+02	2.62E+02	2.62E+02
3	-3.57E+00	7.41E+01	1.86E+02	2.80E+02	3.64E+02	3.64E+02
2	-3.55E+00	1.08E+02	2.33E+02	3.33E+02	4.25E+02	4.25E+02
1	-3.55E+00	1.08E+02	2.33E+02	3.33E+02	4.25E+02	4.25E+02

	NODE 7	NODE 9	NODE 11	NODE 13	NODE 15	ELBOW EXIT
13	-1.56E+03	-1.40E+03	-1.20E+03	-1.02E+03	-7.74E+02	-2.85E+02
12	-1.56E+03	-1.40E+03	-1.20E+03	-1.02E+03	-7.74E+02	-2.85E+02
11	-1.40E+03	-1.32E+03	-1.22E+03	-1.08E+03	-8.44E+02	-3.55E+02
10	-1.16E+03	-1.15E+03	-1.12E+03	-1.04E+03	-8.70E+02	-4.53E+02
9	-8.73E+02	-8.84E+02	-8.85E+02	-8.52E+02	-7.49E+02	-5.01E+02
8	-5.74E+02	-5.80E+02	-5.90E+02	-5.84E+02	-5.36E+02	-4.76E+02
7	-2.84E+02	-2.73E+02	-2.76E+02	-2.84E+02	-2.84E+02	-4.02E+02
6	-2.09E+01	1.74E+01	3.17E+01	1.99E+01	-2.55E+01	-3.04E+02
5	2.04E+02	2.73E+02	3.11E+02	3.07E+02	2.25E+02	-1.99E+02
4	3.81E+02	4.82E+02	5.46E+02	5.61E+02	4.59E+02	-9.75E+01
3	5.06E+02	6.35E+02	7.23E+02	7.63E+02	6.60E+02	-1.30E+01
2	5.89E+02	7.46E+02	8.59E+02	9.26E+02	8.31E+02	4.53E+01
1	5.89E+02	7.46E+02	8.59E+02	9.26E+02	8.31E+02	4.53E+01

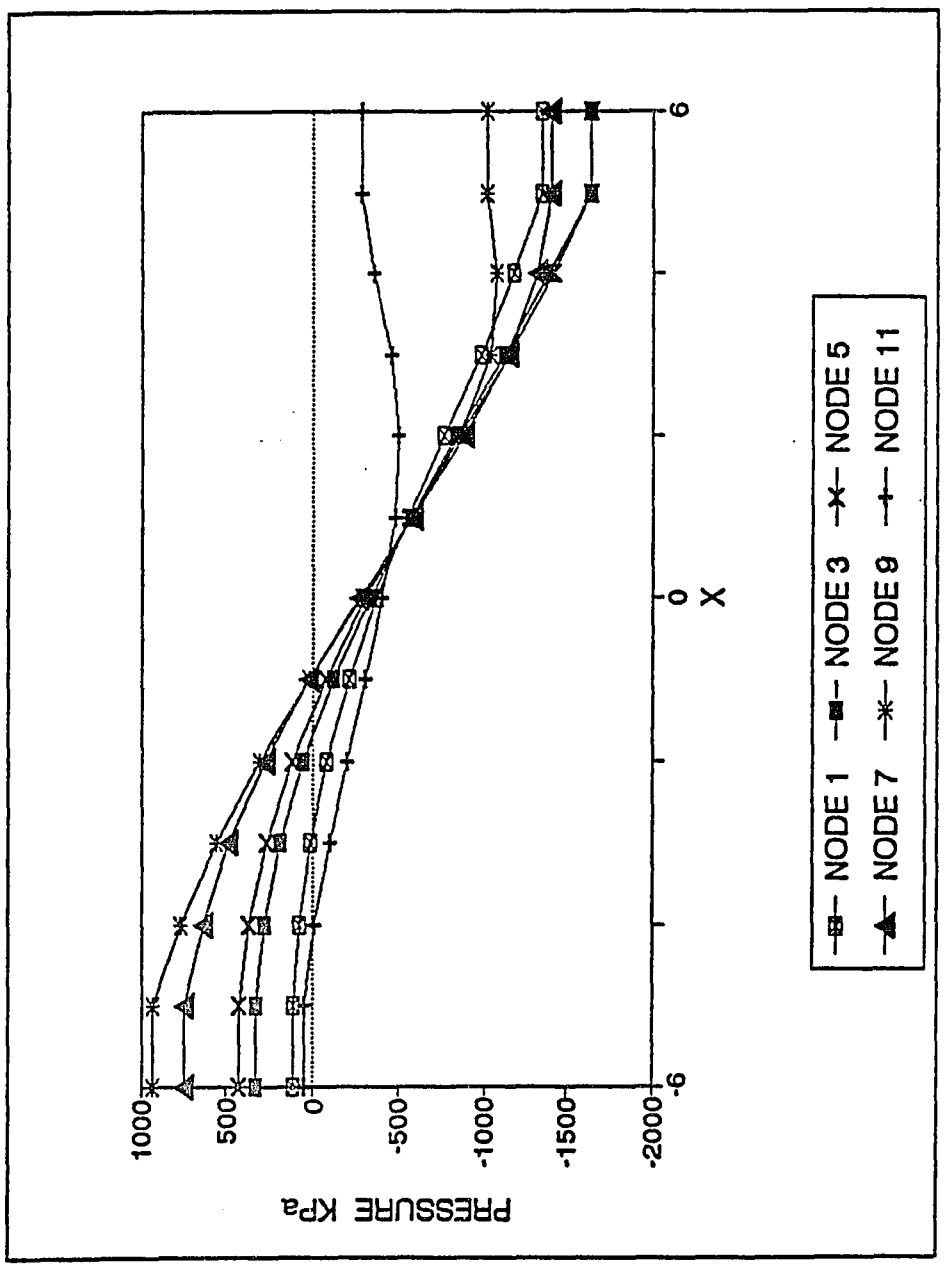

Figure 28. Pressure Profile Across an Elbow, Re 10^5.

only present inside the elbow but also persists downstream of the elbow for a considerable distance. The values listed in the table are not the exact values of pressure at the node points. The exact pressure at a particular node can be calculated by algebraic summation of these values and the reference pressure. With increasing distance, the pressure gradually diminished at the outer wall and increases at the inner wall. After about 34 diameters, the pressure across the pipe became uniform. With a further increase of distance, the pressure decreased uniformly across the pipe. In all the cases of either single or double elbows (both in-plane and out-of-plane) the effects of elbow lasted up to 33-34 diameters. An exception was the single elbow case with Reynold number 10^4 which needed only 29 diameters. Here it can be seen that the presence of two elbows had no effect on the final pressure profile.

Numerical Experiments

Overview

Computational models of single and double elbows were developed to find the length of the pipe required to completely eliminate the elbow effects. Single elbow cases were simulated at three different Reynolds numbers (10^4, 10^5, and 10^6) to find out the effect of elbow. In two elbow cases, the second elbow was placed at different distances

from the first elbow to find out the optimum distance needed between the two elbows and downstream of the second elbow. Since it is possible to have the second elbow at two different planes computational models of both in-plane and out-of-plane were developed. In the double elbow case, the second elbow was placed after 5, 10, and 15 diameters distance from the first elbow in the out-of-plane type and 5 and 15 diameters distance for the in-plane type. All the double elbow cases were simulated at the Reynolds number of 10^5 without considering gravity forces. In the single elbow case, the fluid flowed from the negative Y-direction to the positive X-direction. In out-of-plane, double elbow case, the fluid flowed from negative the Y-direction to the positive X-direction and then finally to the positive Z-direction. In the in-plane, double elbow case, the flow was from the negative Y-direction to the positive X-direction and then to the positive Y-direction.

The following results compare different single and double elbow cases and give the pipe length required to eliminate the elbow effects and establish the fully-developed flow.

The Effect of Reynolds Number on Elbow Flows

In this part of the study, the Reynolds number (Re) was altered in three levels, i.e., 10^4, 10^5 and 10^6. The objective here was to document the influence that Re has on

the development of flow after an elbow. The flow at lower Re of 10^4 (Table 7 and Figure 29) required 60 diameters to fully develop the flow after the elbow. In contrast, the flow at higher Re of 10^5 (Table 4 and Figure 23)and 10^6 (Table 8 and Figure 30) required 67 diameters length.

While Re was selected to be 10^5 for model verification, the Re of 10^6 was chosen because it simulates mill conditions of practical interest with respect to pipe diameters and flow velocity. Figure 31 compares the streamwise velocity profiles for the two cases at different distances from the elbow exit. Both the profiles were statistically the same at all the distances. This implies that the increase in the Reynolds number did not have any significant influence on the elbow effect within the range tested. The profiles of Re 10^6 were slightly flater than the profiles of Re 10^5 and the difference was less than 1%. This result agreed with theoretical analysis in that when the Reynolds number increases, the velocity profile become flattened at the middle of the pipe. However, there was no difference in the requirement of pipe for flow development after the elbow with the increase of Reynolds number. Also the case with Re 10^6 was run for different pipe diameters and the simulation results required same pipe as the case with Re 10^5 after the elbow. This implies that the diameter of the pipe has no influence on the velocity profile.

Table 7

Numerical Values of Streamwise Velocity Along Vertical Axis After the Elbow, Re 10^4

Node Points	Distance from Elbow in Diameters														
	0	1	2	3	4	5	6	7	8	9	10	11	14	16	18
1	0.00	0.00	0.00	0.00	0.00	0.00	0.00	0.00	0.00	0.00	0.00	0.00	0.00	0.00	0.00
2	2.03	2.14	2.06	1.94	1.85	1.80	1.78	1.77	1.76	1.76	1.76	1.75	1.74	1.72	1.70
3	2.16	2.22	2.15	2.09	2.07	2.08	2.11	2.15	2.19	2.23	2.26	2.31	2.34	2.34	2.33
4	2.09	2.05	1.97	1.95	1.98	2.04	2.11	2.17	2.23	2.28	2.32	2.40	2.46	2.52	2.56
5	1.95	1.87	1.82	1.87	1.95	2.03	2.11	2.17	2.22	2.27	2.31	2.38	2.44	2.49	2.53
6	1.79	1.72	1.74	1.84	1.95	2.04	2.11	2.17	2.21	2.25	2.29	2.35	2.39	2.43	2.47
7	1.64	1.62	1.71	1.85	1.96	2.04	2.11	2.15	2.19	2.23	2.25	2.29	2.32	2.34	2.36
8	1.54	1.58	1.72	1.86	1.96	2.03	2.08	2.12	2.14	2.16	2.18	2.20	2.21	2.21	2.22
9	1.49	1.57	1.71	1.84	1.92	1.97	2.00	2.01	2.02	2.03	2.03	2.03	2.02	2.02	2.03
10	1.48	1.54	1.65	1.73	1.77	1.79	1.79	1.78	1.76	1.75	1.74	1.73	1.72	1.72	1.72
11	1.42	1.38	1.39	1.40	1.39	1.38	1.36	1.38	1.34	1.33	1.32	1.31	1.30	1.30	1.30
12	0.00	0.00	0.00	0.00	0.00	0.00	0.00	0.00	0.00	0.00	0.00	0.00	0.00	0.00	0.00

Table 7--Continued

Node Points	Distance from elbow in diameters														
	20	22	25	28	31	34	37	40	43	46	49	52	56	60	70
1	0.00	0.00	0.00	0.00	0.00	0.00	0.00	0.00	0.00	0.00	0.00	0.00	0.00	0.00	0.00
2	1.68	1.66	1.63	1.60	1.57	1.55	1.52	1.51	1.49	1.48	1.48	1.48	1.47	1.47	1.47
3	2.29	2.25	2.20	2.15	2.10	2.07	2.03	2.01	1.99	1.98	1.97	1.97	1.96	1.96	1.96
4	2.59	2.60	2.58	2.53	2.47	2.42	2.38	2.35	2.33	2.31	2.30	2.29	2.29	2.29	2.29
5	2.58	2.61	2.64	2.64	2.61	2.58	2.55	2.52	2.50	2.49	2.48	2.47	2.47	2.47	2.47
6	2.49	2.52	2.55	2.58	2.58	2.58	2.58	2.57	2.56	2.56	2.55	2.55	2.55	2.55	2.55
7	2.38	2.40	2.43	2.46	2.48	2.50	2.52	2.53	2.53	2.54	2.54	2.55	2.55	2.55	2.55
8	2.23	2.25	2.27	2.31	2.34	2.37	2.39	2.42	2.43	2.45	2.46	2.46	2.47	2.47	2.47
9	2.03	2.05	2.07	2.11	2.14	2.17	2.20	2.23	2.25	2.27	2.28	2.28	2.28	2.28	2.28
10	1.73	1.74	1.77	1.80	1.83	1.86	1.89	1.92	1.93	1.95	1.95	1.96	1.96	1.96	1.96
11	1.30	1.31	1.33	1.35	1.37	1.40	1.42	1.44	1.45	1.46	1.47	1.47	1.47	1.47	1.47
12	0.00	0.00	0.00	0.00	0.00	0.00	0.00	0.00	0.00	0.00	0.00	0.00	0.00	0.00	0.00

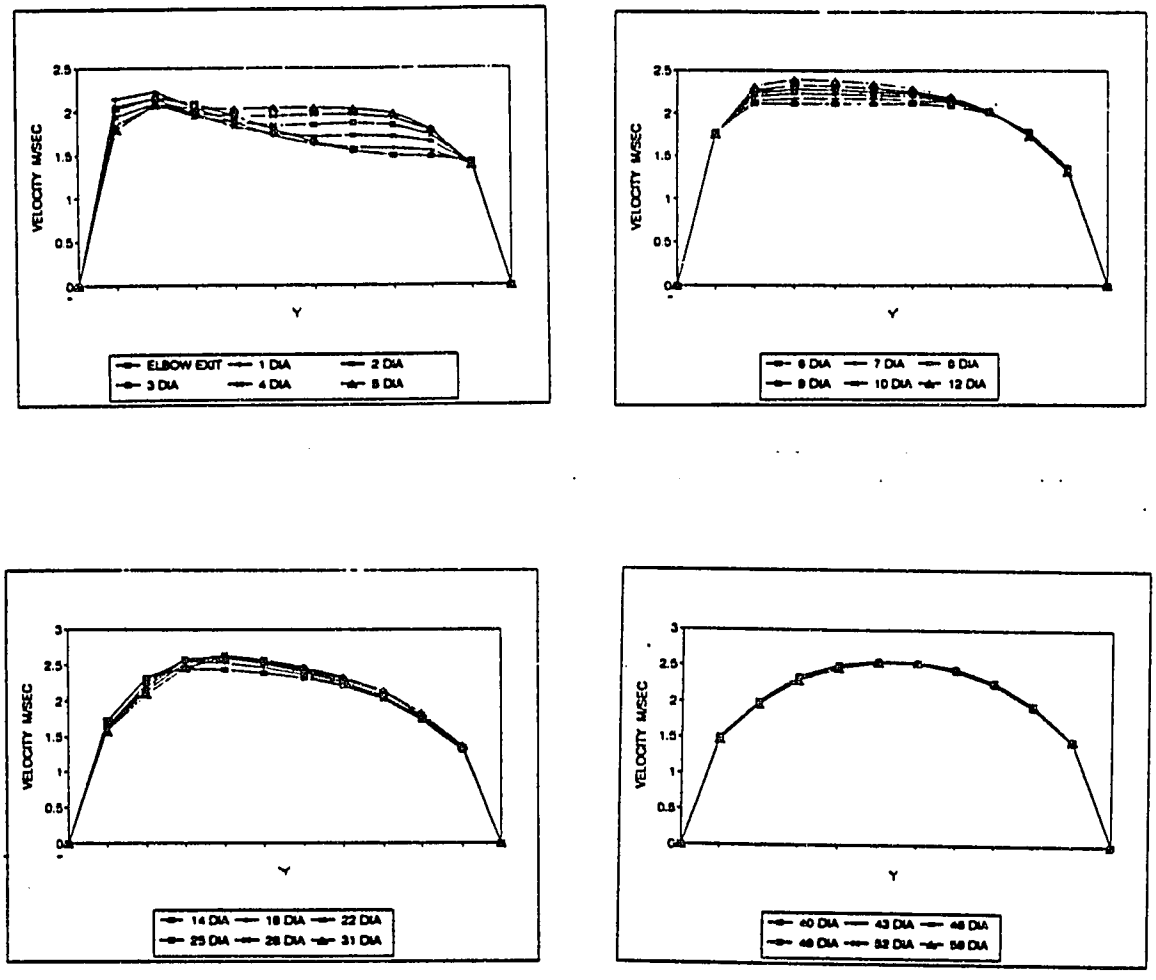

Figure 29. Velocity Profiles at Different Distances Downstream of a Single Elbow, Re 10^4.

Table 8

Numerical Values of Streamwise Velocity Along Vertical Axis After the Elbow, Re 10^6

Node Points	Distance from Elbow in Diameters															
	0	1	2	3	4	5	6	7	8	9	10	11	12	14	16	18
1	0.00	0.00	0.00	0.00	0.00	0.00	0.00	0.00	0.00	0.00	0.00	0.00	0.00	0.00	0.00	0.00
2	3.65	3.87	3.72	3.51	3.38	3.34	3.36	3.39	3.42	3.45	3.46	3.46	3.45	3.42	3.38	3.33
3	3.85	3.91	3.71	3.54	3.51	3.56	3.65	3.75	3.83	3.91	3.98	4.04	4.09	4.16	4.22	4.25
4	3.73	3.60	3.39	3.33	3.41	3.53	3.65	3.76	3.85	3.93	3.99	4.05	4.10	4.19	4.27	4.33
5	3.51	3.30	3.17	3.24	3.39	3.54	3.67	3.77	3.85	3.92	3.98	4.03	4.08	4.16	4.22	4.28
6	3.24	3.05	3.05	3.22	3.41	3.56	3.68	3.78	3.85	3.92	3.97	4.03	4.05	4.12	4.17	4.22
7	2.97	2.87	3.00	3.24	3.43	3.58	3.70	3.78	3.85	3.90	3.94	3.98	4.01	4.07	4.11	4.15
8	2.76	2.77	3.01	3.27	3.46	3.60	3.70	3.77	3.82	3.87	3.90	3.93	3.95	3.99	4.02	4.04
9	2.63	2.75	3.05	3.31	3.48	3.59	3.67	3.72	3.76	3.79	3.82	3.83	3.85	3.86	3.87	3.87
10	2.62	2.79	3.08	3.30	3.44	3.53	3.58	3.61	3.63	3.65	3.65	3.65	3.65	3.63	3.60	3.58
11	2.69	2.82	3.04	3.21	3.29	3.33	3.34	3.32	3.29	3.26	3.23	3.20	3.18	3.13	3.10	3.08
12	2.75	2.72	2.79	3.81	2.78	2.74	2.69	2.66	3.62	2.59	2.56	2.53	2.51	2.47	2.44	2.42
13	0.00	0.00	0.00	0.00	0.00	0.00	0.00	0.00	0.00	0.00	0.00	0.00	0.00	0.00	0.00	0.00

Table 8--Continued

Node Points	Distance from Elbow in Diameters														
	20	23	26	29	32	35	38	41	45	50	55	60	65	68	75
1	0.00	0.00	0.00	0.00	0.00	0.00	0.00	0.00	0.00	0.00	0.00	0.00	0.00	0.00	0.00
2	3.28	3.22	3.17	3.11	3.04	2.98	2.92	2.87	2.80	2.75	2.73	2.72	2.72	2.72	2.72
3	4.27	4.25	4.17	4.06	3.94	3.84	3.76	3.68	3.60	3.53	3.50	3.49	3.49	3.49	3.49
4	4.40	4.49	4.57	4.61	4.58	4.49	4.37	4.27	4.16	4.08	4.04	4.02	4.02	4.02	4.02
5	4.34	4.42	4.51	4.59	4.65	4.68	4.64	4.57	4.47	4.38	4.34	4.33	4.32	4.32	4.32
6	4.27	4.34	4.40	4.47	4.53	4.58	4.61	4.61	4.57	4.52	4.50	4.49	4.48	4.48	4.48
7	4.18	4.23	4.27	4.31	4.36	4.42	4.47	4.50	4.53	4.53	4.53	4.53	4.53	4.53	4.53
8	4.05	4.07	4.09	4.12	4.16	4.21	4.28	4.33	4.40	4.45	4.47	4.48	4.48	4.48	4.48
9	3.86	3.85	3.86	3.88	3.92	3.97	4.04	4.11	4.19	4.26	4.30	4.32	4.32	4.32	4.32
10	3.56	3.54	3.55	3.57	3.60	3.65	3.72	3.79	3.88	3.96	4.00	4.01	4.02	4.02	4.02
11	3.06	3.05	3.06	3.08	3.11	3.16	3.22	3.29	3.37	3.44	3.47	3.48	3.48	3.49	3.49
12	2.40	2.39	2.39	2.40	2.43	2.47	2.51	2.56	2.63	2.68	2.70	2.71	2.72	2.72	2.72
13	0.00	0.00	0.00	0.00	0.00	0.00	0.00	0.00	0.00	0.00	0.00	0.00	0.00	0.00	0.00

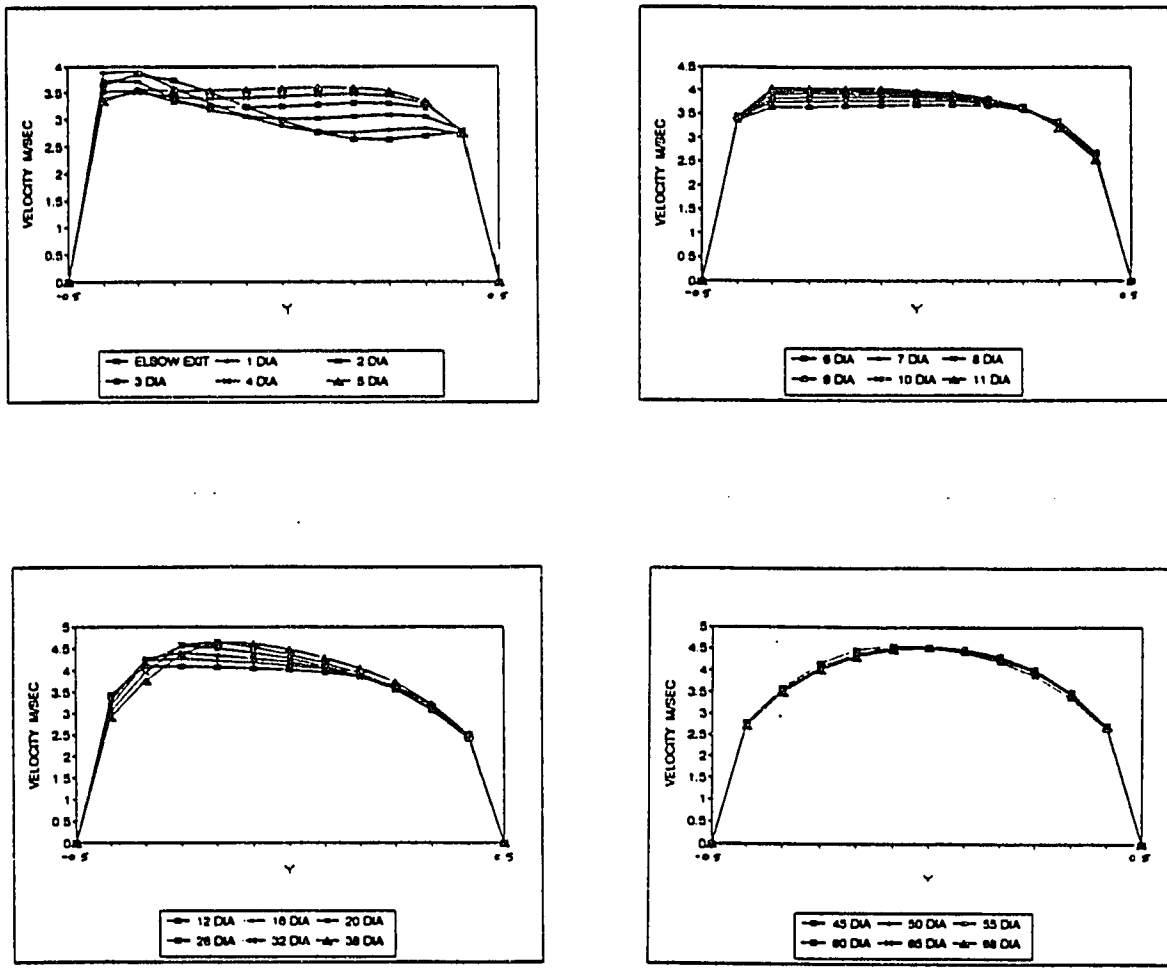

Figure 30. Velocity Profiles at Different Distances Downstream of a Single Elbow, Re 10^6.

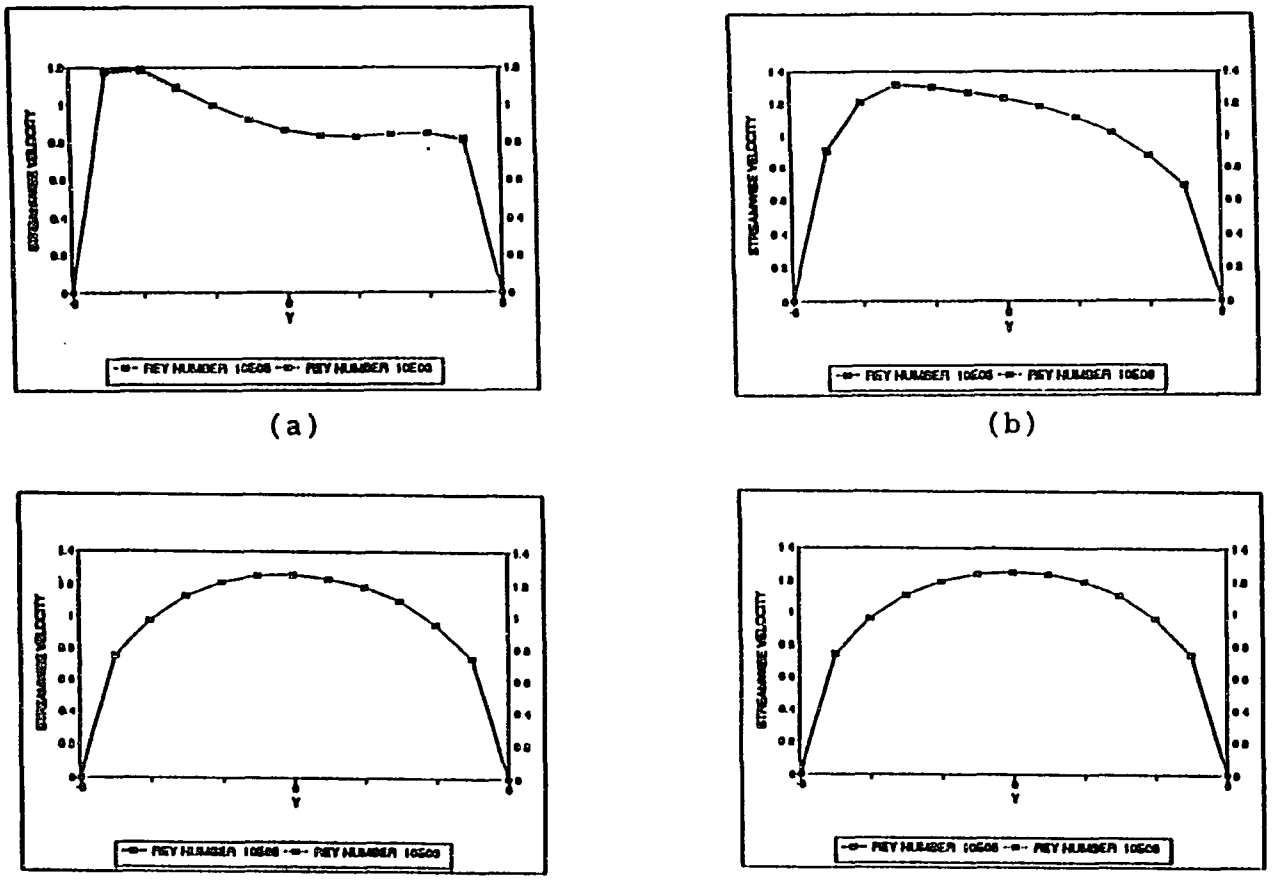

Figure 31. Comparison of Velocity Profiles of Reynolds Number 10^5 10^6 at Different Distances From Elbow: (a) 1 Diameter; (b) 10 Diameters; (c) 40 Diameters; (d) 60 Diameters.

Effect of Out-of-Plane Double elbows

The double elbow cases required more pipe length than required by the single elbow case to get a fully developed profile under the same initial conditions. Quantitative velocity results of double elbows are presented in Tables 9 to 11 and Figures 32 to 34 for 5, 10, and 15 diameters spacing between the two elbows, respectively. The case with 5 diameters spacing required about 78 diameters downstream of the second elbow to completely eliminate the combined effect of both the elbows. Similarly, the case with 10 diameters spacing required about the same distance to eliminate the effect of elbows. In contrast, the case with 15 diameters spacing required only 67 diameters which is equal to the distance required by the single elbow. This results indicate that as the distance between the two elbows increases, the combined effect of elbow diminishes. Since the 15 diameters spaced double elbow case gives the same result as the single elbow case, it can be concluded that there is no combined effect of elbows after 15 or more diameters spacing.

Figures 35 and 36 compare the streamwise velocity along the vertical and horizontal axes of all the out-of-plane cases at 1 and 60 diameters distance after the second elbow. At one diameter distance the case with 5 diameters distance differed from other cases in both vertical and

Table 9

Numerical Values of Streamwise Velocity Along Vertical Axis After the Elbow, 5 Diameters Spaced Double Elbow, Out-of-plane, Re 10^5

Node Points	Distance from Elbow in Diameters														
	1	2	3	4	5	6	7	8	9	10	11	15	18	21	24
1	0.00	0.00	0.00	0.00	0.00	0.00	0.00	0.00	0.00	0.00	0.00	0.00	0.00	0.00	0.00
2	1.80	1.83	1.82	1.79	1.75	1.71	1.67	1.63	1.59	1.55	1.52	1.49	1.40	1.36	1.33	1.30
3	1.96	2.02	2.05	2.06	2.07	2.07	2.06	2.04	2.01	1.99	1.96	1.93	1.83	1.77	1.74	1.69
4	1.99	2.03	2.04	2.05	2.07	2.09	2.12	2.14	2.16	2.17	2.18	2.18	2.16	2.11	2.07	1.99
5	1.95	1.95	1.94	1.95	1.98	2.02	2.06	2.09	2.12	2.14	2.16	2.18	2.20	2.18	2.17	2.13
6	1.84	1.79	1.74	1.75	1.80	1.85	1.89	1.94	1.98	2.01	2.04	2.06	2.13	2.16	2.17	2.19
7	1.77	1.71	1.69	1.72	1.78	1.84	1.89	1.93	1.97	2.01	2.04	2.06	2.15	2.19	2.22	2.26
8	1.84	1.82	1.79	1.81	1.84	1.89	1.93	1.98	2.02	2.05	2.09	2.12	2.21	2.26	2.29	2.34
9	1.94	1.94	1.93	1.93	1.94	1.96	1.99	2.02	2.05	2.08	2.10	2.13	2.22	2.27	2.30	2.33
10	1.99	2.03	2.03	2.03	2.02	2.02	2.01	2.01	2.00	1.99	1.99	1.99	1.99	1.99	2.00	2.00
11	1.86	1.87	1.85	1.81	1.76	1.72	1.68	1.65	1.61	1.58	1.56	1.54	1.50	1.50	1.50	1.51
12	0.00	0.00	0.00	0.00	0.00	0.00	0.00	0.00	0.00	0.00	0.00	0.00	0.00	0.00	0.00	0.00

Table 9--Continued

Node Points	Distance from Elbow in Diameters														
	27	30	33	35	37	39	41	43	45	50	55	60	70	78	85
1	0.00	0.00	0.00	0.00	0.00	0.00	0.00	0.00	0.00	0.00	0.00	0.00	0.00	0.00	0.00
2	1.28	1.27	1.28	1.30	1.32	1.33	1.35	1.36	1.37	1.39	1.40	1.40	1.40	1.40	1.40
3	1.66	1.65	1.67	1.69	1.71	1.73	1.75	1.77	1.79	1.81	1.81	1.81	1.81	1.82	1.82
4	1.95	1.93	1.95	1.97	1.99	2.01	2.03	2.05	2.07	2.08	2.09	2.10	2.10	2.10	2.10
5	2.11	2.11	2.13	2.14	2.16	2.18	2.20	2.22	2.23	2.24	2.25	2.25	2.25	2.25	2.25
6	2.21	2.23	2.26	2.27	2.29	2.30	2.31	2.31	2.32	2.32	2.32	2.32	2.32	2.32	2.32
7	2.30	2.33	2.36	2.37	2.37	2.37	2.36	2.35	2.35	2.33	2.32	2.32	2.32	2.32	2.32
8	2.38	2.40	2.41	2.40	2.38	2.36	2.33	2.31	2.30	2.25	2.26	2.25	2.25	2.25	2.25
9	2.34	2.32	2.29	2.26	2.23	2.21	2.18	2.16	2.14	2.11	2.10	2.10	2.10	2.10	2.10
10	1.99	1.97	1.96	1.94	1.92	1.90	1.88	1.87	1.85	1.84	1.83	1.82	1.81	1.82	1.82
11	1.51	1.51	1.49	1.48	1.47	1.48	1.45	1.44	1.43	1.42	1.41	1.41	1.40	1.40	1.40
12	0.00	0.00	0.00	0.00	0.00	0.00	0.00	0.00	0.00	0.00	0.00	0.00	0.00	0.00	0.00

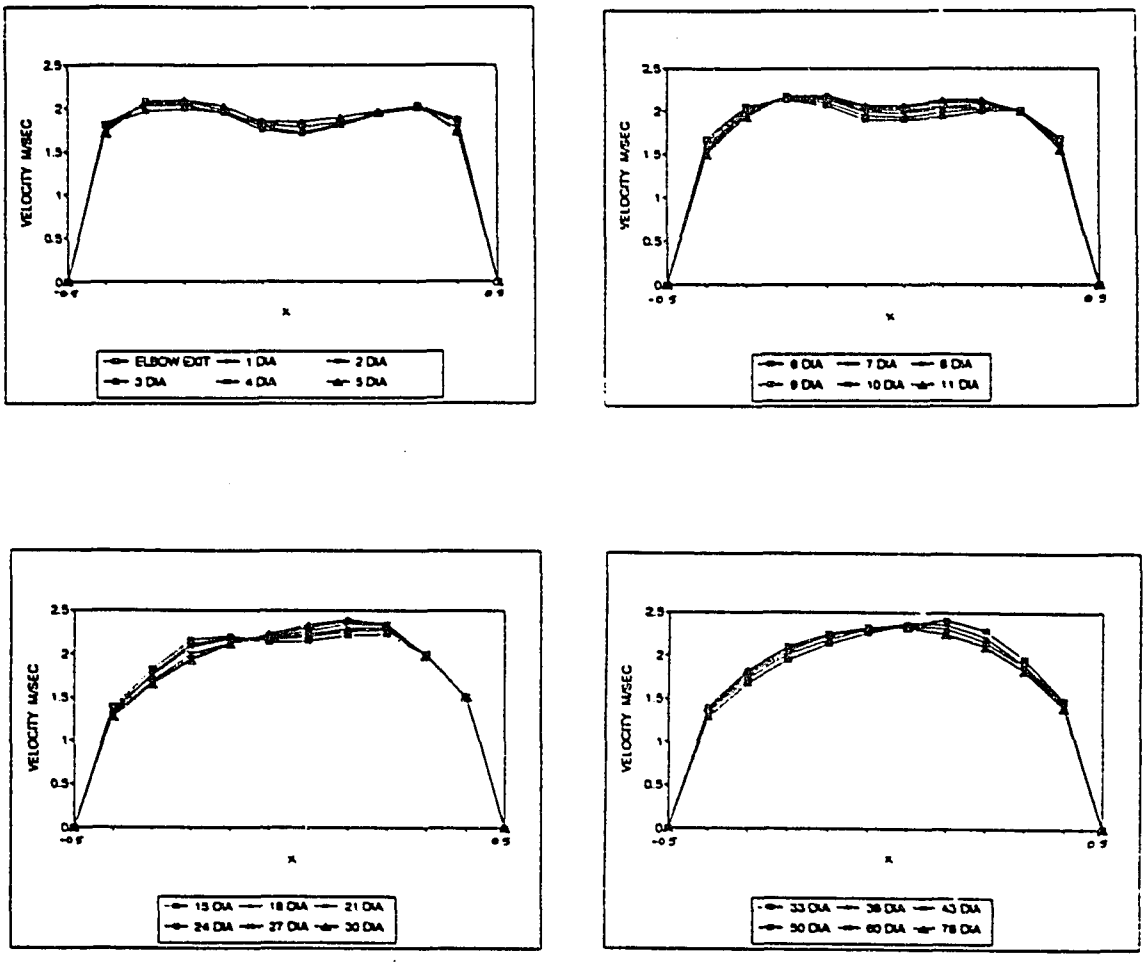

Figure 32. Velocity Profiles at Different Distances Downstream of Second Elbow, 5 Diameters Spacing, Re 10^5, Out-of-Plane.

Table 10

Numerical Values of Streamwise Velocity Along Vertical Axis After the Elbow, 10 Diameters Spaced Double Elbow, Out-of-Plane, Re 10^5

Node Points	Distance from Elbow in Diameters															
	0	1	2	3	4	5	6	7	8	9	10	11	12	13	14	15
1	0.00	0.00	0.00	0.00	0.00	0.00	0.00	0.00	0.00	0.00	0.00	0.00	0.00	0.00	0.00	0.00
2	1.89	1.92	1.89	1.85	1.80	1.74	1.69	1.64	1.59	1.55	1.50	1.47	1.44	1.41	1.38	1.36
3	2.06	2.10	2.10	2.10	2.09	2.08	2.07	2.04	2.01	1.98	1.94	1.90	1.87	1.84	1.81	1.78
4	2.02	2.02	1.99	2.00	2.03	2.06	2.09	2.12	2.13	2.13	2.13	2.12	2.11	2.09	2.07	2.05
5	1.89	1.84	1.80	1.82	1.86	1.91	1.95	1.99	2.02	2.04	2.05	2.06	2.06	2.07	2.06	2.06
6	1.72	1.63	1.61	1.67	1.75	1.82	1.88	1.93	1.97	2.00	2.02	2.04	2.06	2.07	2.08	2.09
7	1.77	1.72	1.70	1.74	1.80	1.87	1.92	1.97	2.01	2.05	2.07	2.10	2.12	2.14	2.15	2.17
8	1.89	1.86	1.83	1.83	1.86	1.90	1.94	1.98	2.02	2.06	2.09	2.12	2.15	2.18	2.20	2.22
9	1.98	1.98	1.96	1.95	1.96	1.97	1.99	2.01	2.04	2.07	2.10	2.12	2.15	2.18	2.20	2.23
10	2.01	2.04	2.05	2.05	2.03	2.02	2.01	2.00	1.99	1.98	1.98	1.99	1.99	2.00	2.01	2.01
11	1.86	1.88	1.87	1.83	1.78	1.73	1.69	1.65	1.61	1.59	1.56	1.55	1.54	1.53	1.53	1.52
12	0.00	0.00	0.00	0.00	0.00	0.00	0.00	0.00	0.00	0.00	0.00	0.00	0.00	0.00	0.00	0.00

Table 10--Continued

Node Points	Distance from Elbow in Diametrs															
	17	19	22	25	30	35	38	41	44	47	50	55	60	67	78	85
1	0.00	0.00	0.00	0.00	0.00	0.00	0.00	0.00	0.00	0.00	0.00	0.00	0.00	0.00	0.00	0.00
2	1.33	1.30	1.28	1.27	1.28	1.32	1.34	1.36	1.37	1.38	1.39	1.40	1.40	1.40	1.40	1.40
3	1.73	1.69	1.66	1.64	1.67	1.72	1.75	1.78	1.80	1.81	1.81	1.81	1.81	1.81	1.82	1.82
4	2.01	1.98	1.94	1.92	1.95	2.01	2.04	2.07	2.08	2.09	2.10	2.10	2.10	2.10	2.10	2.10
5	2.06	2.05	2.05	2.06	2.11	2.18	2.21	2.23	2.25	2.25	2.25	2.25	2.25	2.25	2.25	2.25
6	2.11	2.12	2.15	2.17	2.23	2.29	2.31	2.33	2.33	2.33	2.33	2.32	2.32	2.32	2.32	2.32
7	2.19	2.21	2.25	2.28	2.34	2.37	2.37	2.36	2.35	2.34	2.33	2.32	2.32	2.32	2.32	2.32
8	2.25	2.29	2.33	2.37	2.41	2.38	2.35	2.32	2.29	2.28	2.27	2.26	2.25	2.25	2.25	2.25
9	2.27	2.30	2.33	2.35	2.30	2.23	2.20	2.17	2.15	2.14	2.13	2.12	2.11	2.10	2.10	2.10
10	2.02	2.03	2.02	2.00	1.96	1.92	1.90	1.88	1.86	1.85	1.83	1.82	1.82	1.81	1.82	1.82
11	1.52	1.52	1.52	1.52	1.50	1.48	1.47	1.44	1.43	1.42	1.41	1.41	1.40	1.40	1.40	1.40
12	0.00	0.00	0.00	0.00	0.00	0.00	0.00	0.00	0.00	0.00	0.00	0.00	0.00	0.00	0.00	0.00

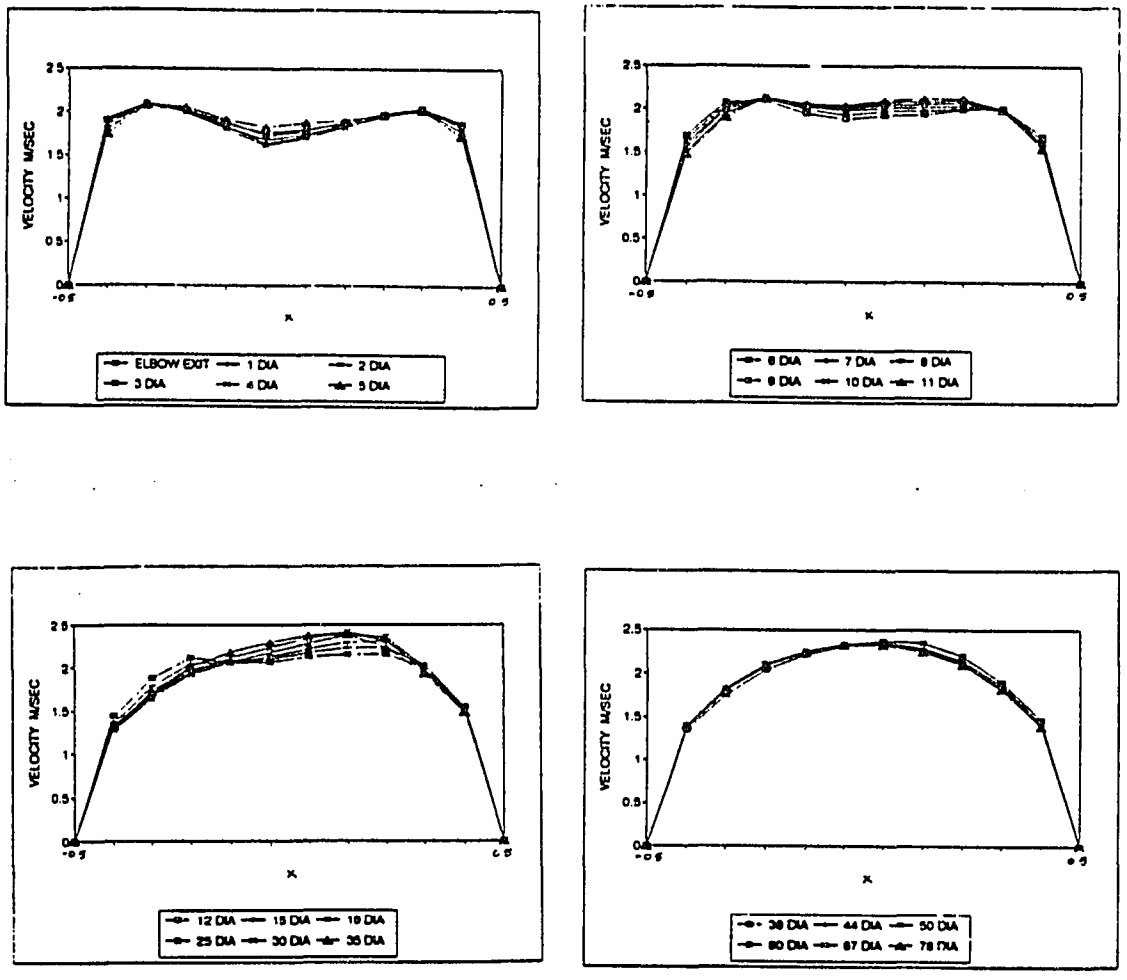

Figure 33. Velocity Profiles at Different Distances Downstream of Second Elbow, 10 Diameters Spacing, Re 10^5, Out-of-Plane.

Table 11

Numerical Values of Streamwise Velocity Along Vertical Axis After the Elbow, 15 Diameters Spaced Double Elbow, Out-of-Plane, Re 10^5

Node Points	Distance from Elbow in Diameters															
	0	1	2	3	4	5	6	7	8	9	10	11	12	13	14	15
1	0.00	0.00	0.00	0.00	0.00	0.00	0.00	0.00	0.00	0.00	0.00	0.00	0.00	0.00	0.00	0.00
2	1.95	1.97	1.93	1.87	1.81	1.75	1.69	1.63	1.58	1.53	1.48	1.45	1.41	1.38	1.36	1.34
3	2.10	2.12	2.11	2.10	2.09	2.07	2.05	2.02	1.99	1.95	1.91	1.87	1.84	1.80	1.77	1.74
4	1.99	1.97	1.94	1.96	1.99	2.02	2.05	2.06	2.06	2.05	2.04	2.02	2.00	1.98	1.97	1.95
5	1.81	1.74	1.71	1.75	1.82	1.88	1.92	1.96	1.98	2.00	2.00	2.01	2.01	2.01	2.01	2.01
6	1.66	1.58	1.59	1.67	1.76	1.84	1.90	1.95	1.98	2.01	2.03	2.04	2.06	2.07	2.08	2.09
7	1.78	1.73	1.71	1.75	1.82	1.88	1.94	1.98	2.02	2.05	2.08	2.10	2.12	2.14	2.15	2.17
8	1.91	1.88	1.84	1.84	1.86	1.90	1.94	1.99	2.03	2.06	2.10	2.13	2.15	2.18	2.20	2.22
9	1.99	1.99	1.97	1.96	1.96	1.97	1.98	2.01	2.04	2.07	2.10	2.13	2.15	2.18	2.20	2.23
10	2.02	2.05	2.06	2.05	2.03	2.01	2.00	1.99	1.98	1.98	1.99	1.99	2.00	2.01	2.02	2.02
11	1.88	1.91	1.89	1.85	1.79	1.74	1.69	1.65	1.62	1.59	1.57	1.56	1.55	1.54	1.54	1.53
12	0.00	0.00	0.00	0.00	0.00	0.00	0.00	0.00	0.00	0.00	0.00	0.00	0.00	0.00	0.00	0.00

Table 11--Continued

Node Points	Distance from Elbow in Diameters															
	17	19	22	25	28	31	34	37	42	46	50	54	60	67	75	80
1	0.00	0.00	0.00	0.00	0.00	0.00	0.00	0.00	0.00	0.00	0.00	0.00	0.00	0.00	0.00	0.00
2	1.31	1.29	1.27	1.27	1.29	1.31	1.33	1.34	1.37	1.38	1.39	1.39	1.40	1.40	1.40	1.40
3	1.70	1.67	1.65	1.65	1.67	1.70	1.73	1.75	1.78	1.80	1.81	1.81	1.82	1.82	1.82	1.82
4	1.93	1.91	1.91	1.92	1.95	1.98	2.01	2.03	2.07	2.08	2.09	2.10	2.10	2.10	2.10	2.10
5	2.01	2.01	2.03	2.06	2.10	2.15	2.17	2.20	2.24	2.25	2.25	2.26	2.25	2.25	2.25	2.25
6	2.10	2.12	2.15	2.18	2.22	2.26	2.28	2.30	2.33	2.33	2.33	2.33	2.33	2.32	2.32	2.32
7	2.19	2.22	2.25	2.29	2.33	2.35	2.36	2.36	2.36	2.36	2.35	2.34	2.33	2.32	2.32	2.32
8	2.26	2.29	2.34	2.38	2.41	2.40	2.38	2.36	2.32	2.30	2.29	2.28	2.26	2.25	2.25	2.25
9	2.27	2.30	2.34	2.34	2.31	2.27	2.24	2.21	2.16	2.15	2.13	2.12	2.11	2.10	2.10	2.10
10	2.03	2.03	2.01	1.99	1.96	1.94	1.92	1.90	1.86	1.85	1.84	1.83	1.82	1.82	1.82	1.82
11	1.53	1.53	1.52	1.51	1.50	1.48	1.47	1.46	1.43	1.42	1.42	1.41	1.40	1.40	1.40	1.40
12	0.00	0.00	0.00	0.00	0.00	0.00	0.00	0.00	0.00	0.00	0.00	0.00	0.00	0.00	0.00	0.00

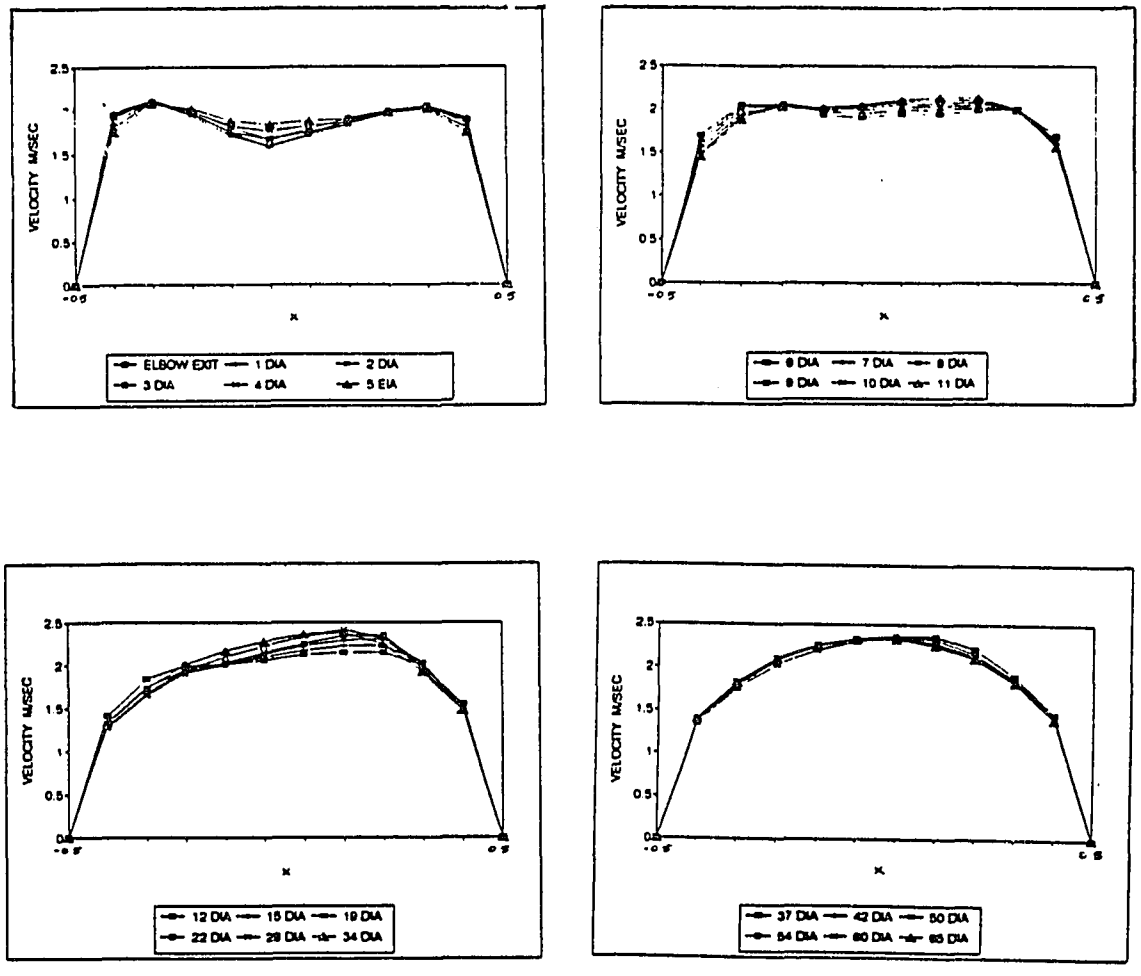

Figure 34. Velocity Profiles at Different Distances Downstream of Second Elbow, 15 Diameters Spacing, Re 10^5, Out-of-Plane.

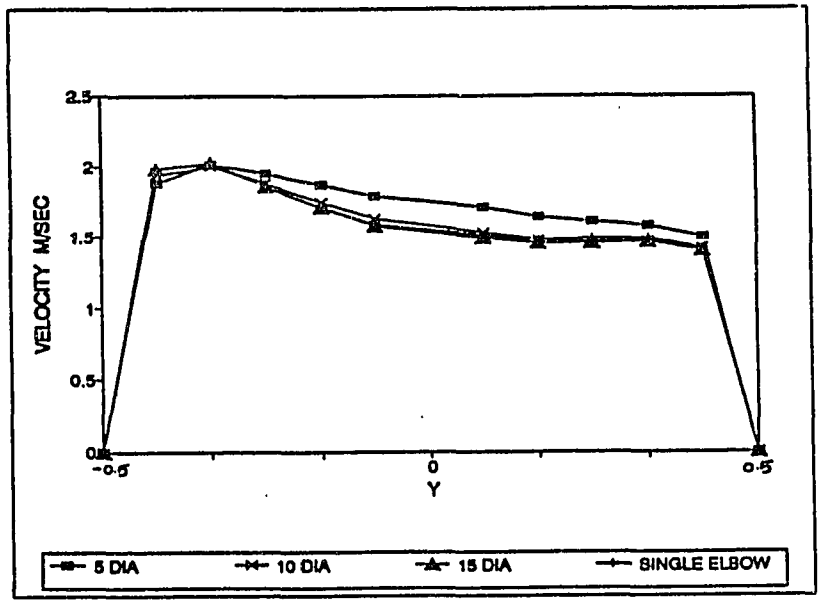

(a)

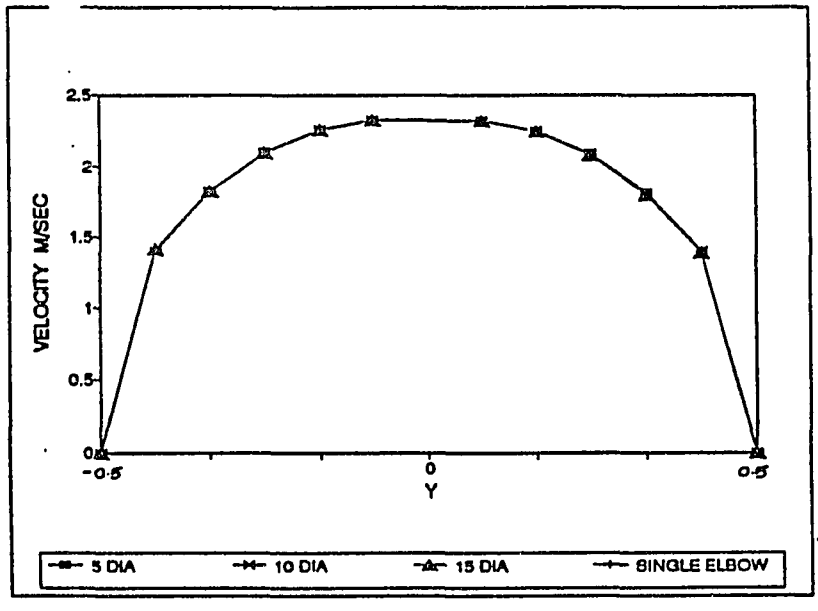

(b)

Legend. (a) 1 Diameter (b) 60 Diameters

Figure 35. Comparison of Streamwise Velocity of Different Out-of-Plane Cases With Single Elbow Case Along Vertical Axis.

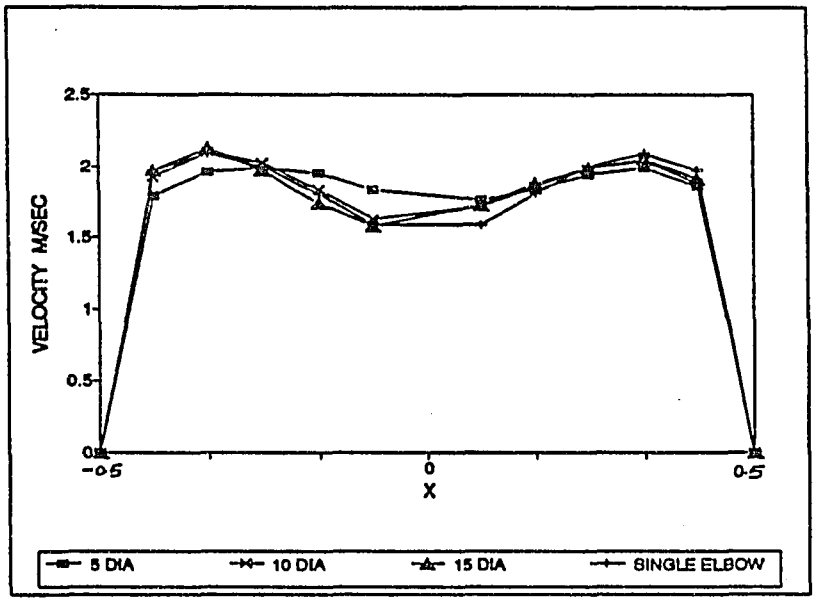

(a)

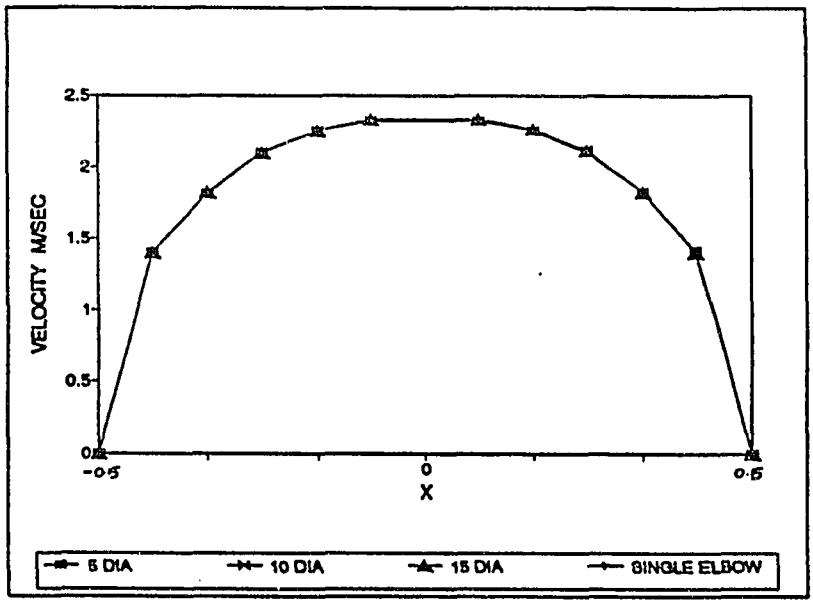

(b)

Legend. (a) 1 Diameter (b) 60 Diameters

Figure 36. Comparison of Streamwise Velocity of Different Out-of-Plane Cases With Single Elbow Case Along Horizontal Axis.

horizontal axes. Because of the short distance between the two elbows, the cross flow coming out of the first elbow influenced the second elbow. As the distance between the elbows increased, the cross flow became weak. Hence the 15 diameters spaced case almost resembled the single elbow case and required the same pipe length to get a fully developed flow. However, all the cases have almost same shape at 60 diameters distance in both vertical and horizontal axis. This implies that there was no considerable difference in the effect of the elbows after 60 diameters, whether it was a single or double elbow case.

Figures 37 and 38 present the cross flows coming out of a single and double elbows of 5 diameters spacing. At the exits of the elbow, the secondary flows coming out of the second elbow in the double elbow case were severe when compared to the secondary flow coming out of the single elbow case. Also the double elbow case required more length of pipe (45 diameters distance) to eliminate the cross flow, whereas the single elbow case required only 32 diameters distance.

Comparison of the Effects of In-Plane and Out-of-Plane Double Elbows

Two computational models with 5 and 15 diameters spaced, in-plane, double elbow cases were tested to compare them with the out-of-plane configuration. They were

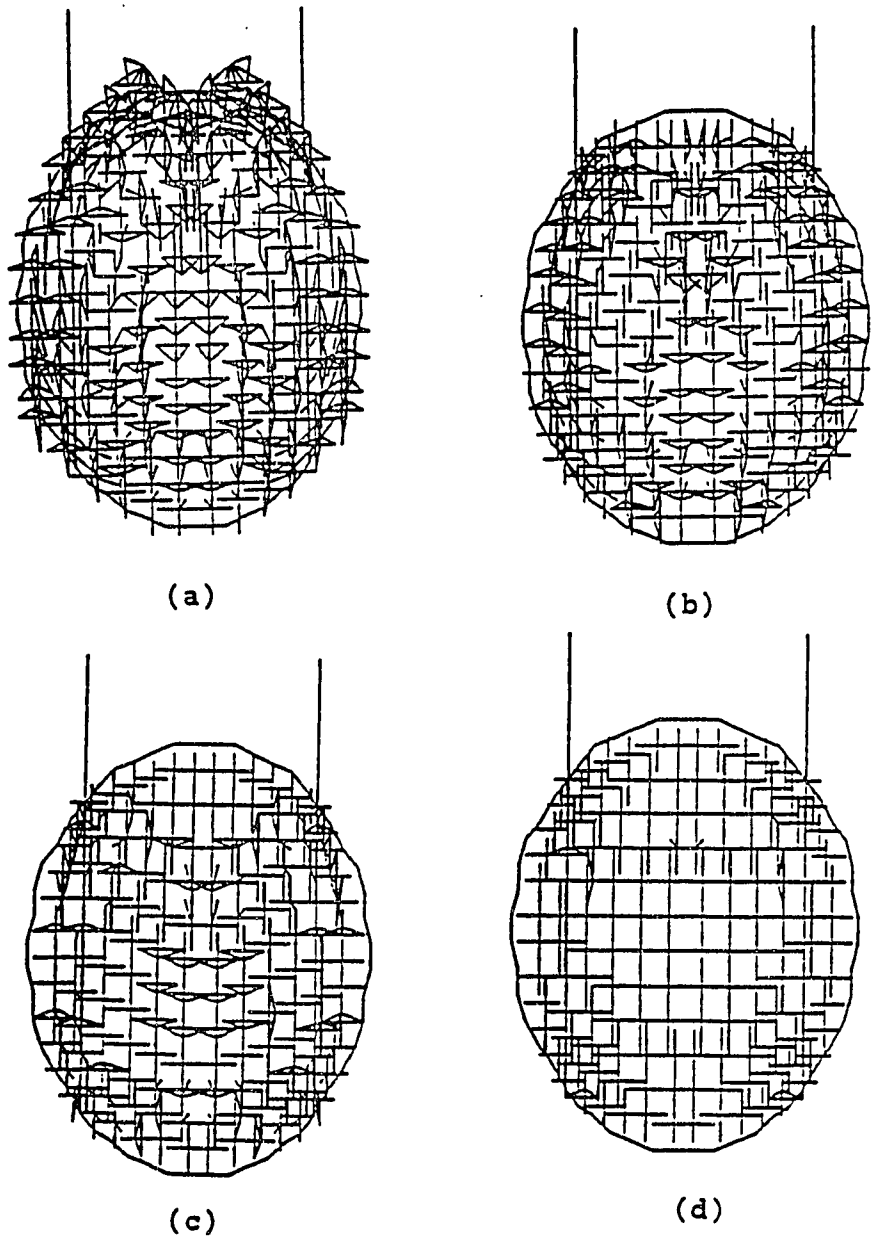

Legend. (a) 1 Diameter (b) 6 Diameters
(c) 15 Diameters (d) 28 Dimaters

Figure 37. Cross Flow Coming Out of a Single Elbow.

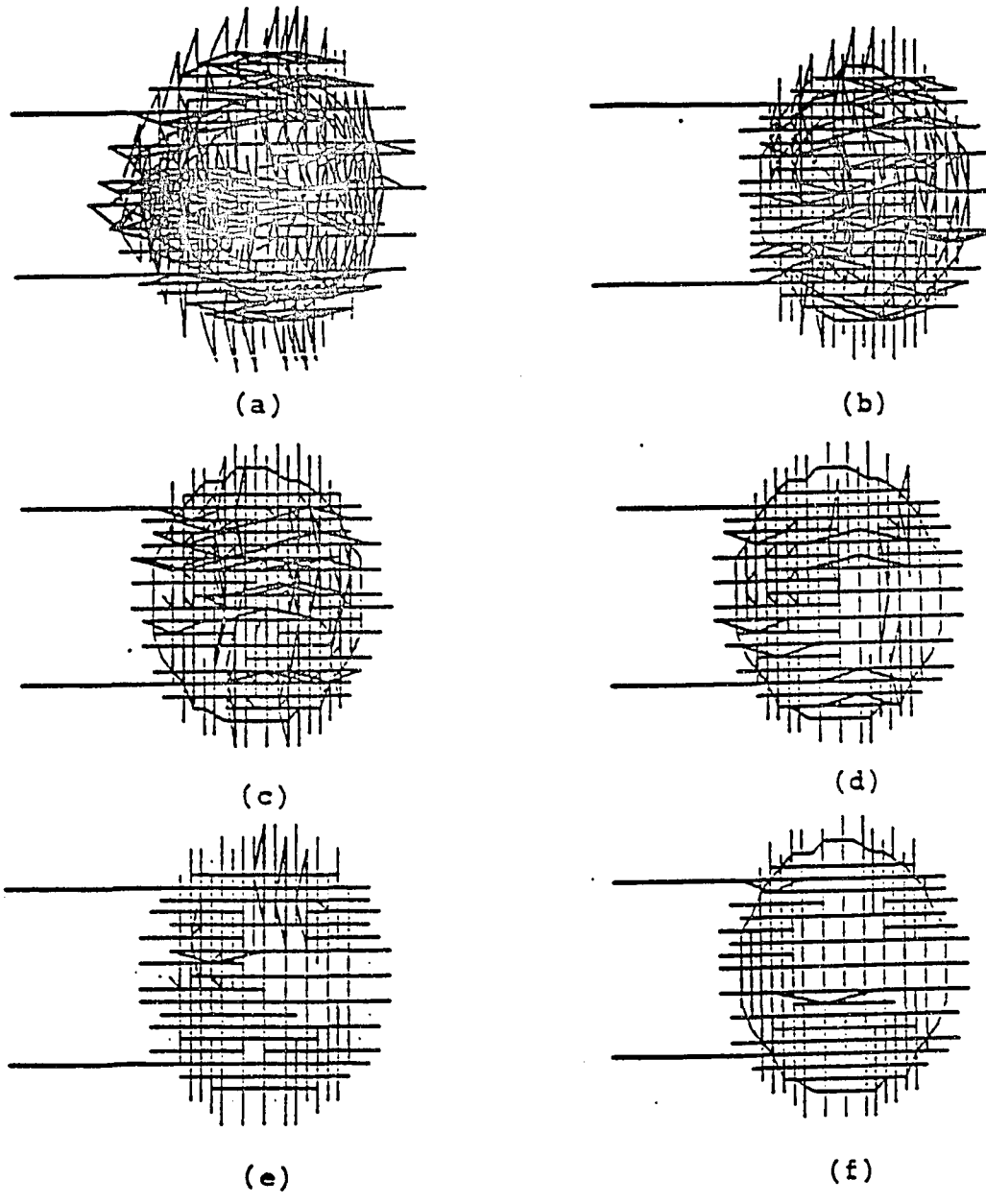

Legend. (a) 1 Diameter (b) 6 Diameters
(c) 15 Diameters (d) 28 Diameters
(e) 35 Diameters (f) 47 Diameters

Figure 38. Cross Flow Coming Out of Second Elbow in 5 Diameters Spaced Double Elbow Case, Out-of-Plane.

simulated with same initial conditions as the out-of-plane type.

The case with 5 diameters spacing (Table 12 and Figure 39) required about 73 diameters distance to completely eliminate the elbow effects, whereas the out-of-plane type required about 78 diameters. The model with 15 diameters spacing (Table 13 and Figure 40) required 67 diameters distance which is same as the out-of-plane case. From these results, it is concluded that the effects due to the out-of-plane type lasted longer than the in-plane type. After 15 diameters spacing the combined effect of elbows had no effect and the distance required to get fully developed flow was the same as in the single elbow case.

Figure 41 compares the velocity profiles of in-plane, out-of-plane and single elbow cases at different distances along the vertical direction. At all locations, the velocity profiles of 5 and 15 diameters in-plane had both qualitative and quantitative similarities with the single elbow case. The case with 5 diameters spacing differed from other profile near the elbow. At 60 diameters distance, all the profiles looked qualitatively the same as single elbow case even though they require different distances to completely eliminate the effects. This implies that after 60 diameters distance, there was no considerable effect due to combined elbows along vertical axes whether they are in-plane or out-of-plane.

Table 12

Numerical Values of Streamwise Velocity Along Vertical Axis After the Elbow, 5 Diameters Spaced Double Elbow, In-Plane, Re 10^5

Node Points	Distance from Elbow in Diametrs															
	0	1	2	3	4	5	6	7	8	9	10	11	13	15	18	21
1	0.00	0.00	0.00	0.00	0.00	0.00	0.00	0.00	0.00	0.00	0.00	0.00	0.00	0.00	0.00	0.00
2	1.57	1.86	1.84	1.77	1.72	1.68	1.66	1.65	1.64	1.64	1.64	1.64	1.63	1.63	1.61	1.59
3	1.69	1.93	1.94	1.92	1.90	1.91	1.92	1.95	1.97	2.00	2.03	2.05	2.09	2.12	2.14	2.13
4	1.70	1.85	1.84	1.83	1.84	1.87	1.90	1.94	1.98	2.02	2.05	2.08	2.14	2.19	2.25	2.31
5	1.70	1.77	1.75	1.76	1.80	1.85	1.89	1.94	1.98	2.01	2.05	2.08	2.13	2.17	2.23	2.28
6	1.69	1.69	1.69	1.73	1.79	1.85	1.90	1.94	1.98	2.01	2.04	2.06	2.11	2.15	2.19	2.24
7	1.66	1.63	1.65	1.72	1.79	1.85	1.90	1.94	1.97	2.00	2.02	2.04	2.07	2.10	2.14	2.16
8	1.62	1.58	1.64	1.73	1.80	1.85	1.89	1.92	1.94	1.96	1.98	1.99	2.01	2.02	2.03	2.04
9	1.58	1.57	1.65	1.73	1.78	1.82	1.84	1.85	1.87	1.81	1.88	1.88	1.88	1.87	1.86	1.86
10	1.59	1.57	1.62	1.67	1.70	1.70	1.70	1.69	1.68	1.66	1.65	1.63	1.61	1.60	1.59	1.59
11	1.64	1.79	1.48	1.46	1.43	1.39	1.36	1.33	1.31	1.29	1.28	1.27	1.25	1.24	1.23	1.23
12	0.00	0.00	0.00	0.00	0.00	0.00	0.00	0.00	0.00	0.00	0.00	0.00	0.00	0.00	0.00	0.00

Table 12--Continued

Node Points	Distance from Elbow in Diameters															
	24	27	30	33	36	39	42	45	48	52	56	60	66	73	90	99 DIA
1	0.00	0.00	0.00	0.00	0.00	0.00	0.00	0.00	0.00	0.00	0.00	0.00	0.00	0.00	0.00	0.00
2	1.58	1.56	1.54	1.52	1.50	1.48	1.46	1.44	1.43	1.41	1.40	1.40	1.40	1.40	1.40	1.40
3	2.10	2.05	2.01	1.98	1.95	1.92	1.90	1.87	1.85	1.83	1.82	1.82	1.81	1.82	1.82	1.82
4	2.35	2.37	2.36	2.32	2.28	2.24	2.20	2.17	2.15	2.12	2.11	2.10	2.10	2.10	2.10	2.10
5	2.33	2.37	2.40	2.41	2.39	2.37	2.34	2.31	2.29	2.27	2.26	2.25	2.25	2.25	2.25	2.25
6	2.27	2.30	2.32	2.34	2.34	2.35	2.34	2.34	2.33	2.32	2.32	2.32	2.32	2.32	2.32	2.32
7	2.18	2.19	2.21	2.23	2.24	2.26	2.27	2.28	2.29	2.30	2.31	2.31	2.31	2.32	2.32	2.32
8	2.05	2.06	2.08	2.09	2.12	2.14	2.16	2.18	2.20	2.22	2.23	2.24	2.24	2.24	2.24	2.24
9	1.87	1.88	1.90	1.92	1.94	1.97	2.00	2.02	2.04	2.07	2.08	2.09	2.09	2.10	2.10	2.10
10	1.60	1.62	1.63	1.65	1.68	1.70	1.73	1.75	1.77	1.79	1.80	1.81	1.81	1.82	1.82	1.82
11	1.24	1.25	1.26	1.27	1.29	1.31	1.33	1.35	1.36	1.38	1.39	1.39	1.39	1.40	1.40	1.40
12	0.00	0.00	0.00	0.00	0.00	0.00	0.00	0.00	0.00	0.00	0.00	0.00	0.00	0.00	0.00	0.00

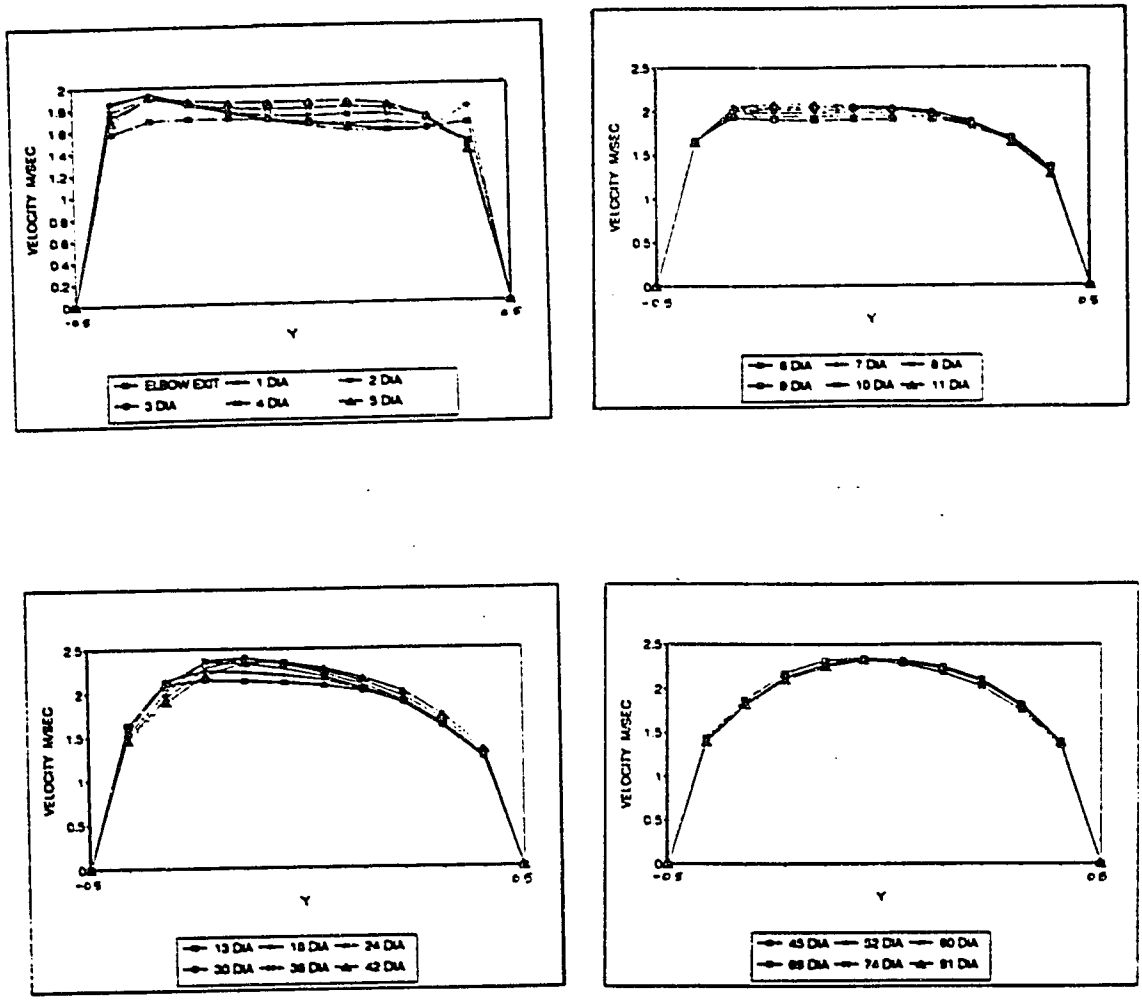

Figure 39. Velocity Profiles at Different Distances Downstream of Second Elbow, 5 Diameters Spacing, Re 10^5, In-Plane.

Table 13

Numerical Values of Streamwise Velocity Along Vertical Axis After the Elbow, 15 Diameters Spaced Double Elbow, In-Plane, Re 10^5

Node Points	Distance from Elbow in Diameters											
	0	1	2	3	4	5	6	7	8	9	10	12
1	0.00	0.00	0.00	0.00	0.00	0.00	0.00	0.00	0.00	0.00	0.00	0.00
2	1.87	1.97	1.92	1.83	1.75	1.70	1.66	1.65	1.65	1.65	1.65	1.66
3	1.99	2.07	2.04	1.97	1.93	1.91	1.92	1.94	1.97	2.00	2.03	2.08
4	1.91	1.92	1.85	1.80	1.81	1.84	1.88	1.93	1.97	2.01	2.05	2.11
5	1.80	1.75	1.69	1.70	1.76	1.82	1.88	1.93	1.97	2.01	2.05	2.10
6	1.66	1.60	1.60	1.67	1.75	1.83	1.89	1.93	1.98	2.01	2.04	2.09
7	1.53	1.51	1.57	1.68	1.77	1.84	1.89	1.94	1.97	2.00	2.02	2.06
8	1.44	1.47	1.58	1.70	1.79	1.85	1.89	1.92	1.95	1.97	1.99	2.01
9	1.41	1.48	1.61	1.72	1.78	1.83	1.85	1.87	1.88	1.89	1.89	1.90
10	1.44	1.49	1.60	1.67	1.71	1.72	1.72	1.72	1.70	1.69	1.67	1.64
11	1.44	1.42	1.45	1.45	1.43	1.40	1.38	1.35	1.33	1.31	1.30	1.27
12	0.00	0.00	0.00	0.00	0.00	0.00	0.00	0.00	0.00	0.00	0.00	0.00

Table 13--Continued

Node Points	Distance from Elbow in Diameters											
	14	17	20	25	30	35	40	45	50	60	68	80
1	0.00	0.00	0.00	0.00	0.00	0.00	0.00	0.00	0.00	0.00	0.00	0.00
2	1.65	1.64	1.62	1.61	1.56	1.52	1.48	1.45	1.42	1.40	1.40	1.40
3	2.12	2.16	2.17	2.16	2.05	1.98	1.92	1.88	1.84	1.82	1.81	1.82
4	2.16	2.23	2.29	2.32	2.38	2.32	2.24	2.18	2.13	2.10	2.10	2.10
5	2.15	2.21	2.26	2.29	2.39	2.40	2.37	2.32	2.28	2.25	2.25	2.25
6	2.13	2.18	2.22	2.24	2.30	2.33	2.34	2.34	2.33	2.32	2.32	2.32
7	2.09	2.13	2.15	2.16	2.19	2.22	2.26	2.28	2.30	2.31	2.32	2.32
8	2.02	2.04	2.04	2.04	2.06	2.09	2.14	2.18	2.21	2.24	2.25	2.25
9	1.89	1.88	1.87	1.87	1.89	1.92	1.97	2.02	2.06	2.09	2.10	2.10
10	1.62	1.60	1.59	1.59	1.62	1.66	1.70	1.75	1.78	1.81	1.81	1.82
11	1.26	1.24	1.23	1.23	1.25	1.28	1.31	1.35	1.37	1.39	1.40	1.40
12	0.00	0.00	0.00	0.00	0.00	0.00	0.00	0.00	0.00	0.00	0.00	0.00

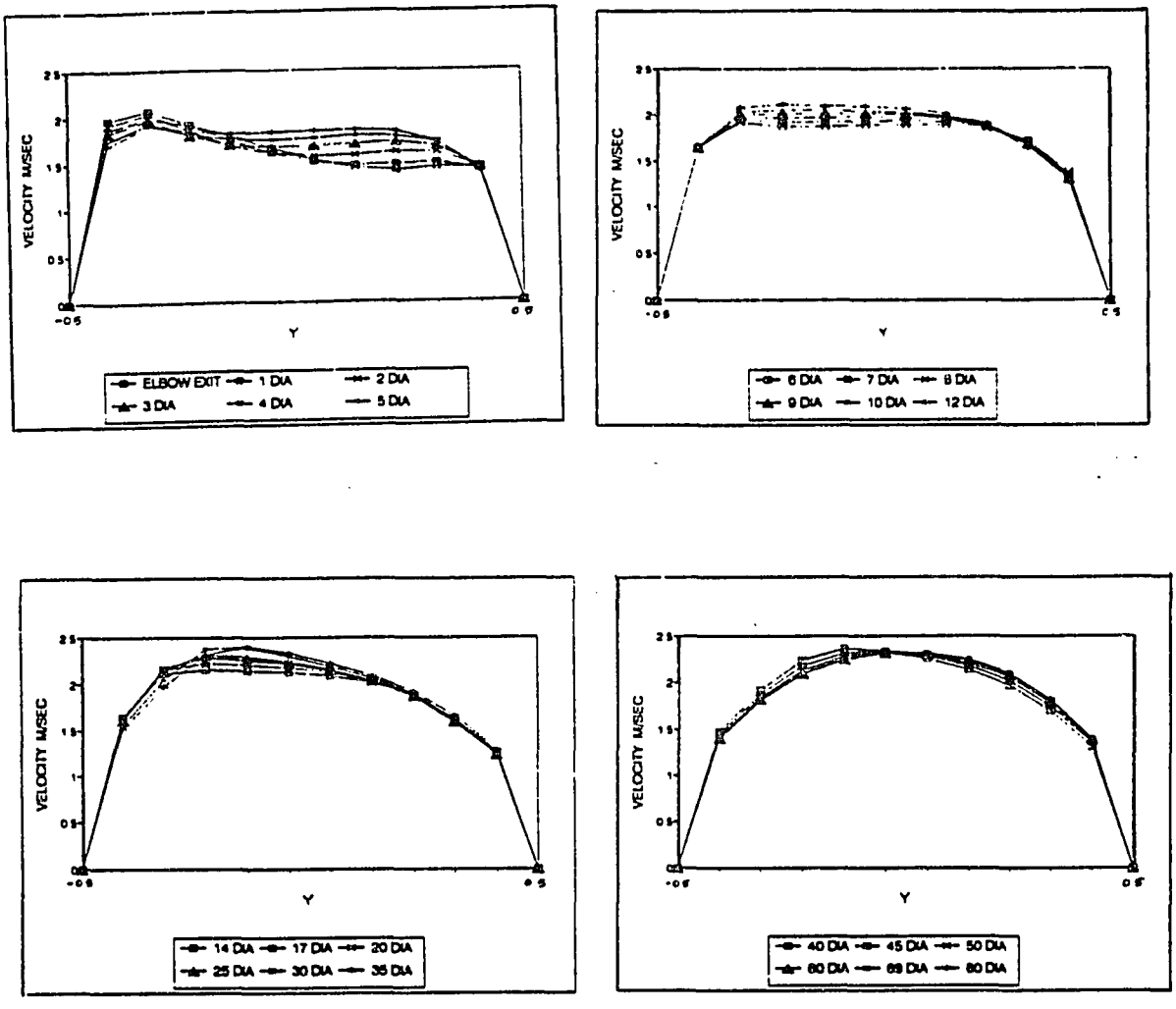

Figure 40. Velocity Profiles at Different Distances Downstream of Second Elbow, 15 Diameters Spacing, Re 10^5, In-Plane.

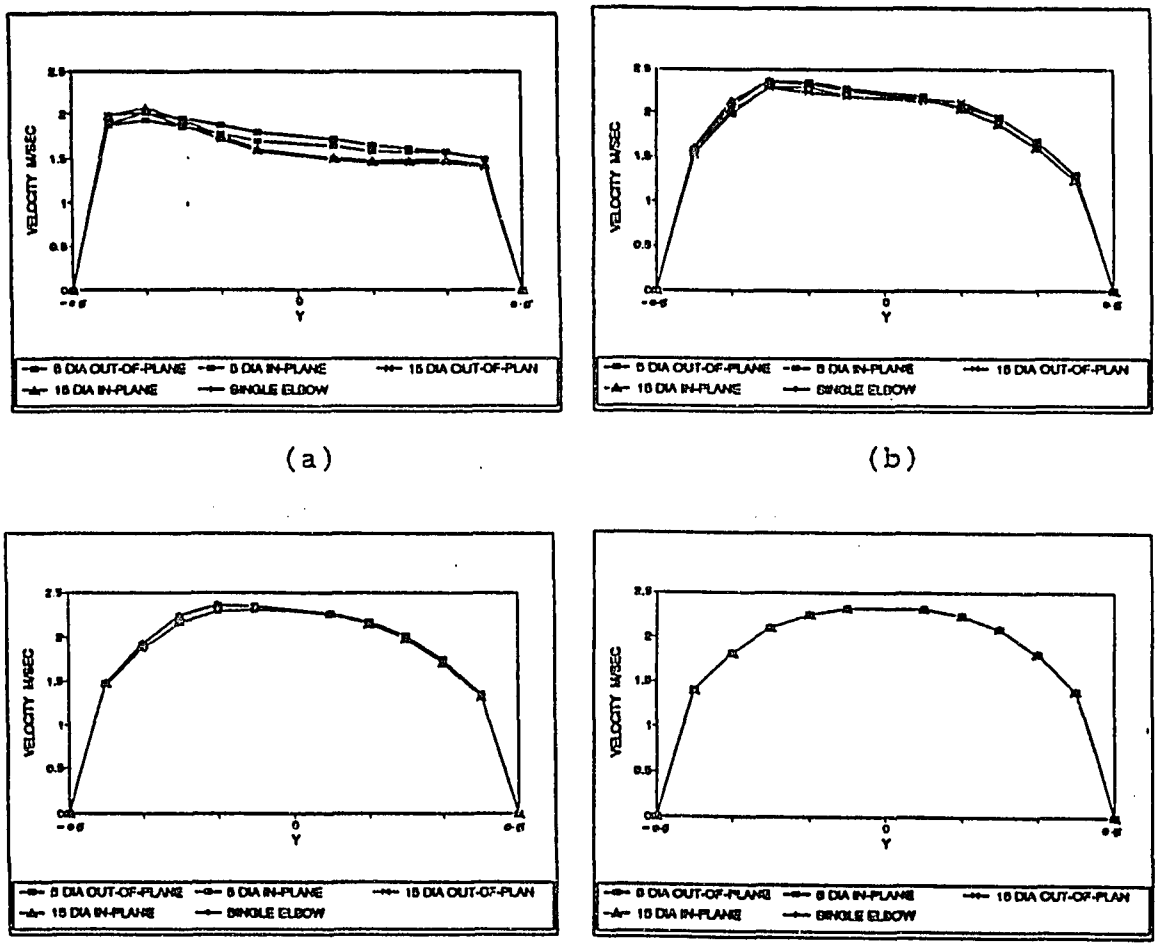

(a) (b)

(c) (d)

Legend. (a) 1 Diameter (b) 25 Diameters
(c) 40 Diameters (d) 60 Diameters

Figure 41. Comparison of Streamwise Velocity Profiles of Different In-Plane and Out-of-Plane Cases at Different Distances Along Vertical Axis.

Figure 42 compares the velocity profiles of in-plane, out-of-plane and single elbow along horizontal axes. At a diameter distance both the 15 diameters spaced in-plane and out-of-plane cases had quantitatively same value as the single elbow. At 25 diameters distance both the out-of-plane cases varied from the single elbow and in-plane cases. At this distance, the velocity profiles of both the in-plane and single elbow were close to a fully developed flow profile, whereas the double elbow cases had the effect of elbows with acceleration near the outer wall. At 40 diameters distance, there was no difference between the profiles of in-plane and single elbow cases. In the out-of-plane cases, the velocity increased at the inner wall and decreased at the outer wall and the profile shapes approached the single elbow case profile. At 60 diameters distance, all the profiles look qualitatively same.

In both of the above comparisons, the velocity profiles from the 5 diameters spaced out-of-plane type were different from other cases at all the distances. It required more distance to get close to the single elbow case, whereas the 15 diameters spaced out-of-plane was in between 5 diameters spaced out-of-plane and single elbow case. In-plane cases were close to the single elbow cases almost at all the distances both along vertical and horizontal directions. However, after a distance of 60 diameters, all the profiles approached to be similar and

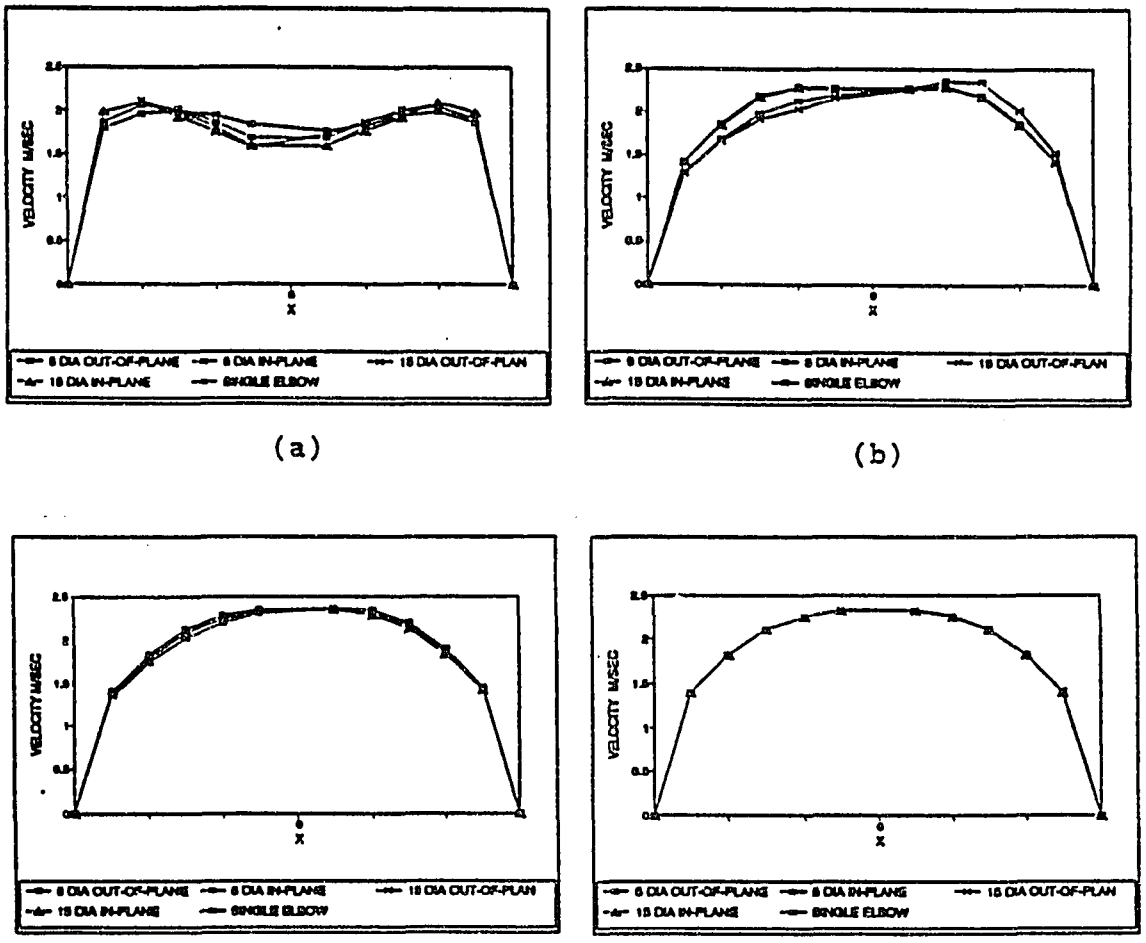

(a) (b)

(c) (d)

Legend. (a) 1 Diameter (b) 25 Diameters
(c) 40 Diameters (d) 60 Diameters

Figure 42. Comparison of Streamwise Velocity Profiles of Different In-Plane and Out-of-Plane Cases at Different Distances Along Horizontal Axis.

the elbow effects could be considered as minimized.

Table 14 gives the length of pipe required to eliminate the elbow effects for different single and double elbow cases.

Table 14

Requirements of Pipe Length for Different Cases to Eliminate the Elbow Effects

Configuration	Re	Length of pipe required in diameters
Single elbow	10^4	64
Single elbow	10^5	67
Single elbow	10^6	67
Double elbows 5 diameters out-of-plane	10^5	78
Double elbows 10 diameters out-of-plane	10^5	78
Double elbows 15 diameters out-of-plane	10^5	67
Double elbows 5 diameters in-plane	10^5	73
Double elbows 15 diameters in-plane	10^5	67

CHAPTER VIII

SUMMARY

Flow field computations were carried out on a computer to determine the effect of elbows. Numerical results showed that the elbows severely distort flow variables like velocity, pressure, and kinetic energy of turbulence. This causes restricting of flow not only within the curved sections themselves but also in the downstream pipe section.

The computational model was verified with experimental data. The analytical solutions demonstrated that numerical modeling can be used with reliability to predict the performance of flow field.

There was a difference in the length of pipe required between the single and double elbow cases. The single elbow case needed about 67 diameters of pipe length to get a fully-developed profile downstream of the elbow. The profile changes ware noticeable up to 45 diameters distance. After that distance, the changes were very small in both the horizontal and vertical axes. Because the results from the cases with Reynolds number of 10^6 and 10^5 were the same, it is concluded that the effects of elbow were not significantly affected by the variation of Reynolds number

within the limits investigated. It was also shown that the elbow effect did not change with different pipe diameters.

In double elbow cases, the elbow effect decreased with increasing distance of spacing between the two elbows. This was true for both in-plane and out-of-plane configurations. However, the required lengths for diminution of the elbow effect were not the same for both in-plane and out-of-plane types. The out-of-plane type required more pipe length to eliminate the combined effects of elbows than the in-plane type. After 15 diameters spacing, both in-plane and out-of-plane required the same length as the single elbow case. In all of the double elbow cases, the effect was not noticeable after about 60 diameters. The profiles approached to be almost identical irrespective of the spacing between the elbows.

Considering the above results, when designing an approach piping system, it is recommended to have 45 diameters distance between the last elbow and the headbox to eliminate the effect of elbows. However, it may not always be practically possible to do this. In that case, the spacing between the last elbow and the headbox should be sufficient enough to eliminate the cross flows and the swirl coming out of the elbow which is about 30 diameters.

There may be many instances that the approach piping system will have two elbows closely in series either in-plane or out-of-plane. The numerical results showed that

the double elbows in the system required more length of pipe than the single elbows. This length varied depending upon the configuration of the elbows whether they are in-plane or out-of-plane and the distance between the elbows. The closer the spacing between elbows, the more was the length of pipe required downstream of the second elbow. In order to avoid the situation of having longer pipe after the second elbow, 15 diameters spacing between the elbows would eliminate the combined effect of the elbows. Hence, if the elbows are placed after 15 diameters spacing, the length of the pipe required downstream of the second elbow would be same as having a single elbow in the system.

CHAPTER IX

CONCLUSIONS

Elbows affected flow variables like velocity, pressure, and kinetic energy of turbulance and generated swirl and cross flows.

For a single elbow, about 67 diameters distance were needed to completely eliminate the elbow effects and to get the axisymmetric velocity profiles. However, the effect was not noticeable after 45 diameters distance in the velocity profile.

In case of pressure profile, about 34 diameters distance were needed to get the uniform pressure profile.

Cross flows that developed from the elbow lasted for about 33 diameters distance.

Swirl angle at the exit of the elbow was -14^0 and at 23 diameters distance it became zero.

Pipe diameter has no influence on the velocity profile.

Effect was severe when there were two elbows in series. The combined effects due to the out-of-plane, double elbows were more severe than in-plane, double elbows and single elbow.

The greater is the distance between the two elbows,

the less is the combined effect. Five diameters spaced, out-of-plane elbows needed 78 diameters distance whereas the in-plane elbows needed 73 diameters to get the fully developed profile. At 15 diameters spacing, the distance needed was 67 diameters for both in-plane and out-of-plane which is same as single elbow. Hence 15 diameters spacing between the elbows decouple the combined elbow effects.

CHAPTER X

SUGGESTIONS FOR FUTURE WORK

While determining the effect of double elbows, it was determined that double elbows, whether in-plane or out-of-plane, with 15 diameters spacing required the same length as the single elbows, i.e., there was no combined effect after 15 diameters spacing. But at 10 diameters spacing, the elbow effects were different for in-plane and out-of-plane. Hence, there is an optimum distance between 10 and 15 diameters between elbows to eliminate the combined effect of elbows. This distance should be investigated.

When the pulp enters the headbox, the flow turns 90° into the tube banks. The length of the tube and the length of the lexon sheet in the converging zone of the hydraulic headbox are important variables in determining turbulence scale and intensity of the headbox. Simulation of optimum length of tubes and lexon sheets in the converging zone should be studied.

Until recently, headbox design has been exclusively on trial and error experimentation. Relative performance has been based on improved formation and sheet properties. Accurate numerical prediction of headbox flow would provide a rapid and effective guide to improved headbox design.

LITERATURE CITED

1. Headbox piping system -- General Design Guide , TAPPI Technical information series TIS 014-6 (1972).

2. Heissenberger, O.L., Jr., "A Headbox for Paper Quality," Engineering Conference Proceedings, TAPPI, P. 647-654 (1987).

3. Manson, D.W., "Introduction to Wetend Operations," Wet End Operations Proceedings, TAPPI, P. 5-6 (1978).

4. Girard L. C., "From Fan Pump to Slice Approach Piping," Tutorial Seminar presented at CPPA annual meeting, Montreal, Quebec, p. 1-20 (1979, January 31).

5. Kershaw, N.T., "Basic Wet End Hydraulics," Wet End Operations Seminar, TAPPI, p. 5-12 (1987).

6. Shands, J., Beloit Corporation, Beloit, Wisconsin, private communications.

7. Sabersky, R.J., Acosta, A.J., and Hauptmann, E.G., "Fluid Flow," Second Edition, The Macmillan Company, New York. (1971).

8. Geankoplis, Christie. J., "Transport Process and Unit Operations," Allyn and Bacon Inc., MA. p. 72 (1978).

9. McCabe, W.L., Smith, J.C., "Unit Operations of Chemical Engineering," Third edition, McGraw-Hill, New York. p. 51-56 (1976).

10. Idelchik, I.D., "Handbook of Hydraulic Resistance", Hemisphere Publishing Corporation, New York, p. 265-331.(1986).

11. Yeh, T.T., and Mattingly, G.E., "Mixing Motions Produced by Pipe Elbows," NISTR 89-4029, National Institute of Standards and Technology, Gaithersburg, MD 20899 (1989).

12. Yeh, T.T., and Mattingly, G.E., "NBS Industry-Government Consortium Research Program on Flowmeter Installation Effects," NISTR 89-4080, National Institute of Standards and Technology, Gaithersburg, MD 20899 (1989).

13. Newcombe, D., "Headbox Problems and Possible Solutions," Wetend Operations Seminar, TAPPI, p. 137-144 (1987).

14. FLUENT/BFC User's Manual version 3.02, CREARE Incorporated, Hanover, NH 03755 (1990).

15. Triantafillopoulos, N., Rudemiller, G., Farrington, T., Jr. and Lindsay, J., "Numerical Simulation of Short Dwell Coater Fond Flows," Engineering Conference, TAPPI, p. 209-212 (1988).

16. Patankar, S.V., "Numerical Heat Transfer and Fluid Flow," Hemisphere Publishing Corporation, McGraw-Hill Company, New York (1980).

17. Dvinsky, A.S., "FLUENT/BFC: A General Purpose Fluid Modeling Program for All Flow Speeds," Presented at the Fifth International Conference on Numerical Methods in Laminar and Turbulent Flow, Montreal, July 1987.

18. Trufitt, D.A., "Design Aspects of Manifold Type Flowspreader," Australian Paper Manufacturers, Melbourne, Victoria, Australia. p. 46-49 (1987).

19. Ogawa, K., Yoshikawa, S., Ikeda, J., and Ogawa, H., "Pressure Loss and Velocity Profile of Pulp in a Circular Pipe," TAPPI, vol (4): 217-221 (1990).

20. FLUENT manual, Creare Incorporated, Hanover, New Hampshire (1987).

21. Boni, A.A., and Srinivasachar, S., "FLUENT," Journal of Engineering Computing and Applications, p. 63-69 (1987).

22. Mattingly, G.E., National Institute of Standards and Technology, Gaithersburg, MD., private communications.

23. Algers, B.A., "New Examination of Stock Piping," Paper, 18(2), p.16-18 (1981).

24. Jones, G.L., and Ginnow, R. J., "Modelling Headbox Performance with Computational Fluid Mechanics," Engineering Conference Proceedings, TAPPI, p. 15-29 (1988).

25. Pantaleo, S., "Stock Piping Principles and Their Effect on Paper Machine Performance," Wet End Opera-

tions Seminar, TAPPI, p. 21-27 (1987).

26. Duncau, S., "Estimates of Rates of Strain of the Flow in the Approach System of a Papermachine," Engineering Conference, TAPPI, p. 215-221 (1982).

27. Heissenberger, O.L., Jr. "A Headbox for Paper Quality," Engineering Conference, TAPPI, p. 647-654 (1987).

28. Brauns, R.A., "Stock Piping Principles," Beloit Corp., Paper Age, (12) 12-14 (1977).

29. Mardon, J., O'Blenes, G., and Wahlstrom, P.B., "The Hydrodynamics of Papermachine Headbox Approach Piping", Pulp and Paper Magazine of Canada, (4) 36-40 (1958).

30. Duffy, G.G.; "Review and Evaluation of Design Methods for Stock Piping System," Engineering Conference, TAPPI, p.149-155 (1975).

31. Yokogawa, A., Suzuki, M., and Shimuzu, T., "A Study on Flow Characterstics of Pulp Suspension Flow-Measurement of Turbulence Intensity and Fiber Concentration Uneveness," Bulletin of JSME, Vol.28, No.239,(5) 846-853 (1985).

32. Laskey, H.L. "Optimum Design of Pulp Stock Pipelines," TAPPI Vol (6):79-83 (1988).

33. Ewald, J.L., "Design Principles for Approach Piping," Wet End Operations Seminar, TAPPI, p. 15-20 (1979).

34. Schlichting, D., "Boundary Layer Theory," Sixth edition, McGraw-Hill Book Company, New York (1968).

APPENDICES

Appendix A

Theory Utilized by FLUENT/BFC

Theory Utilized by FLUENT/BFC

Geometry Definition

Before a numerical simulation of a fluid problem begins, a finite volume grid must be created. There are two ways to generate a grid, either before or after creating the geometry. If the grid is generated before the geometry, fine tuning of grid will change the geometry. In such situation, modification of the grid could be a long and difficult process. These problems can be eliminated by first specifying a geometry from which the grid is then created. There are three basic geometrical elements: points, curves, and surfaces. The boundaries in two-dimensional problems are specified with curves and in three-dimensional with surfaces.

Domain Discretization

Domain discretization is done by dividing the region of interest into small subdomains, called control volume or cells, by drawing lines that coincide with constant coordinate lines. The simplest coordinate system, the Cartesian coordinate system, is not appropriate because the stair-step approximation of a curved or inclined boundary can cause errors in the calculation of wall shear stress.

This, in turn, may cause inaccuracies in the numerical solution for the entire domain. Furthermore, the cells are wasted in dead region that are used to generate the stair-step boundary approximation. Ideally, a coordinate system must be chosen such that the boundaries of the problem coincide with a grid line. Such a coordinate system is so called a Body Fitted Coordinate (BFC) system. In three dimensions, the BFC system involves a third coordinate, and boundaries are defined by coordinate surfaces instead of the lines in two dimensional geometries.

Figure 43. A Domain in Computational Space

An example of BFC grid generation may elucidate this process. Consider that the domain depicted in Fig. 43 is to be discreticized. By introducing a fixed cartesian coordinate system, (x,y), the position of each point in the domain can be uniquely identified by specifying its x and y coordinates. Alternatively, a natural coordinate system, (ξ,η), can be used such that the left and right boundaries of the domain are lines of constant ξ and the bottom and top boundaries are lines of constant η. Under these conditions, the domain looks simple when depicted in the

(ξ,η) coordinate system, as shown in Fig. 7. A unique correspondence can be specified between each grid node in the ξ-η plane and same point in the x-y plane. This process proceeds in the same manner until all the nodes in the plane correspond to their counterparts in the x-y plane. Once this correspondence is specified, a boundary conforming or a boundary-fitted coordinate system has been generated.

In the grid generation process, a set of grid points is formed by the intersection of the lines (or surfaces in three dimensions) of a boundary-conforming curvilinear coordinate system is accomplished by the differential equations method. Once the body-fitted grid is generated, the governing equations can be expressed in terms of the new coordinates (ξ,η). Transforming a domain, or mapping, means that all the points are expressed in terms of a new coordinate system. Conceptually, this means going from the x-y (physical) plane to (ξ,η) (computational) plane. The constant ξ and η lines that are curvilinear in the physical space, are straight lines in (ξ,η) space. The difference is that any point in the physical space is expressed in terms of ξ and η instead of x and y. The governing differential equations expressed in terms of ξ and η may now be solved in the computational (ξ,η) space using a well-defined square mesh.

Boundary Conditions

For incompressible and subsonic flows, the equations described in the above section are elliptic in nature. Therefore for such flows, boundary conditions must be specified at all boundaries. At inlets, the velocity or stagnation pressure, and values of the appropriate scalars such as temperature, kinetic energy and eddy dissipation, are specified. At outlets, the static pressure may be specified or the zero normal gradient conditions may be imposed. At walls, the slip or no-slip condition may be selected. In the case of slip walls, the wall shear stress and the normal velocity component are taken to be zero. At a no-slip wall, the fluid velocity at the walls is taken to be the velocity of the wall. For turbulent flow, the assumption of an equilibrium turbulent wall shear is made.

Solution Procedure

The discretization process yields the following set of nonlinear, coupled basic algebraic equations for the unknowns:

$$\text{Mass} \quad \partial p/\partial t = \nabla.(\rho \mathbf{v}) = 0 \qquad (9)$$

$$\text{Momentum} \quad \partial/\partial t(\rho \mathbf{v}) + \nabla.(\rho \mathbf{v}\mathbf{v}) = \nabla.(\pi+\pi T) + F \qquad (10)$$

$$\text{Energy} \quad \partial/\partial t(\rho e)+\nabla.(\rho \mathbf{v} e) = -\nabla.(q+q_t)-(p\mathbf{v}.\mathbf{v})+(\tau.\mathbf{v}\mathbf{v})+S_E \qquad (11)$$

where ρ is the density, v is the velocity vector, π, π_t are the molecular and turbulent stress tensors, e is the total energy and q and q_t are the mean heat flux and turbulent heat flux vectors, respectively. In the momentum equation, F represents body forces, momentum sources and sinks. Body forces due to gravitational and centrifugal accelerations are provided as:

$$F = \rho g - 2(\Omega * v) - \Omega * (\Omega * r) \qquad (12)$$

where g is the acceleration vector, Ω is the rotational velocity of the reference frame and r is radius vector.

The velocity and pressure fields are coupled through the continuity equation. In addition, the velocity and temperature fields are coupled due to variable property effects.

For turbulent flows a two-equations model is used in which the turbulent stresses and fluxes are represented by diffusion-like terms containing an effective diffusion coefficient which is related to two turbulence parameters: the turbulence kinetic energy (k) and its rate of dissipation (ϵ). The turbulent stress tensor, is modeled by an isotropic eddy viscosity (π_T):

$$\pi_T = 2\mu_t D - (2/3)kI \qquad (13)$$

where k is the turbulent kinetic energy and μ_t the turbulent

viscosity. The mean heat flux vector and the turbulent heat flux vector are defined as follows:

$$q = k\nabla T \qquad (14)$$

$$q_t = k_t\nabla T \qquad (15)$$

where k and k_t are the mean and thermal conductivies, respectively. Turbulent kinetic energy,k, and the turbulence dissipation rate ,e, are governed by the following equations.

$$\partial/\partial t(\rho vk)+ \nabla.(pvk) = \nabla.((\mu_t/\sigma_k)\ k)+2\mu_t D:D-\rho\epsilon \qquad (16)$$

$$\partial/\partial t(\rho ve)+\nabla.(\rho v\epsilon) = \nabla.((\mu_t/\sigma_\epsilon)\nabla\epsilon)+C_1(2\mu_t D:D)(\epsilon/k)- C_2\rho(\epsilon^2/k) \qquad (17)$$

where $C_1 = 1.43$, $_\epsilon = 1.3$, $_k = 1.0$, $C_2 = 1.92$.

Turbulence kinetic energy and turbulent dissipation are combined algebraically to specify a turbulent viscosity. This turbulent viscosity, along with a number of algebraic constants is used in the momentum equation in place of the molecular viscosity. The turbulent eddy viscosity, u_t is evaluated using the Prandtl-Kolmogorov relationship:

$$\mu_t = \rho C_\mu(k^2/\epsilon) \qquad (18)$$

where $C_u = .09$. A thermodynamic equation of state is used to close the above system.

Discretization process yields a set of nonlinear

coupled algebraic equations for the unknowns. The velocity and pressure fields are coupled through the continuity equation. For turbulent flows, the momentum equations are coupled to two scalar transport equations for the two-equation turbulence model via the eddy viscosity. Since all these equations are non-linear partial differential equations, an iterative solution procedure is used. At each iteration, the total error (residual) for each equation that is being solved will be displayed. These residuals provide a measure of the degree to which each equation is satisfied throughout the flow field. The FLUENT/BFC computes residuals for each conservation equation by summing the imbalance in the equation for all cells in the domain. Generally, a solution will be well converged when the normalized residuals are in the order of $1*10^{-03}$.

In BFC two algorithms are available for the solution of the discreticized equations. The default algorithm is based on a pressure correction method called the SIMPLER procedure of Patankar (16). In the SIMPLER algorithm, a pressure equation is derived by combining the discretized momentum equations with the continuity equation. Following algorithm is used for solving the coupled set of discretized equations, starting from the initial conditions of each time step.

1. Start with a guessed velocity field.

2. Calculate coefficients for the momentum equations and then calculate coefficients for the pressure equations.

3. Solve the pressure equation to obtain the pressure field.

4. Using this pressure field solve the momentum equations.

5. Solve the pressure correction equation

6. Using the pressure correction, correct the velocity field.

7. Solve the discretization equation for other scalars if necessary.

8. Return to step 2 and repeat until convergence.

In this method, the discretized equations are solved sequentially in a step by step manner.

An alternative algorithm, proposed by Dvinsky (17), is available for a class of incompressible flow problems. But this method cannot be used for porous media flows, flows with pressure boundary conditions or compressible flows.

Appendix B

Code to Develop a Model with Two Elbows

Code (Log File) to Deveolp a Model With Two Elbows of 15 Diameter Spacing.

```
(* CREATE INLET PIPE SECTION *)
GEO GEO 3 CREATE POINT
NA A X -.01767 Y 1.175 Z .01767 DO
NA 01 X 0 Y 1.175 Z 0 EXIT
CONS COPY POINT
NA 01 NEW 02 Y -1.1 EXIT
EXIT
CRE CURVE
NA DIR1 NUM 2 P1 01 P2 02 EXIT
CRE ARC
NA AB NUM 3 PIV DIR1 ST A END B ARC -90^0 DO
NA BD ST B END D ARC -90^0 DO
NA CD ST D END C DO
NA AC ST C END TEMP EX
MODIFY MERGE
DUPLICATE TEMP REPLACE A DEL YES EX
REV CURVE
NA CD DO
NA AC EX
EXIT
CRE PATCH
NA INLET 1 AB 2 CD 3 AC 4 BD BOU INLET EX
```

```
CONSTRUCT SWEEP SURFACE
NA INLET DIR DIR1 ORIENT NORMAL U0 FRONT1 U1 REAR1 V0 LEFT1
V1 RIGHT1 TABLE CAP CAP1 EXIT
SD PS CAP Y EX SV ISO EX EX DISPLAY
EXIT
(* CREATE FIRST ELBOW *)
CRE POINT
NA E X .075 T .075 Z .025 DO
NA F X .075 T .075 Z -.025 EX
CRE CURVE
NA EF P1 E P2 F EX
CRE ARC
NA DIR2 NUM 5 PIV EF ST 02 END 03 ARC -90 EX
CONSTRUCT SWEEP SURFACE
NA CAP1 DIR DIR2 ORIENT NORMAL U0 FRONT2 U1 REAR2 LEFT2 V1
RIGHT2 TABLE CAP CAP2 EX
EXIT
(* CREATE STRAIGHT SECTION *)
CRE POINT
NA 04 X .825 Y 0 Z 0 EX
CRE CURVE
NA DIR3 P1 03 P2 04 EX
CONSTRUCT SWEEP SURFACE
NA CAP2 DIR DIR3 ORIENT FIXED U0 FRONT3 U1 REAR3 V0 BOTTOM3
V1 TOP3 TABLE CAP CAP3 EX
```

```
EXIT
(* CREATE SECOND ELBOW *)
CREATE POINT
NA H .825 Y -.025 Z .075 DO
NA G .825 Y .025 Z .075 DO
CRE CURVE
NA GH P1 G P2 H EX
CRE ARC
NA DIR4 NUM 5 PIV GH ST 04 END 05 ARC 90 EX
CONSTRUCT SWEEP SURFACE
NA CAP3 DIR DIR4 ORIENT NORMAL U0 FRONT4 U1 REAR4 V0
BOTTOM4 V1 TOP4 TABLE CAP CAP4 EX
EXIT
(* CREATE THE LAST STRAIGHT SECTION *)
CRE POINT
NA 06 X .875 Y 0 Z 4.575 EX
CRE CURVE
NA DIR5 PA 05 P2 06 EX
CONSRUCT SWEEP SURFACE
NA CAP4 DIR DIR5 ORIENT FIXED U0 LEFT5 U1 RIGHT5 V0
BOTTOM5 V1 TOP5 TABLE CAP OUTLET EX
EXIT
(* BEGIN MAPPING *)
GRID BFC GBC SET
ID 157 JD 11 KD 11 EX
```

```
OUTER MS INLET
I1 1 J1 1 K1 11 I2 1 J2 1 K2 1 I3 1 J3 11 K3 1 DO
SURFACE FRONT1 I2 22 J2 1 K2 11 DO
SURFACE LEFT1 DO
SURFACE REAR1 DO
SURFACE RIGHT1 DO
SURFACE FRONT2 I2 37 J2 1 K2 11 DO
SURFACE LEFT2 DO
SURFACE REAR2 DO
SURFACE RIGHT2 DO
SURFACE FRONT3 I2 52 J2 1 K2 11 DO
SURFACE BOTTOM3 DO
SURFACE REAR3 DO
SURFACE TOP3 DO
SURFACE FRONT4 I2 67 J2 1 K2 11 DO
SURFACE BOTTOM4 DO
SURFACE REAR4 DO
SURFACE TOP4 DO
SURFACE LEFT5 I2 157 J2 1 K2 11 DO
SURFACE BOTTOM5 DO
SURFACE RIGHT5 DO
SURFACE TOP5 EXIT
EXIT EXIT
INTERPOALTE-GRID SP EX EX
VD GO SD NUM 1 SO K SI 5 EX
```

```
SV FRONT EX EX
PG SIDE ISO HARD EXIT
GO SD NUM 1 SO I SI 1 EX SV PLAN EX EX PG SCALE
REDRAW  HARD EX
EXIT
WC U DOUBLE_ELBOW.CAS
QUIT
```

Appendix C

Type of Cells in the Geometry

CELL TYPES I-PLANE 1

J K=	1	2	3	4	5	6	7	8	9	10	11	12	13	14
25	W_1	W_1	W_1	W_1	W_1	W_1	W_1	W_1	W_1	W_1	W_1	W_1	W_1	W_1
24	W_1	I_1	I_1	I_1	I_1	I_1	I_1	I_1	I_1	I_1	I_1	I_1	I_1	W_1
23	W_1	I_1	I_1	I_1	I_1	I_1	I_1	I_1	I_1	I_1	I_1	I_1	I_1	W_1
22	W_1	I_1	I_1	I_1	I_1	I_1	I_1	I_1	I_1	I_1	I_1	I_1	I_1	W_1
21	W_1	I_1	I_1	I_1	I_1	I_1	I_1	I_1	I_1	I_1	I_1	I_1	I_1	W_1
20	W_1	I_1	I_1	I_1	I_1	I_1	I_1	I_1	I_1	I_1	I_1	I_1	I_1	W_1
19	W_1	I_1	I_1	I_1	I_1	I_1	I_1	I_1	I_1	I_1	I_1	I_1	I_1	W_1
18	W_1	I_1	I_1	I_1	I_1	I_1	I_1	I_1	I_1	I_1	I_1	I_1	I_1	W_1
17	W_1	I_1	I_1	I_1	I_1	I_1	I_1	I_1	I_1	I_1	I_1	I_1	I_1	W_1
16	W_1	I_1	I_1	I_1	I_1	I_1	I_1	I_1	I_1	I_1	I_1	I_1	I_1	W_1
15	W_1	I_1	I_1	I_1	I_1	I_1	I_1	I_1	I_1	I_1	I_1	I_1	I_1	W_1
14	W_1	I_1	I_1	I_1	I_1	I_1	I_1	I_1	I_1	I_1	I_1	I_1	I_1	W_1
13	W_1	I_1	I_1	I_1	I_1	I_1	I_1	I_1	I_1	I_1	I_1	I_1	I_1	W_1
12	W_1	I_1	I_1	I_1	I_1	I_1	I_1	I_1	I_1	I_1	I_1	I_1	I_1	W_1
11	W_1	I_1	I_1	I_1	I_1	I_1	I_1	I_1	I_1	I_1	I_1	I_1	I_1	W_1
10	W_1	I_1	I_1	I_1	I_1	I_1	I_1	I_1	I_1	I_1	I_1	I_1	I_1	W_1
9	W_1	I_1	I_1	I_1	I_1	I_1	I_1	I_1	I_1	I_1	I_1	I_1	I_1	W_1
8	W_1	I_1	I_1	I_1	I_1	I_1	I_1	I_1	I_1	I_1	I_1	I_1	I_1	W_1
7	W_1	I_1	I_1	I_1	I_1	I_1	I_1	I_1	I_1	I_1	I_1	I_1	I_1	W_1
6	W_1	I_1	I_1	I_1	I_1	I_1	I_1	I_1	I_1	I_1	I_1	I_1	I_1	W_1
5	W_1	I_1	I_1	I_1	I_1	I_1	I_1	I_1	I_1	I_1	I_1	I_1	I_1	W_1
4	W_1	I_1	I_1	I_1	I_1	I_1	I_1	I_1	I_1	I_1	I_1	I_1	I_1	W_1
3	W_1	I_1	I_1	I_1	I_1	I_1	I_1	I_1	I_1	I_1	I_1	I_1	I_1	W_1
2	W_1	I_1	I_1	I_1	I_1	I_1	I_1	I_1	I_1	I_1	I_1	I_1	I_1	W_1
1	W_1	W_1	W_1	W_1	W_1	W_1	W_1	W_1	W_1	W_1	W_1	W_1	W_1	W_1

Figure 44. Cells at the Inlet in Computational Space.

CELL TYPES I-PLANE 60

J	K= 1	2	3	4	5	6	7	8	9	10	11	12	13	14
25	W_1	W_1	W_1	W_1	W_1	W_1	W_1	W_1	W_1	W_1	W_1	W_1	W_1	W_1
24	W_1	.	.	.	.	.	.	.	.	.	.	.	.	W_1
23	W_1	.	.	.	.	.	.	.	.	.	.	.	.	W_1
22	W_1	.	.	.	.	.	.	.	.	.	.	.	.	W_1
21	W_1	.	.	.	.	.	.	.	.	.	.	.	.	W_1
20	W_1	.	.	.	.	.	.	.	.	.	.	.	.	W_1
19	W_1	.	.	.	.	.	.	.	.	.	.	.	.	W_1
18	W_1	.	.	.	.	.	.	.	.	.	.	.	.	W_1
17	W_1	.	.	.	.	.	.	.	.	.	.	.	.	W_1
16	W_1	.	.	.	.	.	.	.	.	.	.	.	.	W_1
15	W_1	.	.	.	.	.	.	.	.	.	.	.	.	W_1
14	W_1	.	.	.	.	.	.	.	.	.	.	.	.	W_1
13	W_1	.	.	.	.	.	.	.	.	.	.	.	.	W_1
12	W_1	.	.	.	.	.	.	.	.	.	.	.	.	W_1
11	W_1	.	.	.	.	.	.	.	.	.	.	.	.	W_1
10	W_1	.	.	.	.	.	.	.	.	.	.	.	.	W_1
9	W_1	.	.	.	.	.	.	.	.	.	.	.	.	W_1
8	W_1	.	.	.	.	.	.	.	.	.	.	.	.	W_1
7	W_1	.	.	.	.	.	.	.	.	.	.	.	.	W_1
6	W_1	.	.	.	.	.	.	.	.	.	.	.	.	W_1
5	W_1	.	.	.	.	.	.	.	.	.	.	.	.	W_1
4	W_1	.	.	.	.	.	.	.	.	.	.	.	.	W_1
3	W_1	.	.	.	.	.	.	.	.	.	.	.	.	W_1
2	W_1	.	.	.	.	.	.	.	.	.	.	.	.	W_1
1	W_1	W_1	W_1	W_1	W_1	W_1	W_1	W_1	W_1	W_1	W_1	W_1	W_1	W_1

Figure 45. Cells at the Flow Domain in Computational Space.

CELL TYPES I-PLANE 6

J	K= 1	2	3	4	5	6	7	8	9	10	11	12	13	14
25	W_1	W_1	W_1	W_1	W_1	W_1	W_1	W_1	W_1	W_1	W_1	W_1	W_1	W_1
24	W_1	0	0	0	0	0	0	0	0	0	0	0	0	W_1
23	W_1	0	0	0	0	0	0	0	0	0	0	0	0	W_1
22	W_1	0	0	0	0	0	0	0	0	0	0	0	0	W_1
21	W_1	0	0	0	0	0	0	0	0	0	0	0	0	W_1
20	W_1	0	0	0	0	0	0	0	0	0	0	0	0	W_1
19	W_1	0	0	0	0	0	0	0	0	0	0	0	0	W_1
18	W_1	0	0	0	0	0	0	0	0	0	0	0	0	W_1
17	W_1	0	0	0	0	0	0	0	0	0	0	0	0	W_1
16	W_1	0	0	0	0	0	0	0	0	0	0	0	0	W_1
15	W_1	0	0	0	0	0	0	0	0	0	0	0	0	W_1
14	W_1	0	0	0	0	0	0	0	0	0	0	0	0	W_1
13	W_1	0	0	0	0	0	0	0	0	0	0	0	0	W_1
12	W_1	0	0	0	0	0	0	0	0	0	0	0	0	W_1
11	W_1	0	0	0	0	0	0	0	0	0	0	0	0	W_1
10	W_1	0	0	0	0	0	0	0	0	0	0	0	0	W_1
9	W_1	0	0	0	0	0	0	0	0	0	0	0	0	W_1
8	W_1	0	0	0	0	0	0	0	0	0	0	0	0	W_1
7	W_1	0	0	0	0	0	0	0	0	0	0	0	0	W_1
6	W_1	0	0	0	0	0	0	0	0	0	0	0	0	W_1
5	W_1	0	0	0	0	0	0	0	0	0	0	0	0	W_1
4	W_1	0	0	0	0	0	0	0	0	0	0	0	0	W_1
3	W_1	0	0	0	0	0	0	0	0	0	0	0	0	W_1
2	W_1	0	0	0	0	0	0	0	0	0	0	0	0	W_1
1	W_1	W_1	W_1	W_1	W_1	W_1	W_1	W_1	W_1	W_1	W_1	W_1	W_1	W_1

Figure 46. Cells at the Outlet in Computational Space.